Modelling and Control of a Stoker Firing System

Master Thesis

Project Group 1031a

Heine Hansen
Louis Schultz Lantow

Aalborg University
The Faculty of Engineering, Science and Medicine
Department of Electronic Systems
Section of Automation and Control

AALBORG UNIVERSITY

Faculty of Engineering, Science and Medicine
Department of Electronic Systems
Section of Automation and Control
Frederik Bajersvej 7 C3
9220 Aalborg Ø
Phone: +45 96 35 86 00
http://www.control.aau.dk

Title:

Modellering og Regulering af et Stoker System

Project Period:

9^{th} and 10^{th} semester, 3^{rd} of September 2007 - 4^{th} of June 2008

Project Group:

1031a

Participants:

Heine Hansen
Louis Schultz Lantow

Supervisors:

Tom Søndergaard Pedersen
Palle Andersen

Copies: 7

Page numbers: 141

Appendices: 8

Date of completion: 4^{th} of June 2008

Synopsis:

This report concerns the controlling of a stoker firing system from Benekov/Liagro. The stoker firing system is set at our/the University's disposal by Techno-Matic A/S who normally delivers the controllers to Benekov/Liagro.
Two non-linear models of the stoker firing system are derived; one for wood pellets and one for wheat. The non-linear models are based on six first order differential equations which are determined by thermodynamics and laws of physics. The two non-linear models are then verified in SIMULINK with measured data from the plant.
The models are linearized using a first order Taylor series so a controller can be designed. The controller is designed from a state space model of the stoker firing system. This state space model is a representation of the linear model on matrix form.
The controller designed for the stoker firing system contains two optimal controllers, based on linear quadratic regulator theory - one for each solid fuel. Moreover the controller contains a solid fuel estimator capable of determine the solid fuel combusted. The solid fuel estimator is designed from the two models, Kalman filters and Bayers possibility rule.
The three parts of the controller are verified individually in simulations with satisfying results and they are therefore tested on the plant. The simulation of the two optimal controllers is done using the non-linear model as the plant. The performance obtained in simulations is however not reached on the plant therefore the controllers does not fulfill the desired requirements.
The three parts are then assembled to one adaptive controller. This controller is then tested on the plant. Due to lack of time resources has it not been possible to obtain a satisfying result for the adaptive controller.

AALBORG UNIVERSITET

Det Ingeniør-, Natur- og Sundheds-videnskabelige Fakultet
Institut for Elektroniske Systmer
Sektion for Automation og Kontrol
Frederik Bajersvej 7 C3
9220 Aalborg Ø
Telefon: +45 96 35 86 00
http://www.control.aau.dk

Titel:

Modelling and Control of a Stoker Firing System

Projektperiode:

9. og 10. semester, 3. september 2007 - 4. juni 2008

Projektgruppe:

1031a

Deltagere:

Heine Hansen
Louis Schultz Lantow

Vejledere:

Tom Søndergaard Pedersen
Palle Andersen

Oplagstal: 7

Sidetal: 141

Appendiksantal: 8

Afsluttet den: 4. juni 2008

Synopsis:

Denne rapport omhandler regulering af et Stoker system fra Benekov/Liagro. Stoker systemet er stillet til rådighed af Techno-Matic A/S, som normalt laver regulatorer til Benekov/Liagro.
To ulineære modeller af stoker systemet er udledt, en for træpiller og en for hvede. De ulineære modeller er baseret på seks differential ligninger af første orden, som er bestemt ud fra termodynamik og fysiske love. De to ulineære modeller er verificeret i SIMULINK med måledata fra anlægget.
Modellerne er lineariseret ved hjælp af en første ordens Taylor approksimation, så en regulator kan blive designet. Regulatoren er designet ud fra en state space model af stoker systemet. Denne state space model er en fremstilling af den lineære model på matrix form.
Den designede regulator for stoker systemet indeholder to optimale regulatorer, som er baseret på lineær kvadratisk regulator teori - en for hvert brændsel. Regulatoren indeholder også en brændsels estimater, som kan bestemme det brændsel der afbrændes. Brændsel kalkulatoren er designet ud fra de to modeller, Kalman filtre og Bayers sandsynlighedsregel.
De tre dele i regulatoren er verificeret individuelt i simuleringer med tilfredsstillende resultat og er derfor testet på anlægget. Simulationen af de to optimale regulatorer er lavet med den ulineære model som anlægget. De opnåede resultater i simuleringerne, er ikke opnået på anlægget og derfor kan regulatorerne ikke opfylde de ønsket krav.
De tre dele er samlet til en adaptiv regulator. Denne regulator er testet på anlægget. På grund af tidsmangel har det dog ikke været muligt at opnå tilfredsstillende resultater for den adaptive regulator.

Preface

This master thesis is written by group 08gr1031a and documents a project concerning control of an automatic stoker system. The project originates in the project proposal, "Adaptive Control of a Stoker Firing System" proposed by associate professors Tom Søndergaard Pedersen and Palle Andersen at Aalborg University in collaboration with Søren Kildedal Jensen at Techno-matic A/S.

The authors would like to thank Søren Kildedal Jensen for his great assistance regarding the practical issues concerning the stoker firing system including the interface to the system. Moreover most of the preliminary test on the stoker firing system is made in cooperation with J. Karsten N. Boll who finished his bachelor thesis in January 2008 at Aalborg University.

The thesis and project is made at the Department of Electronic Systems at the Section of Automation and Control at Aalborg University under the Master program "Intelligent Autonomous Systems", and is composed during the period from the 3rd of September 2007 to the 4th of June 2008.

The target group for this project is the company Techno-Matic A/S, the supervisors, the censor and others with interest for the subject. For a complete understanding of this report, a technical and scientific level corresponding to that of 10th semester students at the Section of Automation and Control is required.

Literature references are written according to the Harvard-method: [Last name of author, year of publication] whereas data sheets are referred to as: [Name of manufacturer, year of production]. A complete bibliography can be found at page 103. Figures, tables and equations are numbered consecutively inside each chapter and references to appendices are enumerated as: Appendix A, B, etc.

On the last page, a CD-ROM is enclosed, which contains literature, MATLAB-files and the report. A complete description of the contents of the CD-ROM can be found on the CD-ROM in the `read me.txt`-file which also contains information on how to reconstruct the different tests.

Throughout the project, MATLAB has been used for capturing, processing and representation of data. SIMULINK has been used for implementing and simulating the developed models and controllers. The version of MATLAB used is 7.5.0.342 (R2007b) and the SIMULINK version is 7.0 (R2007b). Moreover Maple 9.00 has been used for large algebraic computations.

The report consists of 15 chapters and 8 appendices, which are structured into the five following parts:

Part **I** is an introduction to the project. An overview of the context in which the project should be viewed is given. A system description is given, including the hardware configuration on the stoker firing system. Lastly this part contains a detailed description of the scope of the project.

Part **II** concerns the mathematical modelling of the stoker firing system. This includes modelling the actuators and sensors, as well as making non-linear and linear models.

Part **III** of the report contains the development of a controller. After an introductory analysis of controllers, an optimal controller is designed, which is then extended to an adaptive controller.

Part **IV** is the closing part where the result from the acceptance test is discussed and the conclusion of the project is made. Future improvements are also presented.

Part **V** contains the appendices of the report, which contains further documentation of the project. This include a description of the SIMULINK interface to the stoker firing system, the controller designed by Techno-Matic A/S, the detailed calculation used in the modelling part

and lastly, documentation of the conducted tests on the actuators and sensors.

For easy reference, a nomenclature is appended as the last appendix. This briefly describes the meaning of the used abbreviations and symbols, and contains the values of the different constants.

Each part starts with a brief intro, describing the contents of the part, and each major part is concluded with a brief summary.

Aalborg University, 4^{th} of June, 2008

Made by:

Heine Hansen	Louis Schultz Lantow

Contents

Part I

Introduction

This part contains three chapters which define the scope of the project and describe the stoker firing system used in this project.

The first chapter describes the context of the report in order to specify the area, in which the purpose of this project lies.

In the second chapter a description of the stoker firing system is presented. First are the processes inside the stoker firing system analysed and secondly the hardware is described.

Finally, the scope of the project is given in the third chapter, where possible solution strategies are discussed. The main objective for this project is also presented along with a number of test criteria to test the stoker firing system.

Chapter 1

The Context of the Project

The total net heat requirement in Denmark is approximately 220,000 TJ per year. This means that each Dane uses 42 GJ on average every year to heat buildings and domestic water which correspond to 11.5 MWh. Seen in a larger measure the yearly consumption of heat in a average single-family house ($130m^2$) is approximately 65 GJ or 18.1 MWh [Energistyrelsen, 2004].

In Denmark different types of technologies are used to heat building and domestic water. Most heat consumers (three out of four) receive heat from a public heat supplier. This is done by building plants and laying down pipes in the ground which deliver hot water or steam to the consumers; this is known as district heating. District heating is produced in heating plants or combined heat and power plants. Public heat supply is primarily found in cities and towns. The last group of heat consumers (one out of four) uses oil furnaces, natural gas furnaces or biofuel furnaces to supply the house with heat. Every consumer with own heating furnace have to purchase their own fuel. Every third home in Denmark has an individual heating plant and 39,000 of these are automatic stokers. Common for the public heat supply and the individual heat supply is that the heat transport inside the building is done through a central heat water carrying system. This means that the heat is transported around inside the building through radiators and pipes [Energistyrelsen, 2004].

Every third home in Denmark has an individual heat source (609,000) and 39,000 of these are automatic stokers

The price for district heating for a average single-family house can vary up to 20,000 dkr on a yearly basis depending on where in Denmark they are based. The reason for this is, among others, the connection fee, the depreciation politics and the heating fuel. A good average for a single-family house is around 0.60 dkr per kWh [Dansk Fjernvarme, 2007]. For individual heating the price is depended on the efficiency of the furnace, the price of the heating fuel and the load on the system. For an automatic stoker with a efficiency above 90 %, grain as fuel and high load the price is 0.35 dkr per kWh for a single-family house. For oil and natural gas furnaces under the same conditions as for the automatic stoker the price lies between 0.83 and 0.88 dkr per kWh. For the individual heating system there is a small yearly compulsory inspection fee which is not included in the kWh prices and the acquisition price is also not included. As just mentioned the high efficiencies for the individual heating systems is only guaranteed under high loads which means that the efficiency decreases when the load is decreased meaning that the kWh price increases.

This efficiency problem is especially valid for automatic stokers as the combustion of solid fuel is rather complex. Moreover most of the automatic stokers are capable of burning different

solid fuels, which further complicates the problem. Different companies are therefore dealing with the problem and one of these companies is Techno-Matic A/S which this project is made in cooperation with. Techno-Matic A/S is a Danish company located just outside of Aars in North Jutland. Besides controllers for automatic stokers, Techno-Matic A/S develops high-tech systems for physically demanding environments mostly to forest machinery.

1.1 The Automatic Stoker System

The automatic stoker system which has been put at disposal by Techno-Matic A/S for this project is a Benekov R 25 Tornado stoker which has a maximum performance of 24 kW and can reach an efficiency above 90%. Benekov is a family owned Czech boiler manufacturer with over 50 years experience in heat technology. Benekov has in cooperation with the Danish company Liagro A/S developed specialized automatic stokers which have the ability to burn a variety of different solid fuels; the R 25 Tornado is such a stoker. The automatic stokers from Banekov/Liagro all have a control unit made by Techno-Matic A/S, the newest is called TM3006. The R 25 Tornado Banekov/Liagro stoker with a Techno-Matic controller can be seen in Figure 1.1. Throughout this report R 25 stoker or just stoker refer to this particular automatic stoker system unless otherwise is mentioned.

Figure 1.1: *Front view of the R 25 Tornado automatic stoker from Benekov/Liagro where the TM3006 controller from Techno-Matic A/S can be seen in the top left. The outer dimensions of the stoker in [mm] is 1470 x 930 x 1210 (width x depth x height) and it weighs 360 kg.*

1.2 The Purpose of this Project

The purpose for this project is to support Techno-Matic A/S with modelling and control of the R 25 stoker. The modelling part is made to find the correlation between the different variables. A model based controller can use this knowledge of the system, which should result in a better control, compared to the controller implemented on the stoker and other controllers that do not use this knowledge. The main challenge is to improve the control of the stoker, compared to

the one implemented today. An important step in the controller design is the estimation of the solid fuel as the R 25 stoker can burn a variety of different solid fuels. Each of these solid fuels has different composition and efficiency which requires much of the controller. If the solid fuel can be estimated, different controllers can be designed, which is optimal for the relevant solid fuel. The efficiency of the stoker will then be increased as some supervision can shift between a set of different controllers when the solid fuel is changed. This means that the only interacting between the stoker and the user is when the stoker has to be refuelled. The controller must also take the varying consumer load into account.

Another problem is that the load can be very small, for instance in the summer time when only the domestic water has to be heated. This means that the stoker must be able to keep burning, when no effect is required, this is called "pause burning". The "pause burning" phenomenon does not have the highest prioritization as the tendency is that more and more uses automatic ignition. The automatic ignition must then be taken into account in the controller but it is much easier compared to the "pause burning" phenomenon. However none of these two phenomenons will be considered in this report. As the main purpose is to make an adaptive controller to different fuels.

In the following chapter a detailed description of both the combustion process and the system will be given.

Chapter 2

System Analysis

The R 25 stoker which is at disposal for this project can grossly be divided into five parts, a solid fuel feeding system, a burning chamber, a gas chamber, a load and a control system (see Figure 2.1).

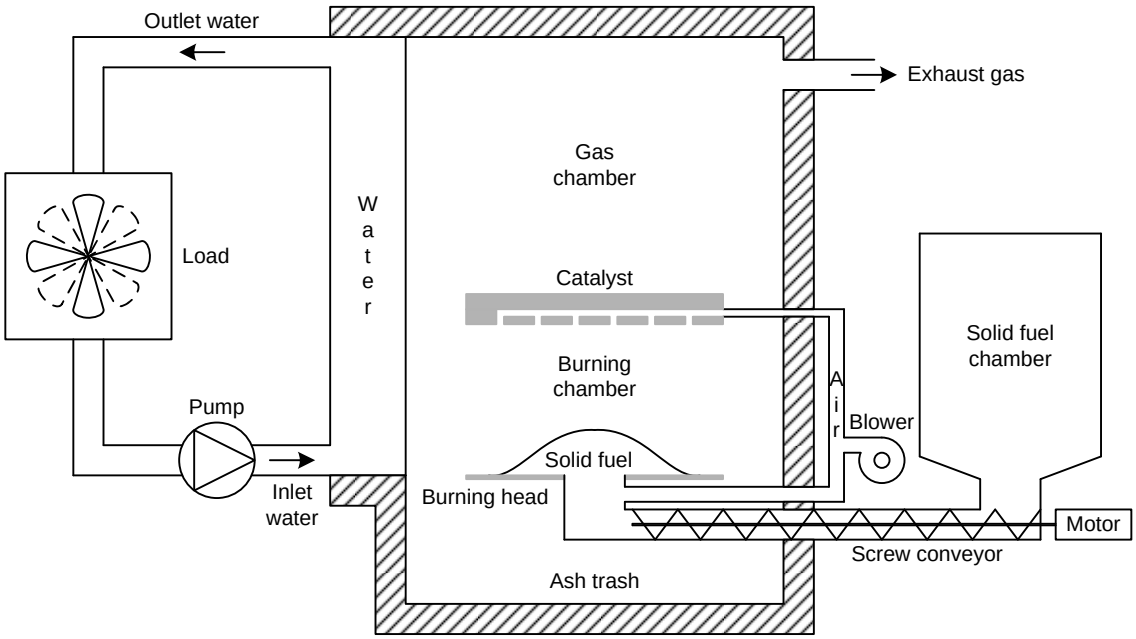

Figure 2.1: *Four of the five parts of the R 25 Tornado stoker which is at disposal for this project. Including the feeding system, the burning chamber, the gas burning chamber and the load.*

The solid fuel feeding system contains a large chamber for solid fuel and a screw conveyor which is driven by a AC motor. This screw conveyor provides the burning chamber with solid fuel. The burning chamber contains a burning head with a hole where the solid fuel comes up like a molehill where a blower provide primary air to the combustion process. Over the molehill is a ceramics plate located to damp down the fire, it also works as a catalyst by supplying secondary air. The gas chamber is the largest area which is in contact with the water pipes, the gas travels around the water pipes until it reaches the exhaust gas chamber and is there led out of a chimney. The gas in the burning chamber, the gas chamber and the exhaust chamber transfers heat to

the water. In the test setup used for this project a calorifier is used as load where the outlet water is led through. The control system on the test setup is different from the original one as the TM3006 controller is replaced with a target PC with an I/O board, two print circuit boards (PCB's) from Techno-Matic A/S and a host PC. A block diagram of the control setup is given in Figure 2.2.

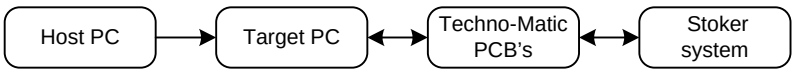

Figure 2.2: *Block diagram of the controller setup for the stoker system where the arrows indicate the signal way.*

Real photos of the stoker system can be found in Appendix F.

In the following the combustion processes inside the stoker will be described in detail, moreover the different solid fuels which can be combusted in a R 25 stoker will be described, and the hardware mounted on the test setup will be described in detail.

2.1 Solid fuel

The R 25 stoker can burn a lot of different solid fuels such as wood pellets, wood chips, grain, olive stones, rape, cacao shells, cherry stones, peat pellets and coal. The solid fuels vary from each other in many ways, but the most distinct are the heating value, the moisture percent and the ash percent. In Table 2.1 the values of these parameters are given.

Solid fuel	Heating value	Humidity content	Ash content
Wood pellets	17.6 MJ/kg	7%	0.3%
Wood chips	17.6 MJ/kg	10%	0.3%
Grain	15.2 MJ/kg	14.5%	3.6%
Olive stones	19.0 MJ/kg	10%	5.0%
Rape pellets	20.8 MJ/kg	7%	8.4%
Cacao shells	17.6 MJ/kg	-	-
Cherry stones	17.2 MJ/kg	15%	1.0%
Peat pellets	16.7 MJ/kg	1.5%	1.7%
Coal	27.2 MJ/kg	10%	10.0%

Table 2.1: *The heating value, humidity content and ash content for the different solid fuels which can be combusted in the R 25 stoker. These solid fuels are tested, approved and recommended by Liagro A/S.*

These values do not only change with different solid fuels, the parameters can also vary as the parameters are depended on the quality of the solid fuel. This is however not investigated further in this project. The values given in Table 2.1 are therefore considered average values. Besides these parameters the different solid fuels can also differ in chemical composition.

This project is limited to dealing with only two different solid fuels; wood pellets and grain which is the two most common solid fuels on the market. These two are described in detail in the following whereas the rest are only described shortly afterwards.

2.1.1 Wood Pellets

Wood pellets are the most distributed solid fuel for stokers and it is made from compacted sawdust. They are usually a by-product of sawmilling or other wood productions. The wood pellets are extremely dense and produced with a low humidity content which allows them to be burned with a high combustion efficiency. Other advantages are the low ash content and the relative high heating value, moreover the wood pellets are highly inflammable. As the wood pellets almost only consists of carbon (C), hydrogen (H), oxygen (O) and water (H_2O) almost no hazardous gases are created during the combustion process. The disadvantage is the price which is more expensive compared to other solid fuels. When the wood pellets are combusted they have a tendency to make a crust, when this crust is burst by the incoming wood pellets the O_2-level will drop briefly. This crust phenomenon is however also present with most of the other solid fuels.

The control of the combustion of wood pellets is relative easy due to the fact that they are highly inflammable. This means that the combustion process can run at a low O_2-level just around 4-8%. The temperature is also easy to control as the wood pellets have a high heating value, meaning that they release a lot of energy during the combustion. The crust formation can be reduced by supplying the stoker with less solid fuel and increasing the number of steps.

2.1.2 Grain

Different sorts of grain can be combusted. In Denmark the most common is wheat and rye. The three parameters for wheat and rye does not differ much, they have the same humidity content but wheat has a lower heating value and a higher ash content. The small difference in the parameters between wheat and rye is assumed to be neglectable. Only wheat is used in this project which is assumed to be sufficient when investigating grain as a solid fuel as wheat has the less optimal parameters. The disadvantage in the grain combustion is the rather low heating value and the high ash content, this is however compensated by the low price on grain. Besides C, H, O and H_2O grain also contains sulphur which creates acid gases during the combustion process. To avoid these acid gases the temperature inside the stoker must be higher than when wood pellets are combusted. Which means that both more grain and more O_2 must be present. The grain is also poor inflammable meaning that even more O_2 must be present.

The control of grain combustions is a bit more complicated compared to combustion of wood pellets. Both the temperature and O_2-level must be sufficiently high. The temperature of the outlet water must be 70-80°C and the O_2-level must be 8-12%.

2.1.3 Alternative Solid Fuels

A number of alternative solid fuels can also be combusted in the R 25 stoker as shown in Table 2.1. All of them have relative small parameter variations compared to each other. The big advantage is the low price which compensates for most of the disadvantages such as low combustion efficiency, low heating value, high moisture and ash contents. The chemical composition of the alternative solid fuels can vary, meaning that different hazardous gases can be created during the combustion process. Common for the combustion of all these alternative solid fuels are the increased demands to the controller.

2.2 The Combustion Processes

As just mentioned the R 25 stoker can burn a lot of different solid fuels, common for all these solid fuels is the chemical structure which mainly consists of C, H, O and H_2O. The combustion process can be divided into five steps (see Figure 2.3).

1. As the wet solid fuel heats up, water is driven off (blue arrows).
2. Drying continues and volatilisation begins (light-orange arrows).
3. Drying and volatilisation continue; volatiles ignite.
4. Drying complete, volatilisation continues and volatiles combustion continues.
5. Volatilisation and volatiles combustion complete; and residual charcoal combusts.

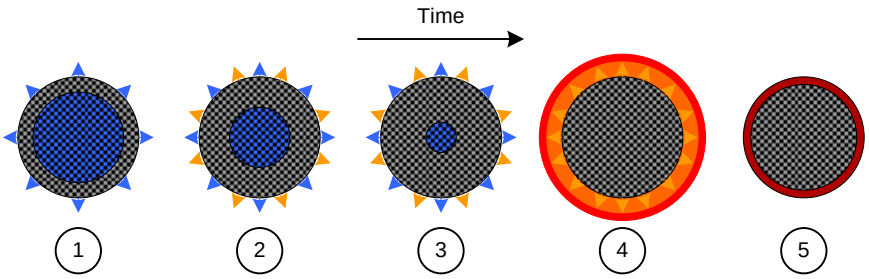

Figure 2.3: *The combustion process of the solid fuel. The arrows indicate volatilisation of gases.*

When modelling this combustion phase two aspects are important: The combustion time of volatiles and the combustion time of charcoal. The latter is much longer than the former.

During the whole combustion process three sets of different chemical reactions can happen, these reactions are important in the modelling phase as they can be used to find the energy supplied from the combustion of the solid fuel. Under supply of air the following reaction happens, this reaction is however not matched [Annamalai & Puri, 2007] [COWI, 2004]:

$$\underbrace{CH_{\kappa_H}O_{\kappa_O}(s) + H_2O(l)}_{\text{solid fuel}} + \underbrace{O_2 + \kappa_N \cdot N_2}_{\text{air}} \rightarrow CO_2 + O_2 + H_2O(g) + CO + \kappa_N \cdot N_2 \tag{2.1}$$

The character in parenthesis indicates the phase of the different substances, where s is solid, g is gas and l is liquid when nothing is mentioned the substance is in the gas phase. The reaction in Equation (2.1) can be split into two reactions; one where no CO_2 is present and one where no CO is present:

I. $CH_{\kappa_H}O_{\kappa_O}(s) + H_2O(l) + O_2 + \kappa_N \cdot N_2 \rightarrow CO + O_2 + H_2O(g) + \kappa_N \cdot N_2$

II. $CH_{\kappa_H}O_{\kappa_O}(s) + H_2O(l) + O_2 + \kappa_N \cdot N_2 \rightarrow CO_2 + O_2 + H_2O(g) + \kappa_N \cdot N_2$

If the combustion of solid fuel is clean no CO is created, this is however not the case most of the time. Therefore both CO and CO_2 will be created during the combustion of solid fuel which means that both reaction I and II happen during the combustion process.

When no air is present the following set of reactions happens:

III. $CH_{\kappa_H}O_{\kappa_O}(s) + H_2O(l) + CO_2 \rightarrow CO + O_2 + (k_1 + k_5) \cdot H_2O(g)$

IV. $CH_{\kappa_H}O_{\kappa_O}(s) + H_2O(l) + H_2O(g) \rightarrow CO + H_2 + O_2 + H_2O(g)$

When the gases created during the combustion process are burned off the following set of reactions happen:

V. $CO + O_2 + \kappa_N \cdot N_2 \rightarrow CO_2 + \kappa_N \cdot N_2$

VI. $H_2 + O_2 + \kappa_N \cdot N_2 \rightarrow H_2O(g) + \kappa_N \cdot N_2$

None of the six reactions are matched. The main information about the six reactions can be seen in Table 2.2.

Reaction	I	II	III	IV	V	VI
Energy	Exo	Exo	Endo	Endo	Exo	Exo
Heat value (h_c) [kJ/kg]	9203.2	32766	-14359.7	-10932	10103	141500
Type	Hetero	Hetero	Hetero	Hetero	Homo	Homo
Dominates	> 800 K	< 800 K	$< O_2$	$< O_2$	-	-

Table 2.2: *Information about the six reactions. Exo/Endo means exothermic/endothermic, the former indicates that the reaction produce energy whereas the latter indicates that the reaction consume energy. The heat value for the first four reactions is per kg carbon, for the 5^{th} reaction it is per kg CO and for the 6^{th} reaction it is per kg H_2. Hetero/Homo means heterogeneous/homogeneous, the former indicates that the reaction happens between species in different phases whereas the latter indicates that the reaction happens between species in the same phases.*

From Table 2.2 it can be seen that reaction III and IV both creates CO and consumes energy, this is not desired in the combustion process, so it is important that the O_2-level is sufficient at all time. Reaction III and IV is however neglected in the rest of the report as it is assumed that the O_2-level is sufficient high during the combustion process. It is assumed that no CO leaves the stoker through the chimney [COWI, 2004], this means that all the CO created during reaction I is created to CO_2 during reaction V. As reaction II contribute with the same amount of energy as reaction I and reaction V it is not important which of reaction I and II that dominates. Reaction II and reaction I and V contribute with the largest amount of energy as the C atoms in the solid fuel has the largest weight. Reaction VI happens when free H_2 reacts with O_2 molecules creating H_2O steam, this reaction creates a lot of energy and is therefore desirable in the combustion process. But as the amount of H is rather small, the contribution from this reaction is small. Moreover is it assumed that no NO_x is created during the combustion. At last it is assumed that the entire C in the solid fuel is incinerated.

These considerations are seen in an energy perspective. For the stoker to be approved it must however fulfil some emission standards. These standards tell how much CO, NO_x and other hazardous gases the exhaust gas must contain. There are no demands regarding the CO_2 emission as the stoker is said to be CO_2 neutral as long as the solid fuel only consists of biofuel. This is because the biofuel absorbs the same amount of CO_2 as it emits in the combustion process. It is assumed that the emission standards are fulfilled as long as the O_2-level is sufficiently high at all time.

2.3 Hardware Description

The hardware on the test setup is somewhat modified compared to the original R 25 stoker, and can be divided into four different types; actuators, sensors, a load and a control system. The actuators can be directly controlled by the control system depending on the measurements from the sensors. The actuators on the test setup are the same as on the original plant, however some extra sensors are mounted on the test setup. As mentioned before a calorifier is used as load on the system. The control system is different from the original controller as the processor is replaced by a target PC with an I/O board and a host PC.

2.3.1 Actuators

The R 25 stoker has two actuators a crew conveyor which is driven by a motor and a blower which provide primary air to the solid fuel and secondary air to the gases.

Screw Conveyor

The screw conveyor is powered by a motor which is controlled with a PWM signal through a solid state relay. The solid state relay is capable of switching on whenever during a sine wave whereas it only can turn off when the sine wave goes through zero. This means that the PWM control signal can be longer than desired, this is illustrated in Figure 2.4.

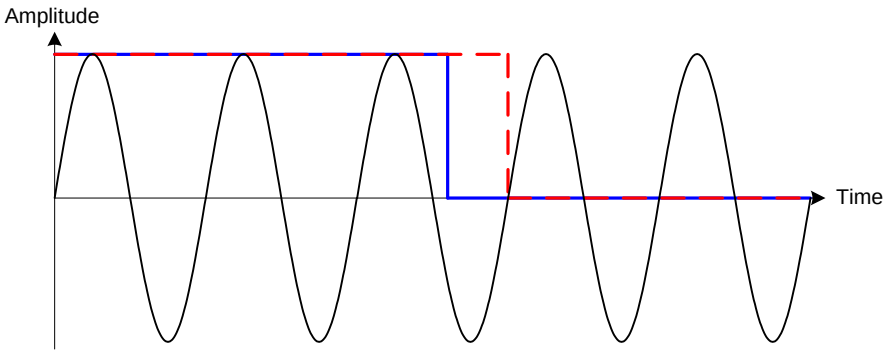

Figure 2.4: *Illustration of how the solid state relay works where the blue line is the desired duty cycle and the red line is the actual duty cycle due to the solid state relay.*

The maximal delay can be calculated as a half period time, at 50 Hz this gives:

$$T_d = \frac{T}{2} = \frac{\frac{1}{50}}{2} = 0.01 \text{ s} \tag{2.2}$$

where T_d is the time delay and T the period time of the power supply to the motor.

The interface to the motor control is a finished SIMULINK-block where the period time can be changed. This block is described in details in Appendix A.

Blower

The blower is used to supply the system with air. It is an AC centrifugal blower from ebmpapst. It has a maximal air flow of 160 m^3/h and is controlled by a PWM signal. As the air coming

from the blower supply both the primary and secondary air via a fork in the pipe, it is impossible to distinguish between primary and secondary air on-line. The interface to the blower control is a finished SIMULINK-block where the period time can be change. This block is described in details in the modelling of actuator and sensor chapter.

2.3.2 Sensors

To make a proper control of the stoker, the system is equipped with six sensors. Three of these sensors are temperature sensors which measure the temperature of the inlet water, the outlet water and the exhaust gas. A lambda oxygen sensor is used to measure the O_2-level in the exhaust gas. Finally two flow meters are used, one to measure the water flow of the inlet water and one to measure the air flow into the stoker which is not mounted on the system. The location of the sensors on the stoker can be seen in Figure 2.5.

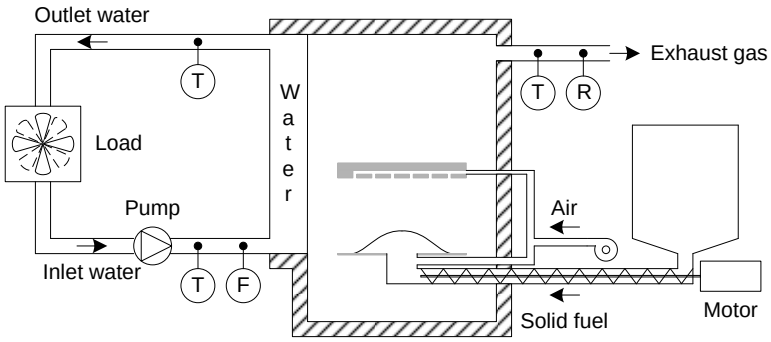

Figure 2.5: *From this simplified sketch the location of the sensors can be seen. T is the temperature sensors, F is the water flow meter and R is the lambda oxygen sensor.*

Normally the stoker is only equipped with three sensors which are the outlet water temperature sensor, the exhaust gas temperature sensor and the lambda oxygen sensor. The extra three sensors are used for modelling purposes in this project. The inlet water temperature sensor can however be used in the controller design, as it gives a good indication of the load on the system. Due to this reason and the price of a temperature sensor it is likely that future stokers from Benekov/Liagro are equipped with an inlet water temperature sensor.

Temperature Sensors

Three different temperature sensors are used to measure temperature. The sensors can be classified into two types depending on the temperature coefficient of the thermistor in the sensor. A thermistor is a type of resistor used to measure temperature changes relying on the change in resistance with changing temperature.

If this temperature coefficient is positive, the resistance increases with increasing temperature and such a sensor is called a positive temperature coefficient (PTC) thermistor temperature sensor. Such a sensor has a linear relation between temperature and resistance. If the coefficient is negative, the resistance decreases with increasing temperature and such a sensor is called a negative temperature coefficient (NTC) thermistor temperature sensor. Such a sensor has a non-linear relation between temperature and resistance.

The temperature sensors used on this stoker are:

- A PT1000 (platinum thermistor) PTC sensor is used to measure the exhaust gas temperature. It is mounted immediately where the exhaust gas leaves the stoker and enters the chimney. The sensor is not mounted in a metal case which means that it is in direct contact with the exhaust gas.
- A 12k NTC sensor is used to measure the outlet water. It is mounted immediately after the outlet water leaves the stoker. The sensor is a standard sensor mounted in a metal case which is immersed in the water.
- A 10k NTC sensor is used to measure the inlet water. It is mounted just before the inlet water enters the stoker. The sensor is a SMD-component which is mounted on the outside of the water pipe with cooling paste. To isolate it from the surroundings the sensor is wrapped in plastic foam.

Lambda Oxygen Sensor

A Bosch LSM 11 lambda oxygen sensor is used to measure the O_2-level in the exhaust gas coming from the burning chambers. The sensor works by measuring the difference in O_2 between the exhaust gas and the external air, and from this difference a voltage is generated. To work effectively the sensor must be heated to approximately 350°C, this is however done by a heating element inside the sensor.

Water Flow Meter

A magnetic flow meter from Fisher & Porter is used to measure the flow of the inlet water. The principle of the flow meter is based on Faraday's induction principle, where a magnetic field is imprinted perpendicular to the flow direction. When water flows through this magnetic field a voltage is induced that is proportional with the magnetic induction, the flow velocity and the pipe diameter. This voltage signal is then converted to a current signal from 4-20 mA.

The input to the I/O board must be a voltage signal so the current output from the flow meter must be converted to voltage. This is done using a current-to-voltage converter.

The water flow meter is only used off-line to measure the water flow for the three velocities for the pump which are used in the modelling phase.

Air Flow Meter

An anemometer from Tasto is used to find the flow of the supply air. An anemometer measures the air velocity and works by an impeller cooling down a thermistor. The flow can then be found by multiplying the velocity by the intake area and the density of air. The anemometer is a hand-held flow meter and is as mentioned earlier not mounted on the system it is only used to measure the relation between the input signal to the blower and the output air flow. The anemometer can also measure the secondary air flow.

2.3.3 Load

The stoker system is not connected to a real load. The load on this test setup consists therefore of a calorifere which is controlled through an Optidrive E. The fan in the calorifere is an axial fan which has a maximum of 1350 RPM. The Otidrive E is a frequency converter from Invertek

Drives which has an operating area from 8 Hz to 50 Hz, which means that the load is controlled through the frequency supplied to the fan. The interface to the frequency converter is a finished SIMULINK-block where the frequency to the calorifere can be changed directly. The calorifere is supplied with hot water from a Grundfos UPS 25-40 circulating pump which has three different velocities.

2.3.4 Controller Setup

As mentioned before the control system on the R 25 stoker consists of a target PC with an I/O board, two PCB's from Techno-Matic A/S and a host PC. This controller setup is illustrated in Figure 2.6. The whole system is controlled by SIMULINK.

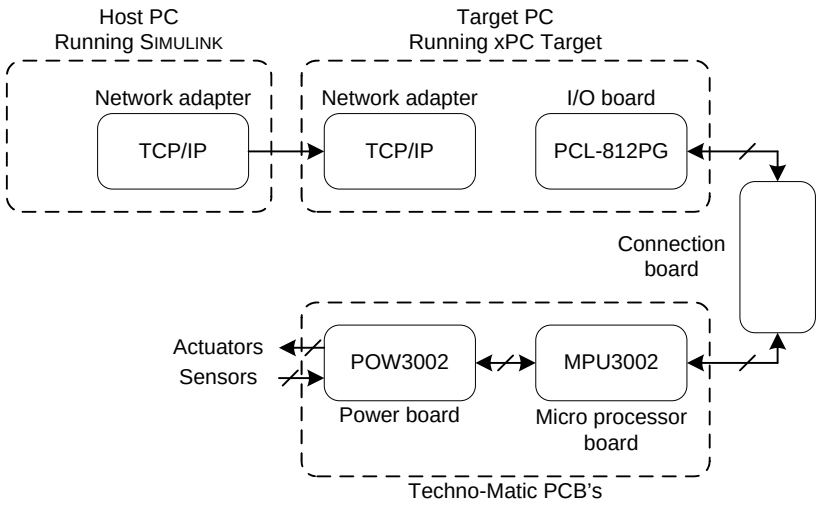

Figure 2.6: *Illustration of the controller hardware setup.*

Target PC

The target PC is a RadiSys rack-mount PC with a Pentium III 500 MHz processor and 512 MB Ram. xPC Target version 3.3 (R2007b) is installed on the target PC's hard drive which enables the connection of SIMULINK models to the physical system and execute them in real time. The xPC target is able to create samples with a base sample time of 1 ms and above, which leaves enough time to execute complex models with a large amount of I/O [MathWorks, 2007]. This means that the target PC basically only works as a "micro processor" only capable of executing SIMULINK models.

An analogue and digital I/O board from MultiLab of the type PCL-812PG is installed in the xPC target which receives the signals from the sensors and transmits the signals to the actuators.

Print Circuit Boards

The two PCB's from Techno-Matic A/S are a MPU3002 board which delivers the computing power and a POW3002 board which delivers the power to the actuators and sensors. The MPU3002 board in this setup is however different from the original as the processor is removed which means that the MPU3002 board only takes care of signal adjustments. The I/O board and the PCB's are connected through a connection board.

Host PC

The host PC is a Znote 6615 laptop from Zepto with an Intel Core 2 Duo T7200 @ 2.00 GHz processor and 2 GB RAM with Windows XP Professional Service Pack 2 installed. MATLAB version 7.5.0.342 (R2007b) with SIMULINK version 7.0 (R2007b) is also installed on the host PC. The controller is created in SIMULINK and built on the host PC, in the building process the controller is compiled with Microsoft Visual C and sent to the xPC target through a TCP/IP connection. After that the host PC is connected to the xPC target and the controller is executed. When the execution is ended it is possible to collect all the data gathered on the xPC target and send it back to the host PC.

The different actuators can be controlled in SIMULINK by adding blocks which generate the PWM signals. The sensors output is available in SIMULINK by adding blocks which convert the mV signals to actual measurements. The calibration of the different sensors and actuators is also done in SIMULINK. This setup allows control of the actual stoker system from SIMULINK, using the host PC. The interfaces to the different actuators and sensors are finished SIMULINK blocks made by Søren Kildedal Jensen from Techno-Matic A/S. See Appendix A for detailed description of the whole SIMULINK interface.

Chapter 3

The Scope of the Project

As mentioned in Chapter 1, this project treats the modelling and control of a stoker firing system. The purpose of this chapter is to give a short description on how this is done. First the strategies used in the problem solution are presented and next is the main objective for the project described.

3.1 Strategies

Two strategies have been used to solve the problem; a modelling strategy and a controller strategy. Firstly a model of the system is made, this is done for the purpose of model based control. This means that the control strategy uses the result of the modelling phase, which should result in a controller that uses the information from the model in the control of the system.

3.1.1 Modelling Strategy

When a mathematical model of a physical system is composed, two different methods can be used. The model can be composed as a black box which is based on a analysis of observations done on the system. The model can also be composed as a physical model which is based on physically laws and considerations.

The black box method uses system identification to determine the parameters in the model from measurements on the real plant so the root mean square error is minimized. This method is rather simple, but it has two major drawbacks as the physically understanding of the system is missing and the structural analogy between the real plant and the model is also missing.

The physical model is normally a set of differential equations. These differential equations can both be partial and non-linear. This method is a time-consuming task but the result gives both a physically understanding of the system and a structural analogy between the real plant and the model. The drawback is that many of the parameters in the system are unknown. In most cases a linear model is preferred for controller design so the non-linear differential equations have to be linearized around an operation point. In the controller design the linearized model will show which physical variables influence the time constants, gains and delays and how these changes in different operation points.

3.1.2 Controller Strategy

Different approaches can be taken when designing the controller. The methods can be divided into two groups. Model based controllers and non-model based controllers. A model based controller, means a controller that use a model of the actual plant, where the different output and states can be found from the model. A non-model based controller can be based on step response of the system, by trial and error or other methods. These techniques require a person that tunes the controller parameters every time some changes in the system are made or a controller that takes the worse case scenario on cost of efficiency. A model based controller can, on the other hand, take care of these problems, but a model based controller require a model, that in general will be more time consuming than the non-model based techniques. It is also necessary to have knowledge of the system, to make a model. But there exist different methods for making both model based and non-model based controllers. Some of these different methods are PID control, robust control, optimal control, predictive control, intelligent control and adaptive control. An overview and description of the different methods, can be found in the controller part, see Chapter 9.1.

3.2 The Main Objective

In the preceding chapter the system is described and solution strategies presented. Techno-Matic A/S wishes a model based controller which in some degree is capable of adjusting it self to the actual environment.

The overall and most important objective is therefore to make a model which describes the stoker system sufficient. A controller can then be designed from this model. Moreover is it desired that the controller can adjust it self to the changes in parameter variations of the plant. The problem can be shorted to:

A model of the stoker system has to be developed from which a controller can be designed. The controller must adjust to different solid fuels on the fly and still suppress any disturbances. Doing so the controller must fulfil the desired requirements to the water temperature and the O_2-level.

The stoker system model is made and verified using SIMULINK. A controller is designed based on this model. The controller is then build in SIMULINK and verified. Lastly is the controller tested on the system to see if it fulfils the requirements which is specified in the following subsection.

3.2.1 Requirement Specification

In order to determine whether the main objective for this report has been achieved a set of requirements is specified. These requirements must be obtained by the controller. The controller must be able to track the system to a reference point for both the water temperature and the O_2-level. Moreover is it desirable that the controller is capable of distinguishing between different solid fuels.

The requirements to the controller are set to the following:

- T_w: ± 5°C from the reference point 90% of the time when disturbances are given to the system.
- O_2-level: $\pm 2\%$ from the reference point 90% of the time when disturbances are given to the system.

The last requirement is that the controller is capable of distinguishing any changes in the composition of the solid fuel within 180 s and change it's parameters to match the new solid fuel composition.

Four tests are made to verify that the requirements set to the controller are fulfilled. The four test are described shortly below.

Test One: To validate if the controller is capable of fulfilling the two first requirements as mentioned earlier when only wood pellets are combusted.

Test Two: To validate if the controller is capable of fulfilling the two first requirements as mentioned earlier when only wheat is combusted.

Test Three: To validate the performance of the final controller.

A more detailed description of the test and the test results for these four test can be found in Chapter 12.

3.2.2 Delimitations

The modelling and controller design is made specific to the test setup at Techno-Matic A/S. This means that some changes must be done for the controller to work on ordinary R 25 stokers from Benekow-Liagro. These changes are both in relation to hardware and software as hardware modifications are made on the test setup and the controller setup is completely replaced.

As mentioned earlier the R 25 stoker can burn a lot of different solid fuel. Due to time constraints this report will only deal with wood pellets and wheat as solid fuels. The procedure for dealing with other solid fuels is however the same as for the two solid fuels used for this report.

Throughout this report different assumptions are used regarding the dimensions of the stoker, the combustion process as mentioned and the physical behaviour of the stoker. As no construction schemes are available for the R 25 stoker, the dimension of the stoker is found from assumptions and measurements done on the test setup. To simplify the energy transport inside the stoker system assumptions are made regarding the combustion process of solid fuel. Lastly assumptions are made to simplify the modelling phase. Care has been taken so none of these assumptions contradict physical laws.

Because of time constrains only normal operation of the stoker system is included in the controller design. This means that both "pause firing" and automatic ignition are disregarded.

Part II

Modelling

In this part a mathematical model of the stoker system is developed. Both a non-linear model and a linear model of the stoker are derived. The part consists of five chapters.

In the first chapter the modelling approach is presented along with some considerations regarding the modelling phase.

The necessity of models for the actuators and sensors are investigated in the second chapter. A model is created where it is found necessary.

The modelling of the stoker starts in the third chapter of this part, where a non-linear model is derived. This model consists of several non-linear differential equations, which are based on energy and mass balance considerations. Through constant and parameter determinations a model is derived for when both wood pellets and wheat is combusted.

In the fourth chapter the non-linear model is linearized through a set of operation points. This linear model is setup in matrix form to create a state space model of the stoker, which is done in the last chapter of this part

All models are discussed, tested and verified. The verification of the models is done using real measurement data from the plant.

Chapter 4

Modelling Approach

The physical model approach described in Chapter 3 is chosen for modelling the stoker system. This means that the mathematical model is setup by non-linear differential equations based on thermodynamics. This model can then be linearized around an operation point. From the linear model a controller can be designed, which can control the states in the system.

The model has three inputs and three outputs. The inputs to the model are; mass flow of solid fuel, mass flow of air and the inlet water temperature. Where the first two inputs are controllable and the last can be seen as a disturbance. The output from the model is the temperature of the outlet water, the temperature of the exhaust gas and the O_2-level of the exhaust gas.

In the test setup at Techno-Matic A/S the actual load is known but in a real setup the load is not as it is given by the customer's heat consumption which is varying. The effect of the load can however be measured through the temperature of the inlet water. If the temperature of the inlet water is known, the load can be taken into account as a known disturbance in the controller design.

It is desirable to control two states in the system; the temperature of the outlet water and the O_2-level of the exhaust gas. The outlet water temperature is controlled to ensure that the water temperature is as desired by the costumer. To ensure an efficient combustion the O_2-level is also controlled.

As the three inputs have influence on all the three outputs, cross coupling is present in the system, and the system is therefore called a Multiple Input Multiple Output (MIMO) system. The system is sketched in Figure 4.1.

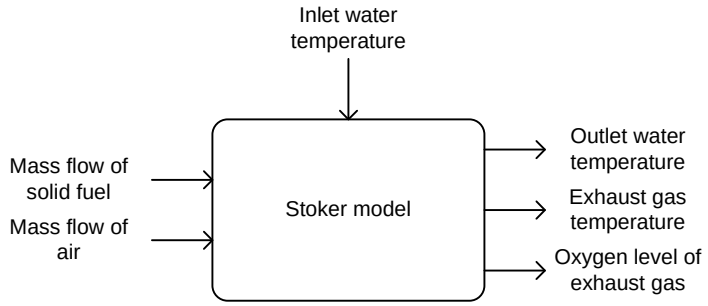

Figure 4.1: *Sketch of the MIMO system where the arrows pointing into the box is input and the arrows pointing out from the box is output.*

4.1 Initial Considerations

Before the modelling phase can begin some aspects must be clarified first. The control volumes and control surfaces of the system, and the state space variables must be determined along with some general physical assumptions.

4.1.1 Control Volumes and Control Surfaces

The stoker system can be divided into several control volumes, from which the mathematical model can be composed. Each control volume is bounded by control surfaces which do not contain any energy or mass. When control volumes are used a place discretizing is made which means that the variables in a control volume only become depended on time and not on time and place. The control volumes are chosen so that the variables can be assumed to be constant in the whole control volume. Three methods can be used in the place discretizing:

- Forward difference: The values of the variables at the input to the control volume are used in the whole control volume.
- Backward difference: The values of the variables at the output of the control volume are used in the whole control volume.
- Central difference: Uses a mean of the input and output as values for the variables. The central difference is also known as the bilinear method.

The forward difference method can give an unstable response and the central difference method can give faulty transients, the backward method is therefore used [Andersen & Pedersen, 2007].

In Figure 4.2 a is pipe illustrated which is divided into two control volumes, moreover it can be seen which variable value there will be used, when the backward method is used. In Figure 4.3 a control surface is used in the transition between air and wall, and wall and water. When a control surface is used it is assumed that the value of the variable jumps in the control surface which is not the case as the variable will change continuously. When looking at the temperature profile, the jumps in the control surfaces tells how the heat transition behaves. The heat transition describes how much heat energy there can be transferred. The larger the temperature jump, the smaller the heat transition between the two mediums is. A high heat transition indicates that a lot of heat energy is transferred hence the temperature jump in the control surface is small. A small heat transition indicates that the medium is poor at transferring heat, which means that the temperature jump in the control surface will be large.

On this background the control volumes and control surfaces are set up for this project. Only the inlet and outlet temperature is known for the water, the water can therefore with advantage be seen as a control volume, as it is assumed that the temperature difference of the water inside the stoker is minimal. The wall between the gas and the water is seen as a control surface, meaning that it contains no energy and only influences the heat transition. The temperature of the exhaust gas is known, but as it is assumed that the difference of the gas temperature inside the stoker is high thus the gas inside the stoker can not be seen as a control volume. The number of control volumes is a trade off between model precision and model order, the higher order the higher precision. It is assumed that dividing the gas inside the stoker into three control volumes is sufficient to give a precise model of the system, keeping the model order relative small. The three control volumes are: The burning chamber where the solid fuel is combusted, the gas chamber where most of the energy is transferred to the water, and the exhaust gas where the gas leaves the stoker. The wall between the gas inside the stoker and the air outside is seen

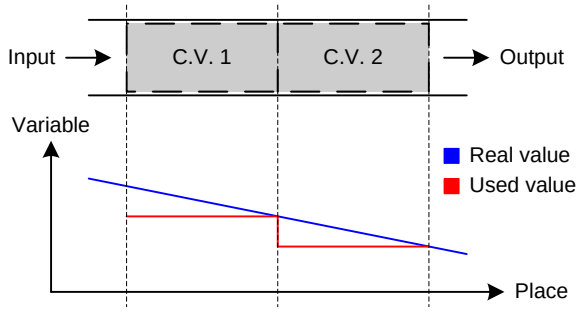

Figure 4.2: *Illustration of two control volumes (C.V.) in a pipe and the corresponding value of the variables when the backward difference method is used.*

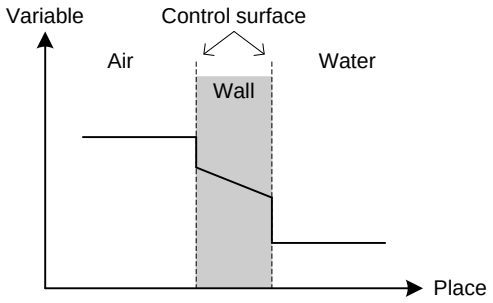

Figure 4.3: *Illustration of two control surfaces for a transition between air and a wall and a wall and water.*

as a control surface, and it is assumed that the heat transition is very poor, meaning that no heat is lost through the wall. To control the energy supply to the stoker, the solid fuel must be monitored, therefore the molehill is chosen as a control volume. From this control volume the solid fuel enters as a solid substance and leaves as gases. The change in O_2 must also be monitored to determine the O_2-level inside the stoker, therefore the O_2 in the gas inside the stoker is seen as a control volume.

4.1.2 State Space Variables

To design a controller from the model, the state space variables must first be determined. These can be used to determine all the different states in the stoker system, and are in this report referred to as states. The states for the model are: The temperature of the outlet water, the temperatures of the gas in the three gas control volumes, the total mass of the solid fuel in the molehill, and the O_2-level of the exhaust gas.

4.1.3 Assumptions

General assumptions concerning the physical behaviour of the stoker system are made, which provide the background for the modelling of the stoker system. These assumptions are made to simplify the model. In the selection of the assumptions, care has been taken, that they do not significantly influence the precision of the model. Moreover none of the assumptions contradict physical laws.

The following assumptions are made:

The mass flow into the stoker is equal to the mass flow out of the stoker: It is assumed that the sum of the mass flows of solid fuel and air is equal to the mass flow of the exhaust gas seen over time.

The mass flow of inlet water is constant and equal to the outlet water: To simplify the energy equation for the water the inlet and outlet water flows are assumed to be constant and equal.

The specific heat capacity in each control volume is constant: To simplify the energy equations the specific heat capacities for the different control volumes are assumed to

be constant.

The ambient temperature is constant: To simplify the equation coming from the energy in the supplied air the ambient temperature is assumed to be constant.

The chemical structure of air is constant: It is assumed that the O_2 volume percent is 21 and the N_2 volume percent is 79 for the air supplied to the combustion processes.

The combustion is 75% clean: This means that under the combustion of solid fuel 75% of the carbon leaves as CO_2 whereas 25% leaves as CO.

The exhausted gas does not contain CO: This means that all the CO released under the combustion is converted to CO_2 before leaving the chimney.

No heat loss through the stoker walls: This means that the only heat loss from the stoker is the exhaust gas leaving the stoker through the chimney.

The mass of the gases are constant: It is assumed that the mass of the gas in the burning chamber, gas chamber and exhaust gas is constant. This assumption simplifies the energy equations for the three gases.

The lumped parameter approach is applied using the backward difference: This means that the variables only depend on time and not both on time and place. The backward difference method is used, which means that the value of the output variable is equal to the value of the variable inside the concerned control volume.

Chapter 5

Actuator and Sensor Models

This chapter will discuss the necessity of modelling the different actuators and sensors on the system. If a necessity is found a model will be derived.

5.1 Actuator Models

The two actuators on the system is the motor which drives the screw conveyor and the motor which drives the blower. They are both controlled by a PWM generator through solid state relays which are placed on the POW3002 PCB. The control signals to the actuators are adjusted by the MPU3002 PCB before they are sent to the actuators.

Screw Conveyor

The screw conveyor motor has a fast response time, compared to the time constants in the actual system. Therefore the dynamic of the screw conveyor motor is neglected in this project and no model of the screw conveyor motor is made.

The time delay from the moment the controller sends a control signal until the the screw conveyor motor reacts can be neglected, as it is assumed that this signal transmission time is very small (around 1 ms) compared with the time constants of the system.

The motor is controlled as sketched in Figure 5.1.

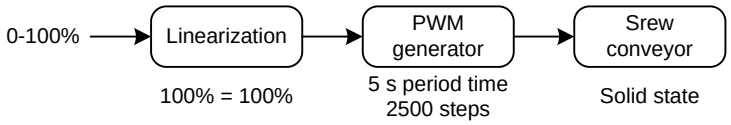

Figure 5.1: *Sketch of the control interface to the screw conveyor motor.*

The input signal is a percentage between 0-100. The gain works like a linearization block, but as the motor is linear, this block can be used to compensate for an oversized motor. This is not the case however so the gain gives one-to-one. The PWM generator generates the actual control signal to the motor, in this block both the period time and step size can be set for the generator. Which respectively are 5 s and 2500 steps in the test setup used in this project. As mentioned

before the motor is controlled through solid state relays, meaning that the period time must be rather high so the zero-passage has small influence on the system.

Blower

The blower used in the system is also assumed to have a fast response time, compared to the time constants in the actual system. Therefore the dynamic of the blower is neglected in this project and no model of the blower is made.

The time delay when the controller sends a control signal to the blower motor reacts can be neglected, as it is assumed that this signal transmission time is very small (around 1 ms) compared to the time constants of the system.

The motor is controlled as sketched in Figure 5.2.

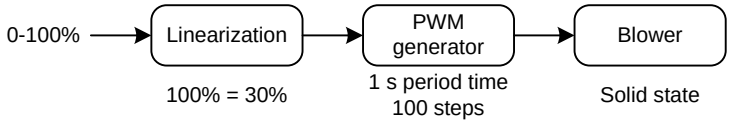

Figure 5.2: *Sketch of the control interface to the blower motor.*

The input signal is a percentage between 0-100. The gain works like a linearization block which is needed as the blower is non-linear. Moreover the blower is oversized for the system which also can be taken into account in the linearization block. The PWM generator generates the actual control signal to the blower, in this block both the period time and step size can be set for the generator. Which respectively are 1 s and 100 steps in the test setup used in this project. The blower is also controlled through solid state relays, meaning that the period time must be rather high so the zero-passage has small influence on the system.

5.2 Sensor Models

The test setup is equipped with five sensors as mentioned earlier. Common for these sensors are that they are powered by the POW3002 PCB and signals to the controller is adjusted by the MPU3002 PCB. The data sheets are only available for the lambda oxygen sensor and the water flow meter. Data for the three temperature sensors are taken from common data sheets for respectively NTC and PT1000 temperature sensors.

Exhaust Gas Temperature Sensor

The temperature sensor that measures the exhaust gas temperature is a PT1000 sensor as mentioned in the hardware description. The change of the exhaust gas temperature inside the stoker is assumed to happen fast. The dynamic of the sensor must therefore be investigated. From Appendix E it is found that the sensor is slow, compared to the changes in the exhaust gas temperature, hence a model of the sensor is therefore necessary. The model of the exhaust gas temperature sensor is derived in Appendix E, and given by the following transfer function.

$$T(s) = \frac{5.148 \cdot 10^{-3}}{33.5 \cdot s + 1} \tag{5.1}$$

Water Temperature Sensors

As mentioned in the hardware description a 10k NTC sensor is used to measure the inlet water temperature and a 12k NTC sensor is used to measure the outlet water temperature. The time constant for the two sensors are assumed to be around 40 s [Bosch, 2002]. The sensors are used to measure the temperature change in the inlet and outlet water. As the water temperature is assumed to change slowly compared to the time constants of the two temperature sensors, the dynamic of the sensors can be neglected and a model of the sensors are therefore not necessary.

Lambda Oxygen Sensor

A lambda oxygen sensor is used to measure the O_2-level in the exhaust gas. According to the data sheet ([Bosch, 2002]), the sensor has a time constant on 1.5 s when the O_2-level increases ("rich" direction) and 2.0 s when the O_2-level decreases ("lean" direction). This is relatively slow compared to how fast the O_2-level can change in the exhaust gas, a model of the lambda oxygen sensor is therefore needed. It is difficult however to conduct any tests on the sensor mounted on the system, as it is hardly accessible and gases with different O_2-levels are needed. The dynamic of the lambda oxygen sensor is therefore not found, but it is assumed that using the time constant as a time delay in the sensor a sufficient model of the lambda oxygen sensor can be found. The transfer function for the sensor is given by Equation (5.2).

$$O_2(s) = \exp\left(-\tau \cdot s\right) \tag{5.2}$$

where τ is 1.5 s in the "rich" direction and 2.0 s in the "lean" direction.

Moreover the measurement is taken in the exhaust gas which may cause a delay in the model if the O_2-level is found inside the stoker.

Water Flow Meter

The circulating pump is used to circulate the outlet water through the calorifere and it can generate three different constant flows. As the water flow is constant, the dynamic of the water flow meter can be neglected. A model of the water flow meter is therefore not necessary for this project.

Chapter 6

Non-linear Model of the Stoker System

To find the state space variables, differential equations are set up for the different control volumes. These differential equations are the product of a modelling phase setting up energy and mass balances for the needed control volumes. The modelling is done by determining the total change in either energy or mass from the supplied and emitted energy or mass, making it possible to control the energy and mass dissipation.

The overall inputs and outputs between the different control volumes are illustrated in Figure 6.1 and the division of the chambers are illustrated in Figure 6.2.

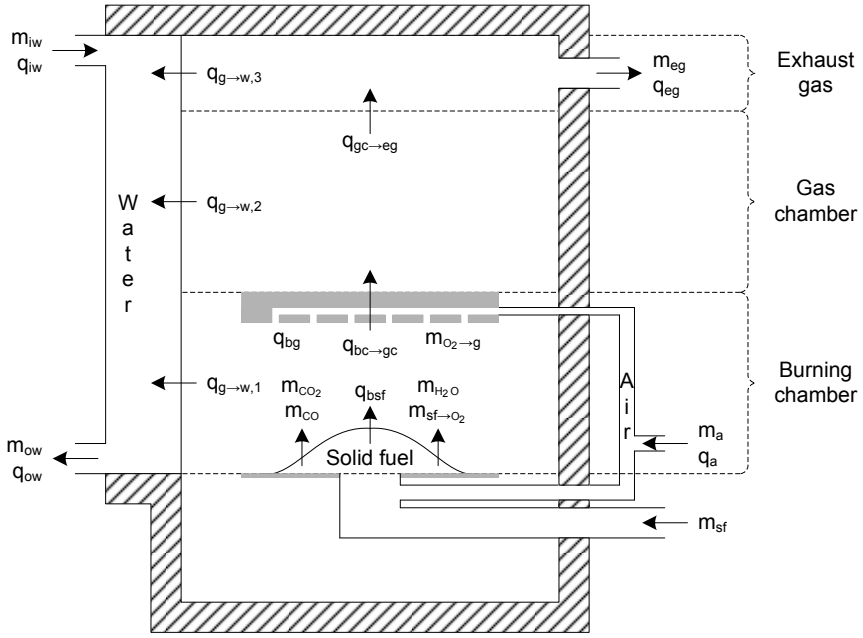

Figure 6.1: *An overview of the energy and mass flows between the different control volumes.*

The change in energy can be expressed by the first theorem of thermodynamics as:

[*change in accumulated energy in c.v. per time unit*] = [*energy from mass flow into c.v.*] − [*energy from mass flow out of c.v.*] + [*supplied power*] − [*heat loss*]

where the accumulated energy can be divided into macroscopic kinetic and potential energy

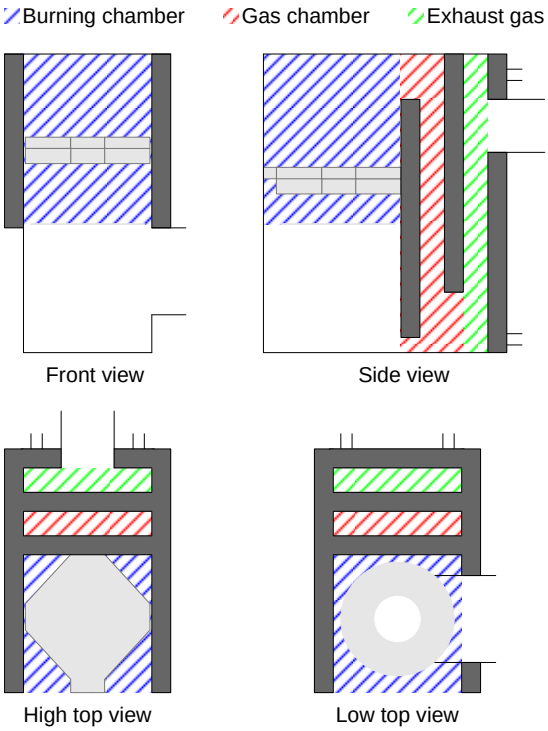

Figure 6.2: *An overview of the division of the three chambers, seen in front, side and two different top views.*

and internal energy which is kinetic energy from the disorderly mutual motion of the individual particles. In this case the macroscopic energy can be neglected [Andersen & Pedersen, 2007].

The change in mass can be expressed as:

[*change in mass in c.v. per time unit*] = [*sum of mass flow into c.v.*] − [*sum of mass flow out of c.v.*]

when the energy and mass balances are used, too many unknowns are present, this is however avoided when the backward difference method is used [Andersen & Pedersen, 2007].

The following energy and mass balances are composed to create a sufficiently precise model of the system and to determine the state space variables.

- Energy balance for the water.
- Energy balance for the gas in the burning chamber.
- Energy balance for the gas in the gas chamber.
- Energy balance for the exhaust gas.
- Mass balance for the solid fuel in the molehill.
- Mass balance for the O_2-level.

These six differential equations form the energy and mass balances are used in a mathematically non-linear model. When this model is created verification is preformed to see if it is in accordance with the real plant. The verification is done in SIMULINK where the non-linear model is build up by different SIMULINK-blocks. This model takes real input from the plant as input and the

model output is then compared with the real output from the plant to see the correctness of the model.

In the following sections the six differential equations are derived but first the combustion process of the carbon in the solid fuel and the mass flow of gas up through the stoker is described in details as it is needed to derive the differential equations.

6.1 Derivation of Model Expressions

In this section the combustion process of the carbon in the solid fuel and the mass flow of gas up through the stoker is derived. These two expressions are used to derive the six differential equations of the system.

6.1.1 Combustion of Carbon

It is assumed that the temperature of the solid fuel, which is about to enter the molehill is just below the ignition point (step three in Figure 2.3). This means that when the solid fuel is pushed in front in the molehill it will ignite at once (step four in Figure 2.3). The ignition happens due to a highly flammable combination of carbon (C) and hydrogen (H) in gas form. After a short time period the flame will die out and only charcoal is left of the solid fuel. Over a longer time period this charcoal will be burnt off due to smouldering (step five in Figure 2.3). A equation can therefore be set up to describe the combustion process of C. The mass flow of C which is ignited, can be given by the mass flow of C in the solid fuel, and a temperature depended time constant.

$$m_{\mathrm{C,gas}}(t) = (1 - \zeta_{\mathrm{char}}(t)) \cdot m_{sf,\mathrm{C}}(t) - \frac{1}{\tau_{\mathrm{gas}}(T_{mh}(t))} \cdot M_{\mathrm{C,gas}}(t) \tag{6.1}$$

where ζ_{char} is the ratio of C converted to charcoal, $m_{\mathrm{C},sf}$ is the mass flow of C in the solid fuel, τ_{gas} is the ignition time and T_{mh} is the temperature in the molehill. The ignition time for the volatiles is much shorter than the combustion time of charcoal. It is therefore assumed that all the volatiles are combusted at once. Equation (6.1) can then be written as:

$$m_{\mathrm{C,gas}}(t) = (1 - \zeta_{\mathrm{char}}(t)) \cdot m_{\mathrm{C},sf}(t) \tag{6.2}$$

where ζ_{char} is depended on the amount of H in the solid fuel and it is derived in Appendix C. The total C in the mass flow of solid fuel ($m_{sf,\mathrm{C}}$) can be written as:

$$m_{sf,\mathrm{C}}(t) = c_{\mathrm{C}} \cdot m_{sf}(t) \tag{6.3}$$

where c_{C} is a term which is depended on the composition of the solid fuel and it is derived in Appendix C and m_{sf} is the mass flow of solid fuel which is given by:

$$m_{sf}(t) = \beta_{\mathrm{motor}} \cdot \text{duty cycle}_{\mathrm{motor}}(t) \tag{6.4}$$

where β_{motor} is the slope rate for the linear relation between the duty cycle of the motor and the mass flow per second of solid fuel which is found in Appendix D. For simplicity m_{sf} is written in its short notation throughout this modelling chapter. Equation (6.2) can then be written as:

$$m_{\mathrm{C,gas}}(t) = (1 - \zeta_{\mathrm{char}}(t)) \cdot c_{\mathrm{C}} \cdot m_{sf}(t) \tag{6.5}$$

The mass flow of charcoal which is under combustion is given by a function which is depended on the primary supply air, the size of the molehill and the temperature in the molehill.

$$m_{\mathrm{C,char}}(t) = f(m_{a,p}(t), M_{\mathrm{C,char}}(t), T_{mh}(t)) \tag{6.6}$$

where $m_{a,p}$ is the mass flow of primary supply air and $M_{\mathrm{C,char}}$ is the mass of charcoal in the molehill. The temperature dependency in the function is neglected as it is almost constant compared with $m_{a,p}$ and $M_{\mathrm{C,char}}$. It is assumed that the temperature at all times is so high that the small changes in the temperature only has a unnoticeable influence on the combustion of charcoal. The function is then only depended on $m_{a,p}$ and $M_{\mathrm{C,char}}$ and it is assumed that the function can be implemented by multiplying a constant on both variables. Equation (6.6) can then be written as:

$$m_{\mathrm{C,char}}(t) = m_{a,p}(t) \cdot \gamma_1 + M_{\mathrm{C,char}}(t) \cdot \gamma_2 \tag{6.7}$$

Both γ_1 and γ_2 must be found from experiments or by trial-and-error. $m_{a,p}$ can be found as:

$$m_{a,p}(t) = \chi \cdot m_a(t) \tag{6.8}$$

where χ is the fraction of supply air which is used as primary supply air (see Appendix D) and m_a is the mass flow of supply air given by:

$$m_a(t) = \beta_{\mathrm{blower}} \cdot \text{duty cycle}_{\mathrm{blower}}(t) \tag{6.9}$$

where β_{blower} is the slope rate for a linear relation between the duty cycle of the blower and the mass flow rate per second of supply air which is found in Appendix D. For simplicity m_a is written in its short notation throughout this modelling chapter.

The overall change of C can now be written as the sum of Equation (6.5) and Equation (6.7).

$$\begin{aligned} m_{\mathrm{C}}(t) &= m_{\mathrm{C,gas}}(t) + m_{\mathrm{C,char}}(t) \\ &= (1 - \zeta_{\mathrm{char}}(t)) \cdot c_{\mathrm{C}} \cdot m_{sf}(t) + \chi \cdot m_a(t) \cdot \gamma_1 + M_{\mathrm{C,char}}(t) \cdot \gamma_2 \end{aligned} \tag{6.10}$$

For simplicity every time m_{C} is written it refers to Equation (6.10).

6.1.2 Mass Flow of Gas

Two different mass flows contribute to the overall mass flow of gas up through the stoker; these are the mass flow coming from the solid fuel and the mass flow of supply air. The mass flow of solid fuel can be split up in four parts; mass flow of CO_2, mass flow of CO, mass flow of H_2O steam and mass flow of O which is released from the solid fuel during the combustion.

The mass flows of CO_2 and CO is added together, as it is assumed that no CO leaves the stoker. The mass flow of CO_2 can then be found from the mass flow of C just derived in the previous section as each C atom binds two O atoms.

$$m_{\mathrm{CO_2}}(t) = \frac{m_{\mathrm{C}}(t)}{n_{\mathrm{C}}} \cdot n_{\mathrm{CO_2}} \tag{6.11}$$

where n is the mole mass of the concerned species.

The mass flow of H_2O can be split into two parts; one coming directly from the solid fuel ($m_{\mathrm{H_2O,1}}$) and one coming during the combustion process, as the H in the solid fuel reacts with the O in the supply air ($m_{\mathrm{H_2O,2}}$). $m_{\mathrm{H_2O,1}}$ can be found from the fraction of liquid water present in the solid fuel.

$$m_{\mathrm{H_2O,1}}(t) = \eta_{\mathrm{H_2O}} \cdot m_{sf}(t) \tag{6.12}$$

where η_{H_2O} is the fraction of liquid H_2O in the solid fuel. $m_{H_2O,2}$ can be found as each H atom in solid fuel binds half an O atom.

$$m_{H_2O,2}(t) = \frac{1}{2} \cdot \frac{m_{sf,H}(t)}{n_H} \cdot n_{H_2O} \tag{6.13}$$

where $m_{sf,H}$ is the mass flow of H released during the combustion and it can be written as:

$$m_{sf,H}(t) = c_H \cdot m_{sf}(t) \tag{6.14}$$

where c_H is a term depended on the composition of the solid fuel and it is derived in Appendix C. The mass flow of H_2O can now be calculated as the sum of Equation (6.12) and Equation (6.13).

$$m_{H_2O}(t) = m_{H_2O,1}(t) + m_{H_2O,2}(t) = \eta_{H_2O} \cdot m_{sf}(t) + \frac{1}{2} \cdot \frac{c_H \cdot m_{sf,H}(t)}{n_H} \cdot n_{H_2O} \tag{6.15}$$

The mass flow of N coming from the supply air is given by Equation (6.16):

$$m_{a,N}(t) = c_N \cdot m_a(t) \tag{6.16}$$

where c_N is a constant which is depended on the composition of the supply air and it is derived in Appendix C.

The last part is the mass flow of O which is not used in the combustion processes. It can be found by looking at the amount of O used in the CO_2 and H_2O reactions, the amount of O released from the solid fuel during the combustion and the amount of O in the supply air.

$$m_O(t) = \left(\frac{m_{a,O}(t)}{n_O} + \frac{m_{sf,O}(t)}{n_O} - 2 \cdot \frac{m_C(t)}{n_C} - \frac{1}{2} \cdot \frac{m_{sf,H}(t)}{n_H} \right) \cdot n_O \tag{6.17}$$

where $m_{a,O}$ is the mass flow of O in the supply air and $m_{sf,O}$ is the mass flow of O released from the solid fuel during the combustion process. These two mass flows are given by:

$$m_{a,O}(t) = c_{a,O} \cdot m_a(t) \tag{6.18}$$

$$m_{sf,O}(t) = c_{sf,O} \cdot m_{sf}(t) \tag{6.19}$$

where $c_{a,O}$ is a constant depended on the composition of the supply air and $c_{sf,O}$ is a term depended on the composition of the solid fuel, both derived in Appendix C.

The mass flow of gas up through the stoker can now be found by adding Equation (6.11), Equation (6.15), Equation (6.16) and Equation (6.17).

$$\begin{aligned} m_g(t) &= m_{CO_2}(t) + m_{H_2O}(t) + m_N(t) + m_O(t) \Leftrightarrow \\ m_g(t) &= \frac{m_C(t)}{n_C} \cdot n_{CO_2} + \eta_{H_2O} \cdot m_{sf}(t) + \frac{1}{2} \cdot \frac{c_H \cdot m_{sf}(t)}{n_H} \cdot n_{H_2O} + c_N \cdot m_a(t) \\ &\quad + \left(\frac{c_{a,O} \cdot m_a(t)}{n_O} + \frac{c_{sf,O} \cdot m_{sf}(t)}{n_O} - 2 \cdot \frac{m_C(t)}{n_C} - \frac{1}{2} \cdot \frac{c_H \cdot m_{sf}(t)}{n_H} \right) \cdot n_O \end{aligned} \tag{6.20}$$

For simplicity every time m_g is written it refers to Equation (6.20).

Now that the mass flow of C released during the combustion process and the mass flow of gas up through the stoker are derived the model phase can continue by deriving the differential equations needed.

6.2 Energy Balances for the Stoker

In this section the first four differential equations are derived. These equations are derived from energy balance considerations.

6.2.1 Energy Balance for the Water

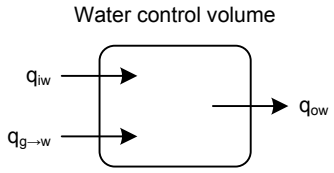

Figure 6.3: *Control volume for the water where arrows going inside indicates supply of energy and arrows going outside indicates energy lost.*

From Figure 6.3 the energy balance for the water can be expressed as energy change in the control volume with respect to time. The energy change is expressed by the energy from the inlet water (q_{iw}), the energy transferred from the gas to the water ($q_{g\to w}$) and the energy from the outlet water (q_{ow}) as seen in Equation (6.21).

$$\frac{\mathrm{d}E_w(t)}{\mathrm{dt}} = q_{iw}(t) + q_{g\to w}(t) - q_{ow}(t) \tag{6.21}$$

The energy in the water (E_w) can be expressed by the mass of the water (M_w), the specific heat capacity of water (c_w) and the temperature of the water (T_w).

$$E_w(t) = M_w \cdot c_w \cdot T_w(t) \tag{6.22}$$

The energy of the inlet water is given by Equation (6.23).

$$q_{iw}(t) = m_{iw} \cdot h_{iw}(t) \tag{6.23}$$

where m_{iw} is the mass flow of inlet water, which is equal to the flow of outlet water and it is therefore denoted m_w and h_{iw} is the enthalpy of the inlet water. As the inlet water only is in one phase, Equation (6.23) can be rewritten to [Andersen & Pedersen, 2007]:

$$q_{iw}(t) = m_w \cdot c_{iw} \cdot T_{iw}(t) \tag{6.24}$$

where c_{iw} is the specific heat capacity of the inlet water and T_{iw} the temperature of the inlet water.

The energy transferred from gas to water can be split into three parts one from each control volume. The energy transferred from the first control volume, the burning chamber, is given by both radiation and convection heat [Cengel, 2003].

$$q_{g\to w,1}(t) = \underbrace{\epsilon_{bcw} \cdot \sigma \cdot A_{bcw} \cdot \left(T_{bc}(t)^4 - T_w(t)^4\right)}_{\text{radiation heat}} + \underbrace{\alpha_{bc} \cdot A_{bcw} \cdot \left(T_{bc}(t) - T_w(t)\right)}_{\text{convection heat}} \tag{6.25}$$

where ϵ_{bcw} is the emissivity of the surface between the burning chamber and the water, σ is the Stefan-Boltzman constant and is equal to $6.57 \cdot 10^{-8}$ W/m^2, A_{bcw} is the surface area of the burning chamber in contact with the water, T_{bc} is the temperature inside the burning chamber

and α_{bc} is the heat transfer coefficient from the burning chamber to the water. The energy transferred from the second control volume, the gas chamber, is only given by convection heat.

$$q_{g\to w,2}(t) = \alpha_{gc} \cdot A_{gcw} \cdot (T_{gc}(t) - T_w(t)) \tag{6.26}$$

where α_{gc} is the heat transfer coefficient from the gas chamber to the water, A_{gcw} is the surface area of the gas chamber in contact with the water and T_{gc} is the temperature of the gas inside the gas chamber. The energy transferred from the third control volume, the exhaust gas, is also given by convection heat.

$$q_{g\to w,3}(t) = \alpha_{eg} \cdot A_{egw} \cdot (T_{eg}(t) - T_w(t)) \tag{6.27}$$

where α_{eg} is the heat transfer coefficient from the exhaust gas to the water, A_{egw} is the surface area of the exhaust gas in contact with the water and T_{eg} is the temperature of the exhaust gas. The complete amount of energy transferred to the water can now be written by Equation (6.28).

$$\begin{aligned} q_{g\to w}(t) &= \epsilon_{bcw} \cdot \sigma \cdot A_{bcw} \cdot \left(T_{bc}(t)^4 - T_w(t)^4\right) + \alpha_{bc} \cdot A_{bcw} \cdot (T_{bc}(t) - T_w(t)) \\ &+ \alpha_{gc} \cdot A_{gcw} \cdot (T_{gc}(t) - T_w(t)) + \alpha_{eg} \cdot A_{egw} \cdot (T_{eg}(t) - T_w(t)) \end{aligned} \tag{6.28}$$

The energy of the outlet water is given by Equation (6.29).

$$q_{ow}(t) = m_{ow}(t) \cdot h_{ow} \tag{6.29}$$

where m_{ow} is the mass flow of outlet water which is equal to the flow of inlet water and it is therefore denoted m_w and h_{ow} is the enthalpy of the outlet water. The assumption used for the inlet water can also be applied for the outlet water, Equation (6.29) can then be rewritten to [Andersen & Pedersen, 2007]:

$$q_{ow}(t) = m_w \cdot c_{ow} \cdot T_{ow}(t) \tag{6.30}$$

where c_{ow} is the specific heat capacity of the outlet water and T_{ow} the temperature of the outlet water. When the backward difference method is used both c_{ow} and T_{ow} is equal to c_w and T_w respectively.

The energy balance for the water can now be expressed by inserting Equation (6.22), Equation (6.24), Equation (6.28) and Equation (6.30) into Equation (6.21) and using some of the assumption defined in Section 4.1.3.

$$\begin{aligned} M_w \cdot c_w \cdot \frac{\mathrm{d}T_w(t)}{\mathrm{dt}} &= m_w \cdot c_{iw} \cdot T_{iw}(t) + \epsilon_{bcw} \cdot \sigma \cdot A_{bcw} \cdot \left(T_{bc}(t)^4 - T_w(t)^4\right) \\ &+ \alpha_{bc} \cdot A_{bcw} \cdot (T_{bc}(t) - T_w(t)) + \alpha_{gc} \cdot A_{gcw} \cdot (T_{gc}(t) - T_w(t)) \\ &+ \alpha_{eg} \cdot A_{egw} \cdot (T_{eg}(t) - T_w(t)) - m_w \cdot c_w \cdot T_w(t) \end{aligned} \tag{6.31}$$

An expression for the change in the water temperature has now been found.

6.2.2 Energy Balance for the Burning Chamber

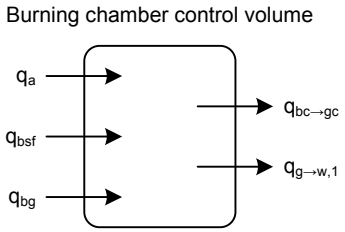

Figure 6.4: *Control volume for the gas in the burning chamber where arrows going inside indicates supply of energy and arrows going outside indicates energy lost.*

From Figure 6.4 the energy balance for the gas in the burning chamber can be expressed as energy change in the control volume with respect to time. The energy change is expressed by the energy of the supplied air (q_a), the energy from burning the solid fuel (q_{bsf}), the energy from burning the gases (q_{bg}), the energy transferred from the burning chamber to the gas chamber ($q_{bc\rightarrow gc}$) and the energy transferred from the burning chamber to the water ($q_{g\rightarrow w,1}$) as seen in Equation (6.32).

$$\frac{\mathrm{d}E_{bc}(t)}{\mathrm{dt}} = q_a(t) + q_{bsf}(t) + q_{bg}(t) - q_{bc\rightarrow gc}(t) - q_{g\rightarrow w,1}(t) \tag{6.32}$$

The energy in the gas in the burning chambers (E_{bc}) can be expressed by the mass of the gas in the burning chamber (M_{bc}), the mass of the ceramic plate (M_{cp}), the specific heat capacity of the gas in the burning chamber (c_{bc}), the specific heat capacity of the ceramic plate (c_{cp}) and the temperature of the gas in the burning chambers (T_{bc}).

$$E_{bc}(t) = (M_{bc} \cdot c_{bc} + M_{cp} \cdot c_{cp}) \cdot T_{bc}(t) \tag{6.33}$$

The energy of the supplied air is given by Equation (6.34).

$$q_a(t) = m_a(t) \cdot c_a \cdot T_a \tag{6.34}$$

where T_a is the temperature of the supply air and c_a is the specific heat capacity of air.

The energy from the combustion of solid fuel is given by the mass flow of C which is under combustion and the heat value of C when it reacts with O [Annamalai & Puri, 2007].

$$q_{bsf}(t) = m_{\mathrm{C}}(t) \cdot \left(\frac{1}{4} \cdot h_{c,\mathrm{I}} + \frac{3}{4} \cdot h_{c,\mathrm{II}}\right) \tag{6.35}$$

where $h_{c,I}$ is the heat value of C during reaction I in Section 2.2, $h_{c,II}$ is the heat value of C during reaction II in Section 2.2 and m_{C} is the mass flow of C in the solid fuel which is under combustion. m_{C} is derived in Section 6.1.1. The fractions indicate how much CO and CO_2 is released during the combustion of the solid fuel.

The energy from the combustion of gases is given by Equation (6.36) [Annamalai & Puri, 2007].

$$q_{bg}(t) = m_{\mathrm{CO}}(t) \cdot h_{c,\mathrm{V}} + m_{\mathrm{H_2}} \cdot h_{c,\mathrm{VI}} \tag{6.36}$$

where m_{CO} is the mass flow of CO in the gases after the combustion of the solid fuel, $h_{c,\mathrm{V}}$ is the heat value of CO during reaction V in Section 2.2, $m_{\mathrm{H_2}}$ is the mass flow of H_2 released during the combustion of the gases and $h_{c,\mathrm{VI}}$ is the heat value of H_2 during reaction VI in Section 2.2.

m_{CO} can be found from the amount of C which is converted to CO which is $\frac{1}{4}$ according to the assumptions.

$$m_{\mathrm{CO}}(t) = \frac{1}{4} \cdot \frac{m_{\mathrm{C}}(t)}{n_{\mathrm{C}}} \cdot n_{\mathrm{CO}} \tag{6.37}$$

$m_{\mathrm{H_2}}$ can be fund from the amount of H in the solid fuel.

$$m_{\mathrm{H_2}} = \frac{1}{2} \cdot \frac{m_{sf,\mathrm{H}}}{n_{\mathrm{H}}} \cdot 2 \cdot n_{\mathrm{H}} = m_{sf,\mathrm{H}} = c_{\mathrm{H}} \cdot m_{sf}(t) \tag{6.38}$$

Equation (6.36) can now be given as:

$$q_{bg}(t) = \frac{1}{4} \cdot \frac{m_{\mathrm{C}}(t)}{n_{\mathrm{C}}} \cdot n_{\mathrm{CO}} \cdot h_{c,\mathrm{V}} + c_{\mathrm{H}} \cdot m_{sf}(t) \cdot h_{c,\mathrm{VI}} \tag{6.39}$$

The energy transferred to the gas chamber is given by transport heat.

$$q_{bc \to gc}(t) = m_{bc \to gc}(t) \cdot c_{bc} \cdot T_{bc}(t) \tag{6.40}$$

where $m_{bc \to gc}$ is the mass flow of gas from the burning chamber to the gas chamber which is equal to m_g derived in Section 6.1.2 and c_{bc} is the specific heat capacity of the gas in the burning chamber.

The energy transferred to the water is derived in Section 6.2.1 as:

$$q_{g \to w,1}(t) = \epsilon_{bcw} \cdot \sigma \cdot A_{bcw} \cdot \left(T_{bc}(t)^4 - T_w(t)^4\right) + \alpha_{bc} \cdot A_{bcw} \cdot \left(T_{bc}(t) - T_w(t)\right) \tag{6.41}$$

The energy balance for the gas in the burning chamber can now be expressed by inserting Equation (6.33), Equation (6.34), Equation (6.35), Equation (6.39), Equation (6.40) and Equation (6.41) into Equation (6.32).

$$\begin{aligned}(M_{bc} \cdot c_{bc} + M_{cp} \cdot c_{cp}) \cdot \frac{\mathrm{d}T_{bc}(t)}{\mathrm{d}t} \quad = \quad & m_a(t) \cdot c_a \cdot T_a + m_{\mathrm{C}}(t) \cdot \left(\frac{1}{4} \cdot h_{c,\mathrm{I}} + \frac{3}{4} \cdot h_{c,\mathrm{II}}\right) \\ & + \frac{1}{4} \cdot \frac{m_{\mathrm{C}}(t)}{n_{\mathrm{C}}} \cdot n_{\mathrm{CO}} \cdot h_{c,\mathrm{V}} + c_{\mathrm{H}} \cdot m_{sf}(t) \cdot h_{c,\mathrm{VI}} \\ & - m_g(t) \cdot c_{bc} \cdot T_{bc}(t) \\ & - \epsilon_{bcw} \cdot \sigma \cdot A_{bcw} \cdot (T_{bc}(t)^4 - T_w(t)^4) \\ & - \alpha_{bc} \cdot A_{bcw} \cdot (T_{bc}(t) - T_w(t))\end{aligned} \tag{6.42}$$

An expression for the change in the gas temperature in the burning chamber has now been found.

6.2.3 Energy Balance for the Gas Chamber

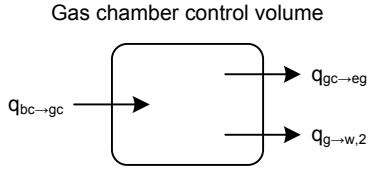

Figure 6.5: *Control volume for the gas in the gas chamber where arrows going inside indicates supply of energy and arrows going outside indicates energy lost.*

From Figure 6.5 the energy balance for the gas in the gas chamber can be expressed as energy change in the control volume with respect to time. The energy change is expressed by $q_{bc\rightarrow gc}$, the energy transferred from the gas chamber to the exhaust gas ($q_{gc\rightarrow eg}$) and the energy transferred from the gas chamber to the water ($q_{g\rightarrow w,2}$) as seen in Equation (6.43).

$$\frac{\mathrm{d}E_{gc}(t)}{\mathrm{dt}} = q_{bc\rightarrow gc}(t) - q_{gc\rightarrow eg}(t) - q_{g\rightarrow w,2}(t) \tag{6.43}$$

The energy in the gas (E_{gc}) can be expressed by the mass of the gas in the gas chamber (M_{gc}), the specific heat capacity of the gas in the the gas chamber (c_{gc}) and the temperature of the gas in the gas chamber (T_{gc}).

$$E_{gc}(t) = M_{gc} \cdot c_{gc} \cdot T_{gc}(t) \tag{6.44}$$

The energy transferred from the burning chamber is derived in Section 6.2.2 as:

$$q_{bc\rightarrow gc}(t) = m_g(t) \cdot c_{bc} \cdot T_{bc}(t) \tag{6.45}$$

The energy transferred to the exhausted gas from the gas is given by transport heat transfer.

$$q_{gc\rightarrow eg}(t) = m_{gc\rightarrow eg}(t) \cdot c_{gc} \cdot T_{gc}(t) \tag{6.46}$$

where $m_{gc\rightarrow eg}$ is the mass flow of gas from the gas chamber to the exhaust gas which is equal to m_g derived in Section 6.1.2 and c_{gc} is the specific heat capacity of the gas in the gas chamber.

The energy transferred from the gas chamber to the water is derived in Section 6.1.1 as:

$$q_{g\rightarrow w,2}(t) = \alpha_{gc} \cdot A_{gcw} \cdot (T_{gc}(t) - T_w(t)) \tag{6.47}$$

The energy balance for the gas can now be expressed by inserting Equation (6.44), Equation (6.45), Equation (6.46) and Equation (6.47) into Equation (6.43).

$$\begin{aligned} M_{gc} \cdot c_{gc} \cdot \frac{\mathrm{d}T_{gc}(t)}{\mathrm{dt}} &= m_g(t) \cdot (c_{bc} \cdot T_{bc}(t) - c_{gc} \cdot T_{gc}(t)) \\ &\quad -\alpha_{gc} \cdot A_{gcw} \cdot (T_{gc}(t) - T_w(t)) \end{aligned} \tag{6.48}$$

An expression for the change in the gas temperature in the gas chamber has now been found.

6.2.4 Energy Balance for the Exhausted Gas

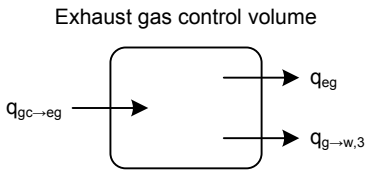

Figure 6.6: *Control volume for the exhaust gas where arrows going inside indicates supply of energy and arrows going outside indicates energy lost.*

From Figure 6.6 the energy balance for the exhaust gas can be expressed as energy change in the control volume with respect to time. The energy change is expressed by $q_{gc\rightarrow eg}$, the energy in

the exhausted gas (q_{eg}) and the energy transferred from the exhaust gas to the water ($q_{g\to w,3}$) as seen in Equation (6.49).

$$\frac{\mathrm{d}E_{eg}(t)}{\mathrm{dt}} = q_{gc\to eg}(t) - q_{eg}(t) - q_{g\to w,3} \tag{6.49}$$

The energy in the exhaust gas (E_{eg}) can be expressed by the mass of the exhaust gas (M_{eg}), the specific heat capacity of the exhaust gas (c_{eg}) and the temperature of the exhaust gas (T_{eg}).

$$E_{eg}(t) = M_{eg} \cdot c_{eg} \cdot T_{eg}(t) \tag{6.50}$$

The energy transferred from the gas chamber to the exhaust gas is derived in Section 6.2.3 as:

$$q_{gc\to eg}(t) = m_g(t) \cdot c_{gc} \cdot T_{gc}(t) \tag{6.51}$$

The energy in the exhausted gas is given by Equation (6.52).

$$q_{eg}(t) = m_{eg}(t) \cdot c_{eg} \cdot T_{eg}(t) \tag{6.52}$$

where m_{eg} is the mass flow of the exhausted gas which is equal to m_g derived in Section 6.1.2, c_{eg} is the specific heat capacity of the exhaust gas and T_{eg} is the temperature of the exhausted gas.

The energy transferred from the exhaust gas to the water is derived in Section 6.2.1:

$$q_{g\to w,3}(t) = \alpha_{eg} \cdot A_{egw} \cdot (T_{eg}(t) - T_w(t)) \tag{6.53}$$

The energy balance for the exhaust gas can now be expressed by inserting Equation (6.50), Equation (6.51), Equation (6.52) and Equation (6.53) into Equation (6.49).

$$\begin{aligned} M_{eg} \cdot c_{eg} \cdot \frac{\mathrm{d}T_{eg}(t)}{\mathrm{dt}} &= m_g(t) \cdot (c_{gc} \cdot T_{gc}(t) - c_{eg} \cdot T_{eg}(t)) \\ &\quad -\alpha_{eg} \cdot A_{egw} \cdot (T_{eg}(t) - T_w(t)) \end{aligned} \tag{6.54}$$

An expression for the change in the exhaust gas temperature has now been found.

6.3 Mass Balances for the Stoker

In this section the last two differential equations are derived. These equations are derived from mass balance considerations.

6.3.1 Mass Balance for the Solid Fuel

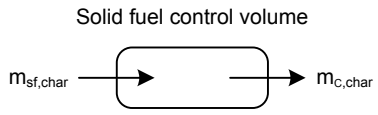

Figure 6.7: *Control volume for the solid fuel where arrows going inside indicates supply of mass and arrows going outside indicates mass lost.*

From Figure 6.7 the mass balance for the solid fuel can be expressed as mass change in the control volume with respect to time. Only the charcoal is monitored as it is assumed that all

the gases in the solid fuel combust instantly. The mass change of solid fuel is therefore given by the mass change of charcoal which can be expressed by the mass flow C in the solid fuel which is converted to charcoal ($m_{sf,\mathrm{char}}$) and the mass flow of C in the charcoal which is under combustion ($m_{\mathrm{C,char}}$) as seen in Equation (6.55).

$$\frac{\mathrm{d}M_{sf}(t)}{\mathrm{dt}} = \frac{\mathrm{d}M_{\mathrm{C,char}}(t)}{\mathrm{dt}} = m_{sf,\mathrm{char}}(t) - m_{\mathrm{C,char}}(t) \tag{6.55}$$

The mass flow of C in the solid fuel which is converted to charcoal is given by the ratio of C converted to charcoal and the C in the solid fuel.

$$m_{sf,\mathrm{char}}(t) = \zeta_{\mathrm{char}}(t) \cdot c_{\mathrm{C}} \cdot m_{sf}(t) \tag{6.56}$$

The mass flow of C in the charcoal which is under combustion is derived in Section 6.1.1 as:

$$m_{\mathrm{C,char}}(t) = \chi \cdot m_a(t) \cdot \gamma_1 + M_{\mathrm{C,char}}(t) \cdot \gamma_2 \tag{6.57}$$

The mass balance for the solid fuel can now be expressed by inserting Equation (6.56) and Equation (6.57) into Equation (6.55).

$$\frac{\mathrm{d}M_{\mathrm{C,char}}(t)}{\mathrm{dt}} = \zeta_{\mathrm{char}}(t) \cdot c_{\mathrm{C}} \cdot m_{sf}(t) - \chi \cdot m_a(t) \cdot \gamma_1 - M_{\mathrm{C,char}}(t) \cdot \gamma_2 \tag{6.58}$$

An expression for the change in the mass of the solid fuel is now found.

6.3.2 Mass Balance for the O_2-Level

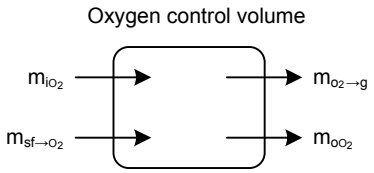

Figure 6.8: *Control volume for the O_2 where arrows going inside indicates supply of mass and arrows going outside indicates mass lost.*

From Figure 6.8 the mass balance for the O_2 can be expressed as mass change in the control volume with respect to time. The mass change is expressed by the mass flow of O_2 in the supply air (m_{iO_2}), the mass flow of O_2 which is released from the solid fuel during the combustion process (m_{sf,O_2}), the mass flow of O_2 which is converted to gas during the combustion process ($m_{O_2\to g}$) and the mass flow of O_2 in the exhaust gas (m_{oO_2}) as seen in Equation (6.59).

$$\frac{\mathrm{d}M_{O_2}(t)}{\mathrm{dt}} = m_{iO_2}(t) + m_{sf,O_2}(t) - m_{O_2\to g}(t) - m_{oO_2}(t) \tag{6.59}$$

The inlet O_2 can be found as the composition of the supply air is known.

$$m_{iO_2}(t) = \frac{1}{2} \cdot \frac{m_{a,\mathrm{O}}(t)}{n_{\mathrm{O}}} \cdot 2 \cdot n_{\mathrm{O}} = c_{a,\mathrm{O}} \cdot m_a(t) \tag{6.60}$$

m_{sf,O_2} is the mass flow of O_2 in the solid fuel and can be found by multiplying one half on the amount of O in the solid fuel. This amount can be found from $m_{sf,\mathrm{O}}$ which is derived in Section 6.1.2.

$$m_{sf,O_2}(t) = \frac{1}{2} \cdot \frac{m_{sf,\mathrm{O}}(t)}{n_{\mathrm{O}}} \cdot 2 \cdot n_{\mathrm{O}} = c_{sf,\mathrm{O}} \cdot m_{sf}(t) \tag{6.61}$$

$m_{O_2 \to g}$ is the mass flow of O_2 which is used in CO, CO_2 and H_2O molecules. But as all the CO is converted to CO_2 this intermediate result is included in the conversion to CO_2. Both The mass flow of O used in the CO_2 and H_2O reactions are derived in Section 6.1.2 as:

$$m_{O_2 \to CO_2} = \frac{1}{2} \cdot 2 \cdot \frac{m_C(t)}{n_C} \cdot 2 \cdot n_O = 2 \cdot \frac{m_C(t) \cdot n_O}{n_C} \tag{6.62}$$

and

$$m_{O_2 \to H_2O} = \frac{1}{4} \cdot \frac{m_{sf,H}(t)}{n_H} \cdot 2 \cdot n_O = \frac{1}{2} \cdot \frac{c_H \cdot n_O}{n_H} \cdot m_{sf}(t) \tag{6.63}$$

$m_{O_2 \to g}$ can now be written as the sum of Equation (6.62) and Equation (6.63) as:

$$m_{O_2 \to g} = 2 \cdot \frac{m_C(t) \cdot n_O}{n_C} + \frac{1}{2} \cdot \frac{c_H \cdot n_O}{n_H} \cdot m_{sf}(t) \tag{6.64}$$

The mass flow of O_2 out of the stoker is given by the flow of exhaust gas and the fraction of O_2 in the exhaust gas.

$$m_{oO_2}(t) = O_2(t) \cdot m_{eg}(t) \tag{6.65}$$

where m_{eg} is the mass flow of exhaust gas which is equal to m_g derived in Section 6.1.2.

The change of O_2-level inside the stoker can now be expressed by inserting Equation (6.60), Equation (6.61), Equation (6.64) and Equation (6.65) into Equation (6.59) and divide with the total mass of gas inside the stoker ($O_2 = M_{O_2}/M_{total}$).

$$\begin{aligned} M_{total} \cdot \frac{dO_2(t)}{dt} &= c_{a,O} \cdot m_a(t) + c_{sf,O} \cdot m_{sf}(t) - 2 \cdot \frac{n_O \cdot m_C(t)}{n_C} \\ &\quad - \frac{1}{2} \cdot \frac{c_H \cdot n_O}{n_H} \cdot m_{sf}(t) - O_2(t) \cdot m_g(t) \end{aligned} \tag{6.66}$$

An expression for the change in the O_2-level is now found.

The six differential equations needed to create the mathematical model of the system is now derived. It can be seen that the model is non-linear as the differential equations contain products of terms which are time depended. This non-linear model has to be validated to see the accuracy of the model.

6.4 Constant and Parameter Determination

Now that the non-linear model has been derived, the constants and parameters used in the equations must be determined. The constants are stated by physical elements and they stay constant independent of the solid fuel composition and the time. Most of the constants are physical quantities which can be found in look-up tables and books. Other constants are measured on the stoker setup at Techno-Matic A/S. Some of these constants are derived in Appendix G whereas the rest are found in Appendix H.

There are two different types of parameters in the system. One type which is dependent of the solid fuel. They will not be fitted and are constant for a certain solid fuel. These parameters are also found from look-up tables and books. Some of these parameters are derived in Appendix G whereas the rest are found in Appendix H.

The last part of the parameters has to be fitted to obtain a sufficient model. These parameters are the two γ-values which has to be fitted from engineering intuition and trial-and-error using

real measurement data from the plant. Both γ_1 and γ_2 are dependent on the composition of the solid fuel. Under combustion of wood pellets γ_1 is found to 0.05 and γ_2 is found to 4.0 and under the combustion of wheat γ_1 is found to 0.12 and γ_2 is found to 2.0. The result has shown, that the γ-values primary influence the dynamic of the system. γ_1 mainly change the dynamic when a step in m_a is performed, where γ_2 mainly change the dynamic when a step in m_{sf} is made. However a change in a γ-value effects both the dynamic for a step in m_a and m_{sf}.

6.5 Verification of the Non-linear Model

The non-linear model is constructed in SIMULINK to verify the accuracy of the model. The SIMULINK model take steps in the plant input as input and the model output is then compared with the plant output. The SIMULINK model can be found on the enclosed CD.

The model is verified from six states; T_w, T_{eg}, T_{bc}, T_{gc}, M_{sf}, O_2. Only three of these states, T_w, T_{eg} and O_2, can be measured and the model is primary verified from these states. However the last three states are also used in the verification as their dynamics are known. The non-linear model is verified on different step and steady state test.

It is expected that a step in solid fuel (m_{sf}) will increase the temperature in the stoker as the surface of the molehill will increase, this means that the contact area between the air and the solid fuel is increased. It will however influence the O_2-level which will decrease because more O_2 react with the solid fuel.

When a step in the supply air (m_a) is conducted it is expected that the temperature in the stoker will increase as more O_2 is accessible for the combustion process it is however assumed that the O_2-level also increases.

In Figure 6.9 is the simulated state (T_w, T_{eg} and O_2) and measured state from a steady state test with wood pellets shown.

As it can be seen in the first graph in Figure 6.9 the simulated water temperature is about one degree below the measured water temperature. In the second graph the exhaust gas temperature is shown which is a little above the measured exhaust gas temperature. In the third graph the O_2-level is shown, here a fine accordance between the measured data and the model is found. The reason why the O_2 measurement is oscillating is due to the PWM signal which the screw conveyor motor receives. The period time of the PWM signal is too long which means that too much solid fuel is supplied during a step which decreases the O_2-level. In the period time where no solid fuel is supplied will the O_2-level increase again. Using a smaller period time with more steps would solve this problem which can be seen in future figures.

In Figure 6.10 is the simulated state of the non measurable states shown (M_{sf}, T_{bc} and T_{gc}).

The first graph shows the mass of the solid fuel in the molehill. It can be seen that the mass is constant during the whole steady state test which is as expected. Moreover the mass is just above 0.45 kg which is also as expected, as it is assumed that the size of the molehill is just around 0.4 - 0.5 kg.

The temperature in the burning and gas champers is shown in the two subsequent graphs in Figure 6.10. The temperatures are around 450°C and 200°C respectively, which is assumed to be fine as the temperatures has been estimated to be in that area, see Appendix G for details.

The same model with the same constants and parameters is also used in a step test with wood pellets. The result from this step test can be seen in Figure 6.11 and Figure 6.12 where the first figure has outputs that can be compared with measured outputs from the plant.

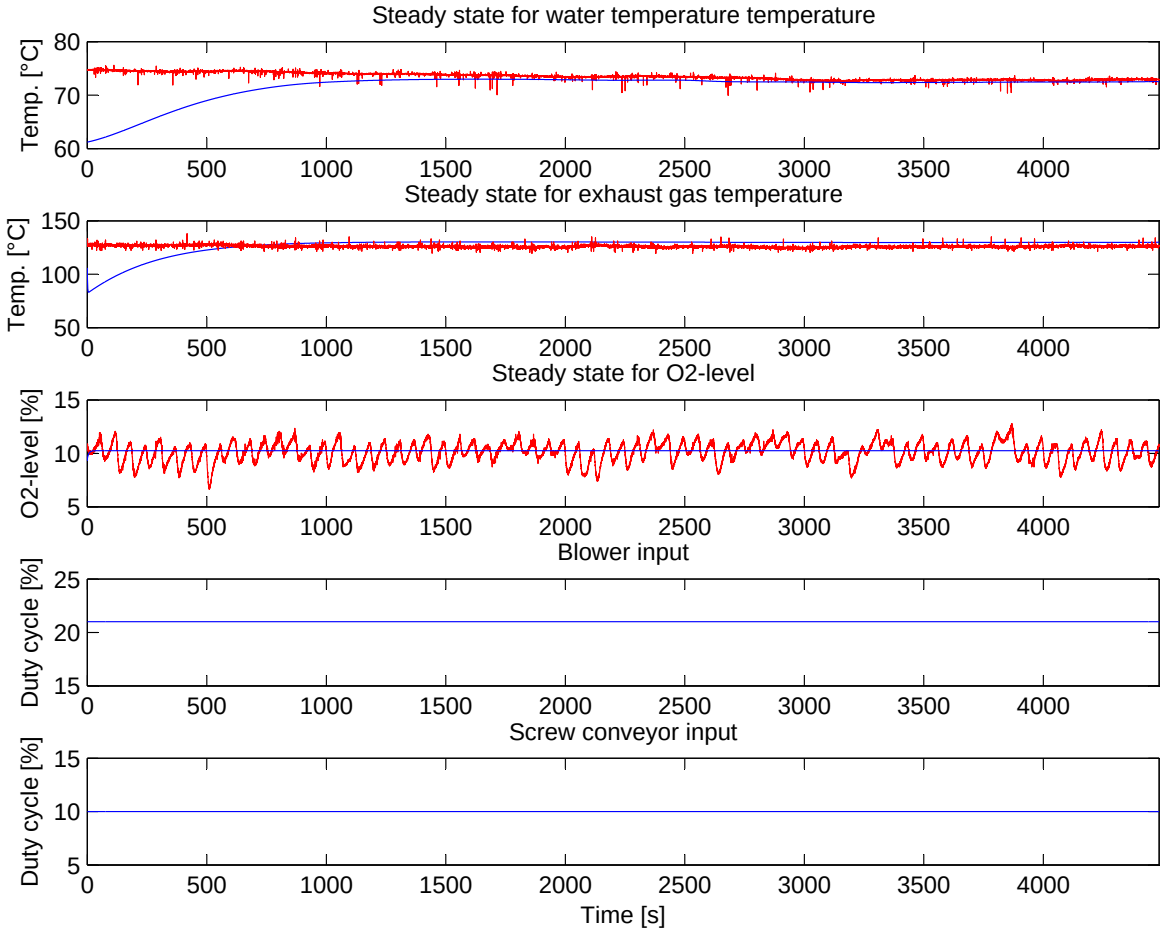

Figure 6.9: *The simulated and measured water temperature, exhaust gas temperature and O_2-level from a steady state test where red is measured values and blue is simulated values. The last two graphs show the input to the actuators.*

As it is shown in the first graph in Figure 6.11 the simulated water temperature and measured water temperature are close to each other, the largest difference is around one degree. The parameters γ_1 and γ_2 can be tuned, so the simulated and measured data is equal in one desired point on the curve. But as it is chosen to fit the model to both a step and a steady state measurement the γ-values are the same as they were for the steady state test. The water temperature is increasing as expected when a step in the supply air and solid fuel is made. The dynamic of the model is also following the real plant, so the model is sufficient to find this state.

The exhaust gas temperature is shown in the second graph. As it can be seen the dynamic has the right behaviour when steps in the supply air and the solid fuel are performed. The simulated temperature is however nearly 15°C from the measured, when the temperature is below 125°C. This can be fitted with the γ-values, so it is correct at lower temperatures also, but then the difference will be larger when the temperature increases. The dynamic of the model is also a little to fast, especially when a step in the supply air is made. The final simulated temperature is around 4°C below the measured exhaust gas temperature. It is however assumed that the model of the exhaust gas temperature is sufficient.

The O_2-level is shown in the third graph in Figure 6.11. The simulated and measured level is following each other very well. The dynamic is also as expected. The O_2-level is increasing when a step in the supply air is performed and the O_2-level is decreasing when a step in the

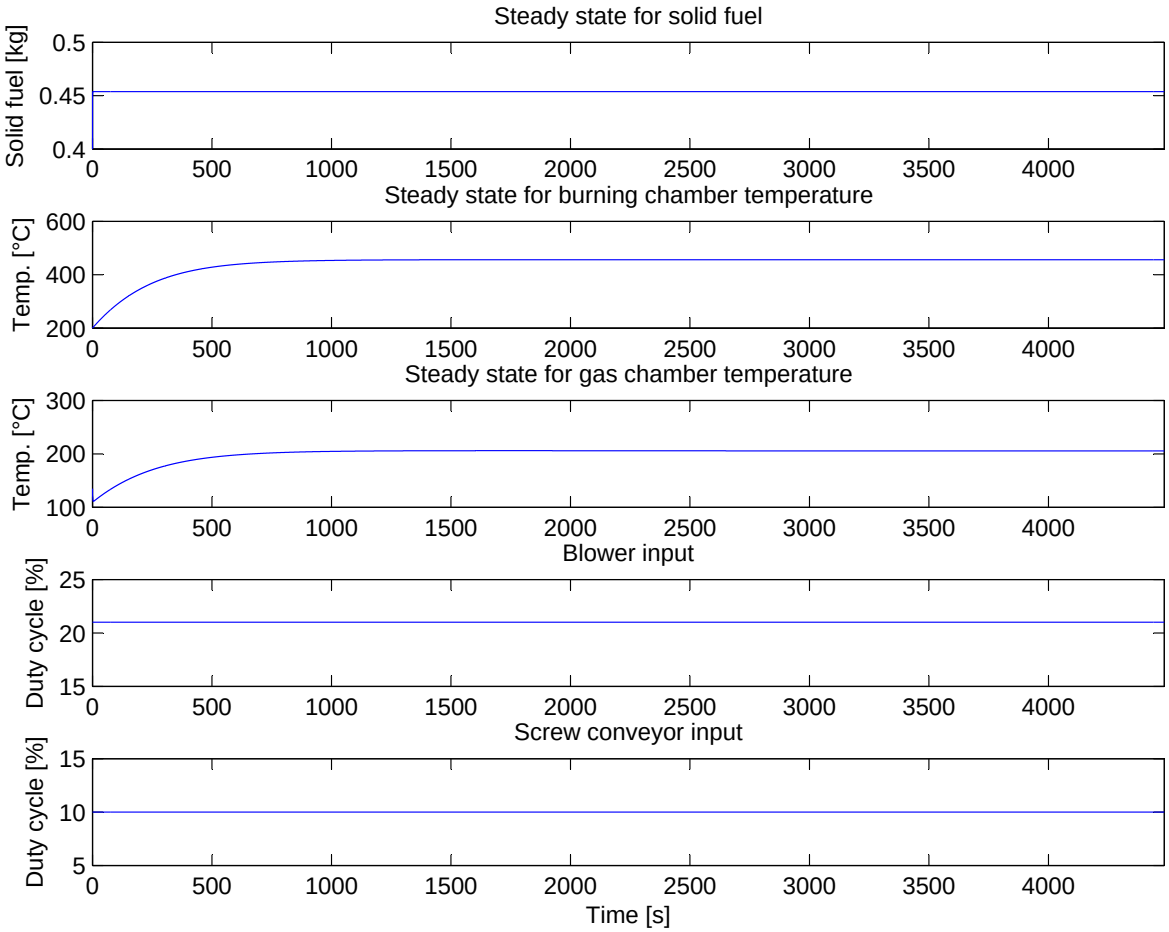

Figure 6.10: *The simulated values for the mass of the solid fuel, the burning chamber temperature and the gas chamber temperature from a steady state test. The last two graphs show the input to the actuators.*

solid fuel is performed. The O_2-level from the model is close enough to the actual plant, so the model is sufficient to describe the O_2-level. The oscillation phenomenon is also present in this measurement.

The mass of solid fuel is shown in the first graph in Figure 6.12. The dynamic of the mass of the molehill is, as assumed, as the mass of solid fuel is decreased when a step in the supply air is performed and increased when a step in the solid fuel is performed. The level of the mass of the molehill is also, as expected, as it is assumed that the molehill is around 0.4 - 0.5 kg.

The temperature of the burning chamber and the gas chamber can be seen in the subsequent two graphs in Figure 6.12. The dynamic is doing as expected in these chambers, as the temperature is increasing when steps are performed in the supply air and the solid fuel. The temperature is around 400°C and 200°C for the two champers respectively, which is in accordance with the tests that have been made for the two campers, see Appendix G.

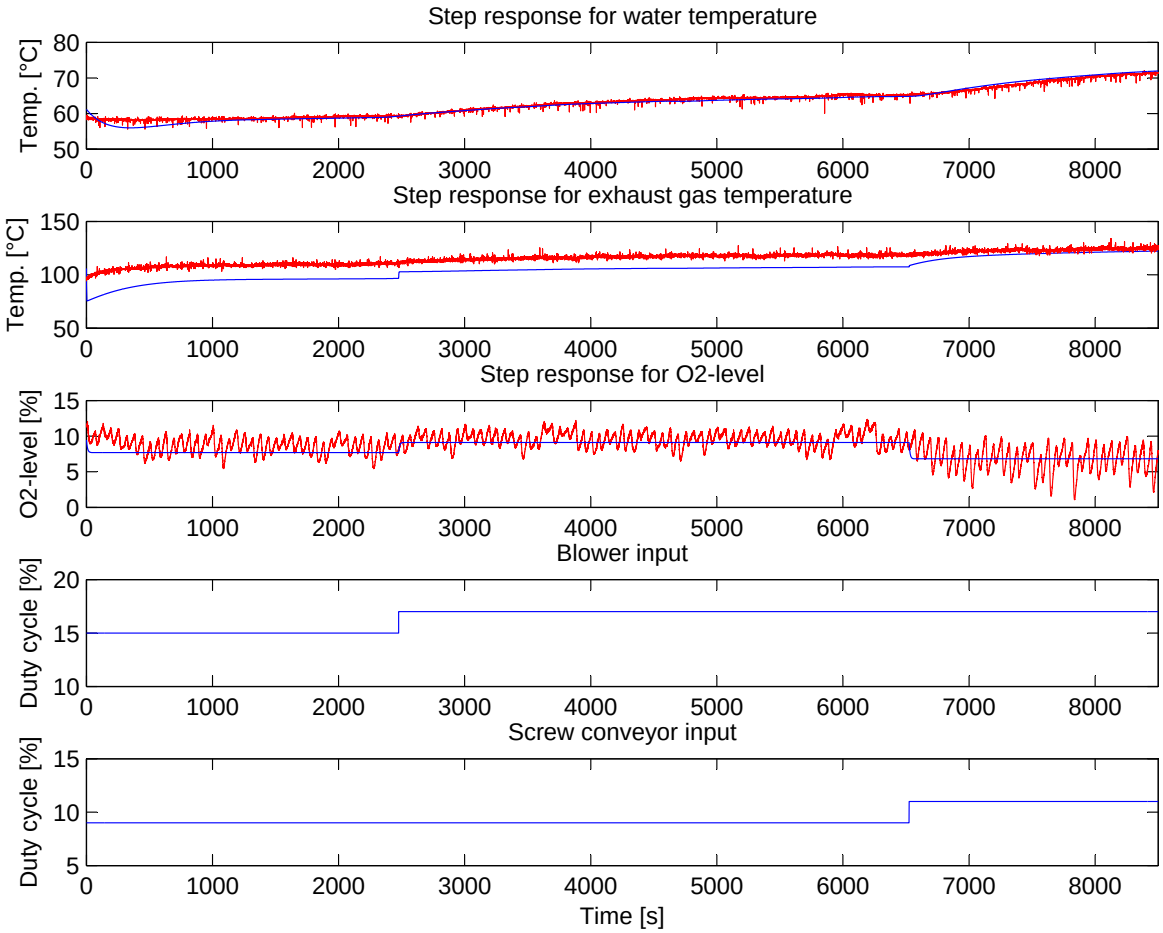

Figure 6.11: *The simulated and measured water temperature, exhaust gas temperature and O_2-level from a step test where red is measured values and blue is simulated values. The last two graphs show the input from to actuators.*

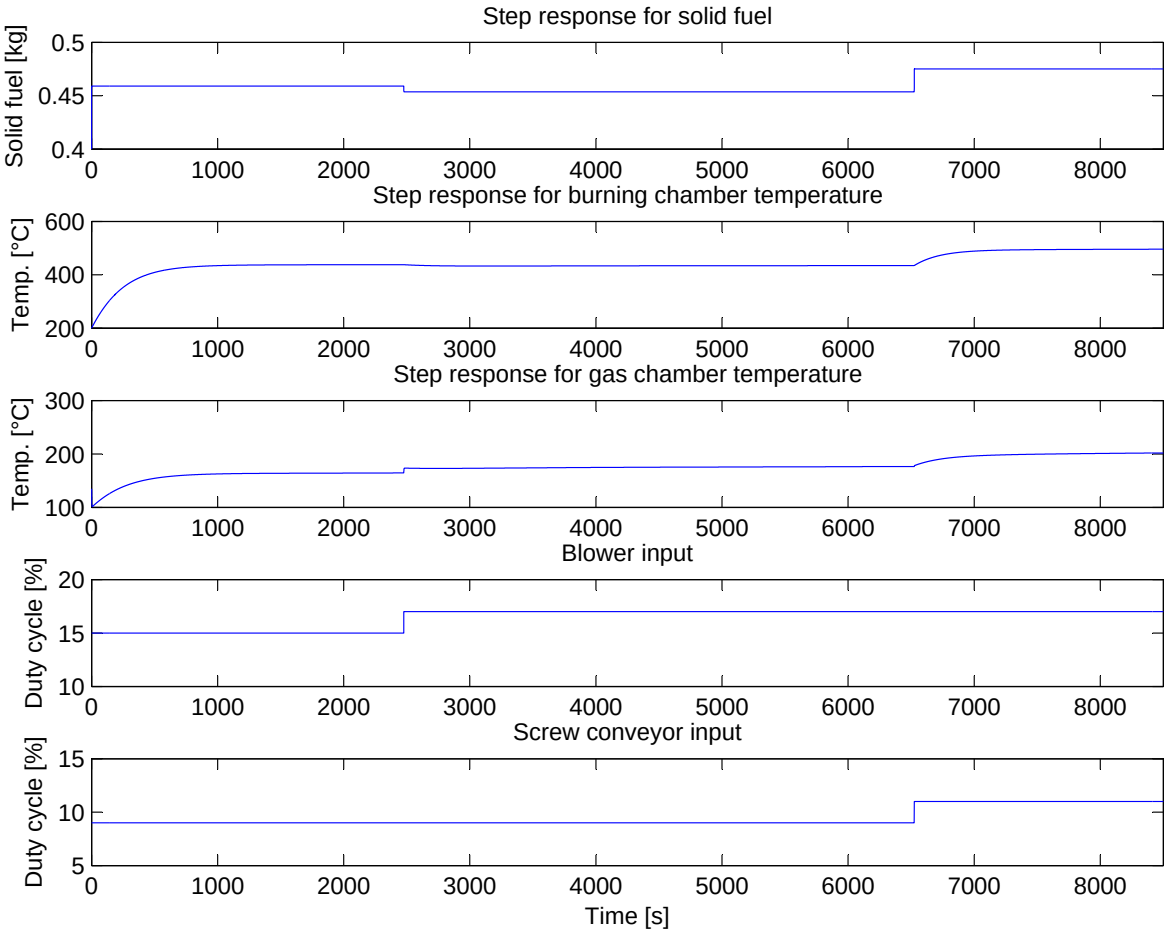

Figure 6.12: *The simulated values for the mass of the solid fuel, the burning chamber temperature and the gas chamber temperature from a step test. The last two graphs show the input from the actuators.*

6.6 Model with a Different Solid Fuel

It is assumed that the non-linear model just derived and verified under combustion of wood pellets also can be used for other solid fuels. For this to a apply, some of the parameters must be changed. This section will investigate which parameters are needed to change for the model to be sufficient for another solid fuel. The project is limited to dealing with only two different solid fuels; as wood pellets and wheat.

The same parameters as used for wood pellets are examined first, to see how well the model fits with these parameters when wheat is combusted. This is seen in Figure 6.13 where both the simulated (blue) and measured (red) state along with the actuator inputs are shown.

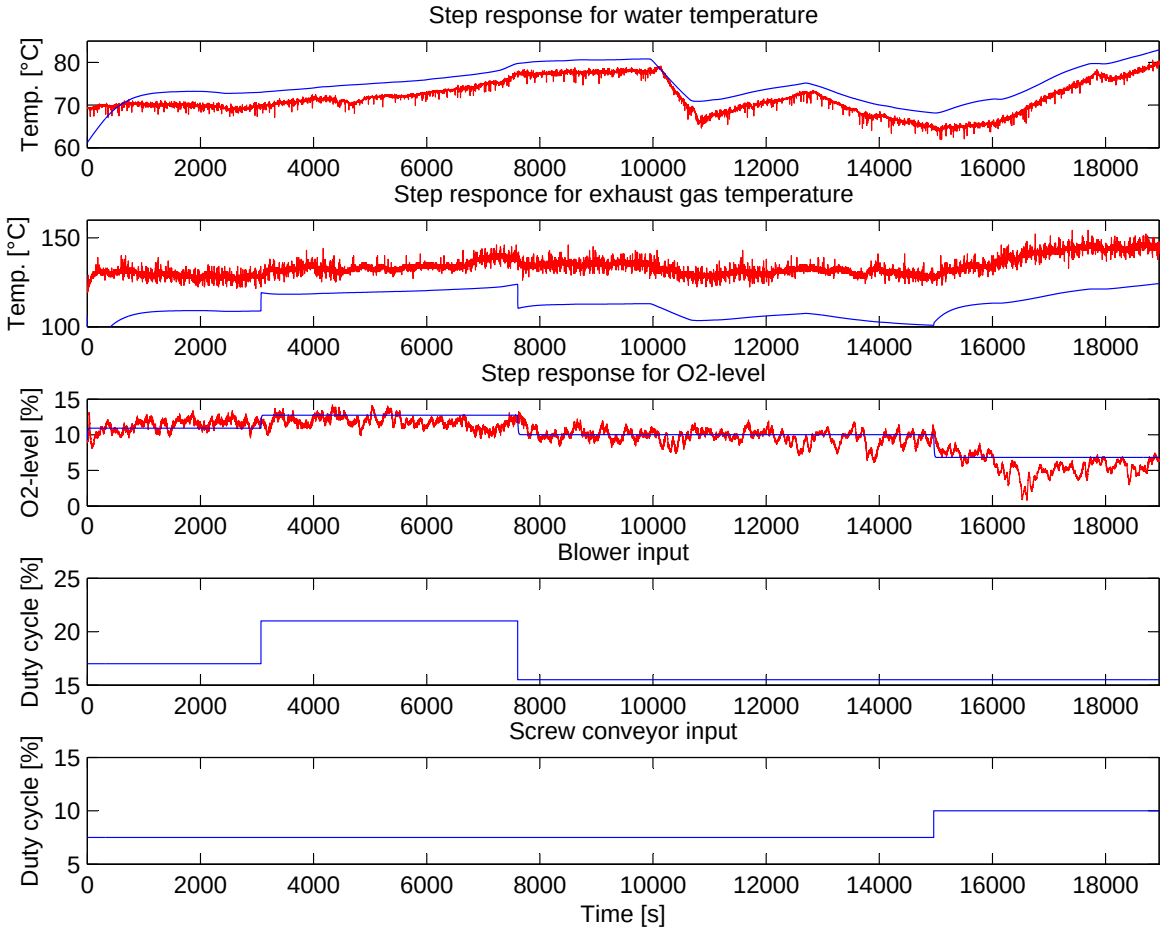

Figure 6.13: *The water temperature, exhaust gas temperature and O_2-level with parameters fitted to wood pellets but with wheat as the actual solid fuel. The last two graphs show the input to the actuators.*

As it can be seen in the graphs, the parameters used for wood pellets will not give a sufficient output result for the water temperature and the exhaust gas when wheat is combusted. Therefore some of the parameters must be changed. β_{motor} is changed as wheat has a different density (see Appendix D). The heat transfer coefficients are also changed because the temperatures are higher when wheat is combusted which gives another set of operating points (see Appendix G). Finally the two γ-parameters must be changed for the dynamics to fit.

The parameters are fitted to a step test. The step test is only comparing the model outputs with

the measurable outputs and the results can be seen in Figure 6.14.

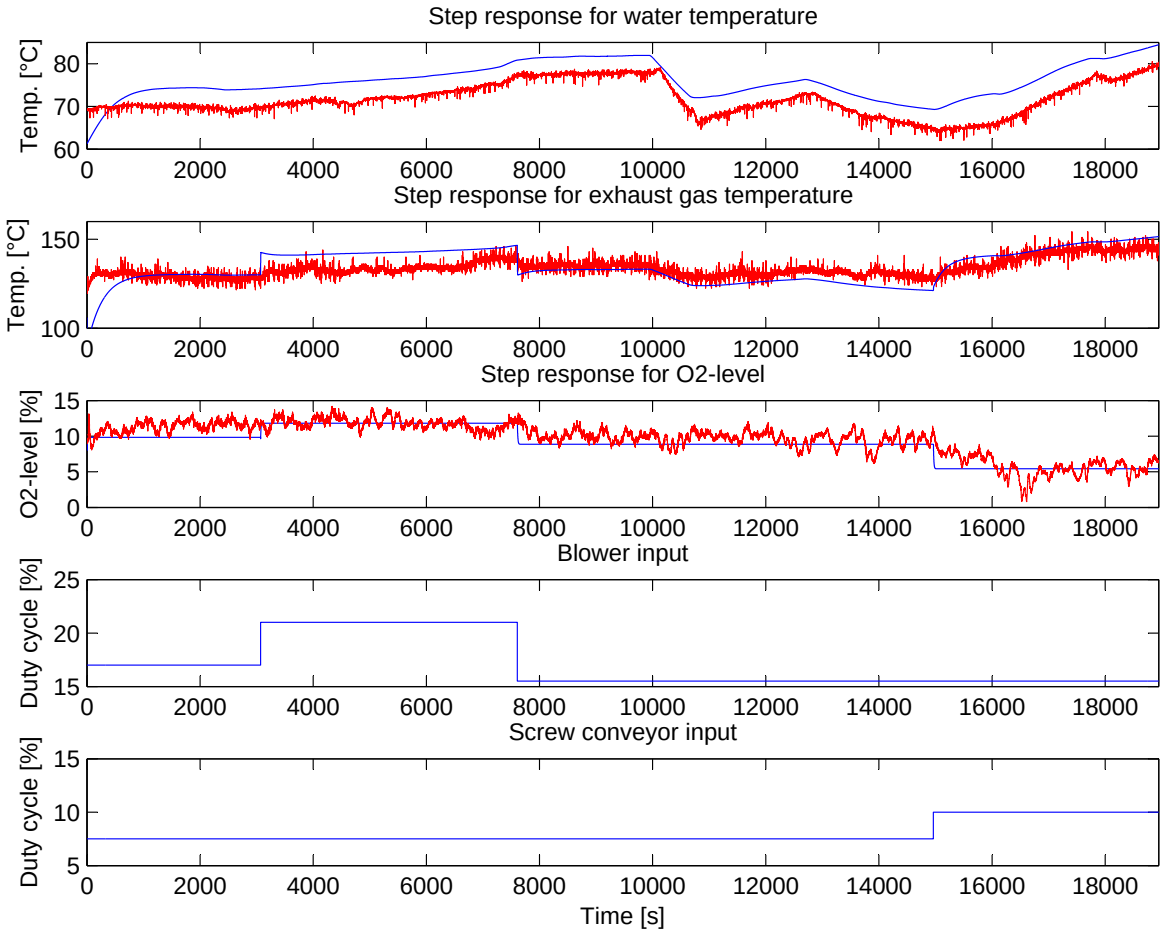

Figure 6.14: *The water temperature, exhaust gas temperature and O_2-level with constants fitted to wheat. The last two graphs show the input to the actuators.*

It can be seen that both the water temperature and the exhaust gas temperature fits better with the wheat constants, moreover can it be seen that the O_2-level fits fine, independent of the parameters for wheat and wood pellets. From Figure 6.13 and Figure 6.14 is it assumed that it will be possible to find differences between the two models when wood pellets and wheat is combusted. This also means that the non-linear model of the stoker system using wheat as solid fuel is verified with success.

To see the differences between the actual plant output and the wheat model, when wood pellets parameters are used, one more test is performed. The result can be seen in Figure 6.15.

The differences when the model for wheat is used with wood pellets as solid fuel are mainly seen in the exhaust temperature and a little in the water temperature. This fits well with the opposite test, that also showed that the largest difference was in the exhaust temperature.

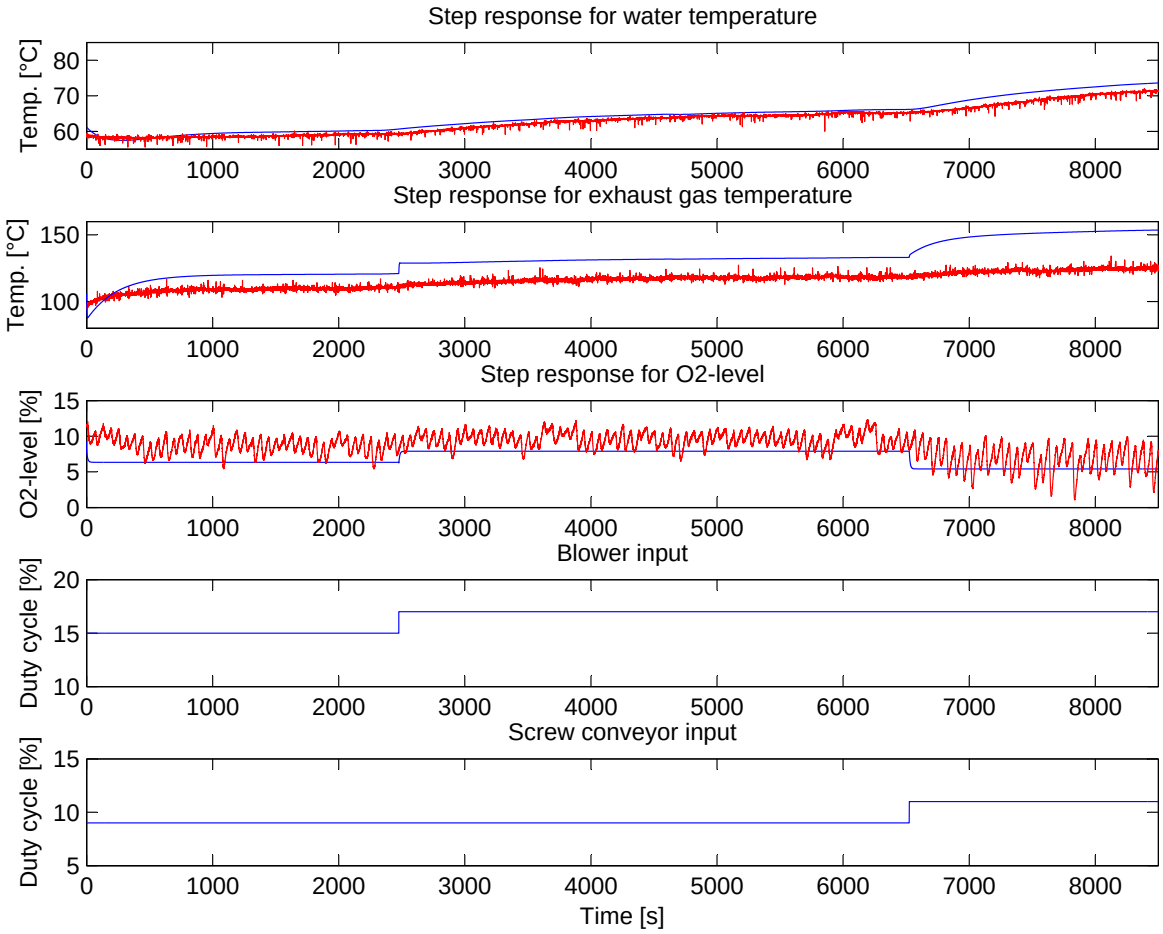

Figure 6.15: *The water temperature, exhaust gas temperature and O_2-level with parameters fitted to wheat but with wood pellets as actual solid fuel. The last two graphs show the input to the actuators.*

Chapter Summery

In this chapter a non-linear model of the stoker system is derived. The non-linear model consists of ordinary first order differential equations which are based on energy and mass balance considerations. The modelling is divided into six control volumes. The water, the burning chamber, the gas chamber, and the exhaust gas where the temperature is found from energy balance considerations and the mass of the solid fuel, and the O_2-level is found from mass balance considerations. However before these six differential equation can be derived the combustion of C and the mass flow of gas up through the stoker is found. The six differential equation is seen in the following six equations.

The energy balance for the water temperature:

$$\begin{aligned} M_w \cdot c_w \cdot \frac{\mathrm{d}T_w(t)}{\mathrm{dt}} &= m_w \cdot c_{iw} \cdot T_{iw}(t) + \epsilon_{bcw} \cdot \sigma \cdot A_{bcw} \cdot \left(T_{bc}(t)^4 - T_w(t)^4\right) \\ &\quad + \alpha_{bc} \cdot A_{bcw} \cdot (T_{bc}(t) - T_w(t)) + \alpha_{gc} \cdot A_{gcw} \cdot (T_{gc}(t) - T_w(t)) \\ &\quad + \alpha_{eg} \cdot A_{egw} \cdot (T_{eg}(t) - T_w(t)) - m_w \cdot c_w \cdot T_w(t) \end{aligned}$$

The energy balance for the burning chamber temperature:

$$\begin{aligned}(M_{bc}\cdot c_{bc}+M_{cp}\cdot c_{cp})\cdot\frac{\mathrm{d}T_{bc}(t)}{\mathrm{dt}} &= m_a(t)\cdot c_a\cdot T_a+m_{\mathrm{C}}(t)\cdot\left(\frac{1}{4}\cdot h_{c,\mathrm{I}}+\frac{3}{4}\cdot h_{c,\mathrm{II}}\right)\\ &\quad+\frac{1}{4}\cdot\frac{m_{\mathrm{C}}(t)}{n_{\mathrm{C}}}\cdot n_{\mathrm{CO}}\cdot h_{c,\mathrm{V}}+c_{\mathrm{H}}\cdot m_{sf}(t)\cdot h_{c,\mathrm{VI}}\\ &\quad-m_g(t)\cdot c_{bc}\cdot T_{bc}(t)\\ &\quad-\epsilon_{bcw}\cdot\sigma\cdot A_{bcw}\cdot(T_{bc}(t)^4-T_w(t)^4)\\ &\quad-\alpha_{bc}\cdot A_{bcw}\cdot(T_{bc}(t)-T_w(t))\end{aligned}$$

The energy balance for the gas chamber temperature:

$$\begin{aligned}M_{gc}\cdot c_{gc}\cdot\frac{\mathrm{d}T_{gc}(t)}{\mathrm{dt}} &= m_g(t)\cdot(c_{bc}\cdot T_{bc}(t)-c_{gc}\cdot T_{gc}(t))\\ &\quad-\alpha_{gc}\cdot A_{gcw}\cdot(T_{gc}(t)-T_w(t))\end{aligned}$$

The energy balance for the exhaust gas temperature:

$$\begin{aligned}M_{eg}\cdot c_{eg}\cdot\frac{\mathrm{d}T_{eg}(t)}{\mathrm{dt}} &= m_g(t)\cdot(c_{gc}\cdot T_{gc}(t)-c_{eg}\cdot T_{eg}(t))\\ &\quad-\alpha_{eg}\cdot A_{egw}\cdot(T_{eg}(t)-T_w(t))\end{aligned}$$

Mass balance for the solid fuel in the molehill:

$$\frac{\mathrm{d}M_{\mathrm{C,char}}(t)}{\mathrm{dt}} = \zeta_{\mathrm{char}}\cdot c_{\mathrm{C}}\cdot m_{sf}(t)-\chi\cdot m_a(t)\cdot\gamma_1-M_{\mathrm{C,char}}(t)\cdot\gamma_2$$

Mass balance for the O_2-level inside the stoker:

$$\begin{aligned}M_{\mathrm{total}}\cdot\frac{\mathrm{dO}_2(t)}{\mathrm{dt}} &= c_{a,\mathrm{O}}\cdot m_a(t)+c_{sf,\mathrm{O}}\cdot m_{sf}(t)-2\cdot\frac{n_{\mathrm{O}}\cdot m_{\mathrm{C}}(t)}{n_{\mathrm{C}}}\\ &\quad-\frac{1}{2}\cdot\frac{c_{\mathrm{H}}\cdot n_{\mathrm{O}}}{n_{\mathrm{H}}}\cdot m_{sf}(t)-\mathrm{O}_2(t)\cdot m_g(t)\end{aligned}$$

These equations are implemented in SIMULINK and verified through steady state and step tests using real measurement data from the plant when wood pellets are combusted. It is found that the non-linear equations describe the system acceptable with only small deviations from the real plant.

Furthermore the parameters which are depended on the solid fuel is changed to them of wheat and a model is found when wheat is combusted in the stoker. This model is also verified with acceptable results through a step test.

Chapter 7

Linear Model of the Stoker System

The non-linear models, just derived in the previous chapter, can be linearized to create a linear model of the stoker system, from which a controller can be designed. This linear model is only valid in a limited area as the linearization take its starting point from a set of predefined operation points. The linearization is done by a first order Taylor series which in general for one variable is written as:

$$f(\bar{x},\hat{x}) = f(\bar{x}) + \frac{\partial}{\partial x}\cdot f(x)\Big|_{x=\bar{x}}\cdot\hat{x} + \text{rest}(\hat{x}) \tag{7.1}$$

where $\bar{}$ indicate a steady-state value and $\hat{}$ indicates a small signal value. The term rest($\hat{x}$) goes toward zero faster than the first order term when $\hat{x}$ goes toward zero. The rest-term is disregarded in the linearization and Equation (7.1) can then be written as:

$$f(\bar{x},\hat{x}) \approx f(\bar{x}) + \ f_x(x)\Big|_{x=\bar{x}}\cdot\hat{x} \tag{7.2}$$

To complete the linearization the steady-state values are subtracted from Equation (7.2) which gives:

$$\begin{aligned} f(\bar{x},\hat{x}) - f(\bar{x}) &= f(\bar{x}) + \ f_x(x)\Big|_{x=\bar{x}}\cdot\hat{x} - f(\bar{x}) \Leftrightarrow \\ f(\hat{x}) &= f_x(x)\Big|_{x=\bar{x}}\cdot\hat{x} \end{aligned} \tag{7.3}$$

The variables in the stoker model are the state space variables, the system inputs and the disturbance. When the non-linear equations are inserted in Figure 7.3 the partial differentiations become rather complex to calculate. Maple version 9.0 is therefore used to differentiate the different expressions.

The linearization of the non-linear differential equations gives an overview of the dynamics of the system, which cannot be achieved from the non-linear differential equations alone. In the following sections each non-linear differential equation is linearized, but first two sets of operation points are found. One for when wood pellets are combusted and one when wheat is combusted.

7.1 Operations Points

The operation points for the linearization can be seen in Table 7.1 and Table 7.2 respectively when wood pellet and wheat are combusted. The operation points are found when the stoker is

Operation point:	$\bar{T}_w$	$\bar{T}_{bc}$	$\bar{T}_{gc}$	$\bar{T}_{eg}$
Value:	60°C	400°C	180°C	100°C
Operation point:	$\bar{m}_{sf}$	$\bar{m}_a$	$\bar{M}_{\mathrm{C,char}}$	$\bar{\mathrm{O}}_2$
Value:	$0.859 \cdot 10^{-3}$ kg/s	$4.531 \cdot 10^{-3}$ kg/s	$1.912 \cdot 10^{-3}$ kg	8%

Table 7.1: *The values of the operating points for the linearization when wood pellets are combusted.*

Operation point:	$\bar{T}_w$	$\bar{T}_{bc}$	$\bar{T}_{gc}$	$\bar{T}_{eg}$
Value:	70°C	450°C	200°C	115°C
Operation point:	$\bar{m}_{sf}$	$\bar{m}_a$	$\bar{M}_{\mathrm{C,char}}$	$\bar{\mathrm{O}}_2$
Value:	$1.054 \cdot 10^{-3}$ kg/s	$4.780 \cdot 10^{-3}$ kg/s	$1.912 \cdot 10^{-3}$ kg	12%

Table 7.2: *The values of the operating points for the linearization when wheat is combusted.*

in steady state. This means that when step test is preformed on the linearized model inaccuracies between the plant and the non-linear model can occur.

The operation values are chosen from plant outputs and by looking at the non-linear model.

Now that the operation points are found the linearization process can begin. To reduce some of the linear equations, the linear expressions regarding m_{C} and m_g are derived first.

7.2 Linearization of the Model Expressions

The partial differentiate of $m_{\mathrm{C}}(t)$ and $m_g(t)$ with respect to m_{sf} is rather complex, so they are derived in this section and a reduced notation is used in the rest of the linearization process of the non-linear differential equations. The two expressions are given be the following two equations.

$$\tilde{m}_{\mathrm{C}} = \left.\frac{\partial m_{\mathrm{C}}}{\partial m_{sf}}\right|_{m_{sf}=\bar{m}_{sf}} = \frac{2 \cdot c_{\mathrm{C}} \cdot c_{\mathrm{H}} \cdot \bar{m}_{sf}}{n_{\mathrm{H}} \cdot \left(\frac{2 \cdot c_{\mathrm{C}} \cdot \bar{m}_{sf}}{n_{\mathrm{C}}} + 2\right)} - \frac{2 \cdot {c_{\mathrm{C}}}^2 \cdot c_{\mathrm{H}} \cdot {\bar{m}_{sf}}^2}{n_{\mathrm{C}} \cdot n_{\mathrm{H}} \cdot \left(\frac{2 \cdot c_{\mathrm{C}} \cdot \bar{m}_{sf}}{n_{\mathrm{C}}} + 2\right)^2} \tag{7.4}$$

$$\tilde{m}_g = \left.\frac{\partial m_g}{\partial m_{sf}}\right|_{m_{sf}=\bar{m}_{sf}} = \frac{(n_{\mathrm{CO2}} - 2 \cdot n_{\mathrm{O}}) \cdot \tilde{m}_{\mathrm{C}}}{n_{\mathrm{C}}} + \frac{(n_{\mathrm{H2O}} - n_{\mathrm{O}}) \cdot c_{\mathrm{H}}}{2 \cdot n_{\mathrm{H}}} + \eta_{\mathrm{H2O}} + c_{sf,\mathrm{O}} \tag{7.5}$$

Also an expression for m_{C} and m_g in the operation point are derived to reduce the notation in the linearization process.

$$\bar{m}_{\mathrm{C}} = \frac{c_{\mathrm{C}} \cdot c_{\mathrm{H}} \cdot {\bar{m}_{sf}}^2}{n_{\mathrm{H}} \cdot \left(\frac{2 \cdot c_{\mathrm{C}} \cdot \bar{m}_{sf}}{n_{\mathrm{C}}} + 2\right)} + \chi \cdot \gamma_1 \cdot \bar{m}_a + \gamma_2 \cdot \bar{M}_{\mathrm{C,char}} \tag{7.6}$$

$$\bar{m}_g = \frac{(n_{\mathrm{CO2}} - 2 \cdot n_{\mathrm{O}}) \cdot \bar{m}_{\mathrm{C}}}{n_{\mathrm{C}}} + \left(\frac{(n_{\mathrm{H2O}} - n_{\mathrm{O}}) \cdot c_{\mathrm{H}}}{2 \cdot n_{\mathrm{H}}} + \eta_{\mathrm{H2O}} + c_{sf,\mathrm{O}}\right) \cdot \bar{m}_{sf} + (c_{\mathrm{N}} + c_{a,\mathrm{O}}) \cdot \bar{m}_a \tag{7.7}$$

The linearization of the non-linear differential equations can now begin. Each term in the linearized equation is named by letters and a consecutive number.

7.3 Linearization of the Energy Balance Equations

In this section the first four non-linear differential equations are linearized.

7.3.1 Linearization of the Water Equation

The non-linear differential equation for the water temperature (Equation (6.31)) is linearized as just described in the beginning of this chapter. Equation (7.8) shows the non-linear equation whereas Equation (7.9) shows the linear equation for the water temperature.

$$\begin{aligned} M_w \cdot c_w \cdot \frac{\mathrm{d}T_w(t)}{\mathrm{dt}} &= m_w \cdot c_{iw} \cdot T_{iw}(t) + \epsilon_{bcw} \cdot \sigma \cdot A_{bcw} \cdot \left(T_{bc}(t)^4 - T_w(t)^4\right) \\ &\quad + \alpha_{bc} \cdot A_{bcw} \cdot (T_{bc}(t) - T_w(t)) + \alpha_{gc} \cdot A_{gcw} \cdot (T_{gc}(t) - T_w(t)) \\ &\quad + \alpha_{eg} \cdot A_{egw} \cdot (T_{eg}(t) - T_w(t)) - m_w \cdot c_w \cdot T_w(t) \end{aligned} \tag{7.8}$$

$$\begin{aligned} \overbrace{M_w \cdot c_w}^{tw_1} \cdot \frac{\mathrm{d}\hat{T}_w(t)}{\mathrm{dt}} &= \overbrace{m_w \cdot c_{iw}}^{tw_2} \cdot \hat{T}_{iw}(t) + \overbrace{\left(4 \cdot \epsilon_{bcw} \cdot \sigma \cdot \bar{T}_{bc}{}^3 + \alpha_{bc}\right) \cdot A_{bcw}}^{tw_3} \cdot \hat{T}_{bc}(t) \\ &\quad + \overbrace{\alpha_{gc} \cdot A_{gcw}}^{tw_4} \cdot \hat{T}_{gc}(t) + \overbrace{\alpha_{eg} \cdot A_{egw}}^{tw_5} \cdot \hat{T}_{eg}(t) \\ &\quad - \Big\{ \overbrace{\left(4 \cdot \epsilon_{bcw} \cdot \sigma \cdot \bar{T}_w{}^3 + \alpha_{bc}\right) \cdot A_{bcw}}^{tw_{6.1}} \\ &\quad + \overbrace{\alpha_{gc} \cdot A_{gcw} + \alpha_{eg} \cdot A_{egw} + m_w \cdot c_w}^{tw_{6.2}} \Big\} \cdot \hat{T}_w(t) \end{aligned} \tag{7.9}$$

A linear expression for the change in the water temperature is now found.

7.3.2 Linearization of the Burning Chamber Equation

The non-linear differential equation for the gas temperature in the burning chamber (Equation (6.42)) is linearized as described in the beginning of this chapter. Equation (7.10) shows the non-linear equation whereas Equation (7.11) shows the linear equation for the gas temperature in the burning chamber.

$$\begin{aligned} (M_{bc} \cdot c_{bc} + M_{cp} \cdot c_{cp}) \cdot \frac{\mathrm{d}T_{bc}(t)}{\mathrm{dt}} &= m_a(t) \cdot c_a \cdot T_a + m_{\mathrm{C}}(t) \cdot \left(\frac{1}{4} \cdot h_{c,\mathrm{I}} + \frac{3}{4} \cdot h_{c,\mathrm{II}}\right) \\ &\quad + \frac{1}{4} \cdot \frac{m_{\mathrm{C}}(t)}{n_{\mathrm{C}}} \cdot n_{\mathrm{CO}} \cdot h_{c,\mathrm{V}} + c_{\mathrm{H}} \cdot m_{sf}(t) \cdot h_{c,\mathrm{VI}} \\ &\quad - m_g(t) \cdot c_{bc} \cdot T_{bc}(t) \\ &\quad - \epsilon_{bcw} \cdot \sigma \cdot A_{bcw} \cdot (T_{bc}(t)^4 - T_w(t)^4) \\ &\quad - \alpha_{bc} \cdot A_{bcw} \cdot (T_{bc}(t) - T_w(t)) \end{aligned} \tag{7.10}$$

$$
\begin{aligned}
\overbrace{(M_{bc} \cdot c_{bc} + M_{cp} \cdot c_{cp})}^{tbc_1} \cdot \frac{\mathrm{d}\hat{T}_{bc}(t)}{\mathrm{dt}} &= -\overbrace{\left(\left(4 \cdot \epsilon_{bcw} \cdot \sigma \cdot {\bar{T}_{bc}}^3 + \alpha_{bc}\right) \cdot A_{bcw} + \bar{m}_g \cdot c_{bc}\right)}^{tbc_3} \cdot \hat{T}_{bc}(t) \\
&\quad + \overbrace{\left(\left(4 \cdot \epsilon_{bcw} \cdot \sigma \cdot {\bar{T}_{w}}^3 + \alpha_{bc}\right) \cdot A_{bcw}\right)}^{tbc_6} \cdot \hat{T}_{w}(t) \\
&\quad + \Bigg\{ \overbrace{\tilde{m}_{\mathrm{C}} \cdot \left(\frac{h_{c,\mathrm{I}} + 3 \cdot h_{c,\mathrm{II}}}{4}\right) + \frac{\tilde{m}_{\mathrm{C}} \cdot n_{\mathrm{CO}} \cdot h_{c,\mathrm{V}}}{4 \cdot n_{\mathrm{C}}} + c_{\mathrm{H}} \cdot h_{c,\mathrm{VI}}}^{tbc_{7.1}} \\
&\quad - \overbrace{\tilde{m}_g \cdot c_{bc} \cdot \bar{T}_{bc}}^{tbc_{7.2}} \Bigg\} \cdot \hat{m}_{sf}(t) \\
&\quad + \Bigg\{ \overbrace{c_a \cdot T_a + \left(\frac{h_{c,\mathrm{I}} + 3 \cdot h_{c,\mathrm{II}}}{4} + \frac{n_{\mathrm{CO}} \cdot h_{c,\mathrm{V}}}{4 \cdot n_{\mathrm{C}}}\right) \cdot \chi \cdot \gamma_1}^{tbc_{8.1}} \\
&\quad - \overbrace{\left(\frac{(n_{\mathrm{CO_2}} - 2 \cdot n_{\mathrm{O}}) \cdot \chi \cdot \gamma_1}{n_{\mathrm{C}}} + c_{\mathrm{N}} + c_{a,\mathrm{O}}\right) \cdot c_{bc} \cdot \bar{T}_{bc}}^{tbc_{8.2}} \Bigg\} \cdot \hat{m}_a(t) \\
&\quad + \Bigg\{ \overbrace{\left(\frac{h_{c,\mathrm{I}} + 3 \cdot h_{c,\mathrm{II}}}{4} + \frac{n_{\mathrm{CO}} \cdot h_{c,\mathrm{V}}}{4 \cdot n_{\mathrm{C}}}\right) \cdot \gamma_2}^{tbc_{9.1}} \\
&\quad - \overbrace{\frac{(n_{\mathrm{CO_2}} - 2 \cdot n_{\mathrm{O}}) \cdot c_{bc} \cdot \bar{T}_{bc}}{n_c} \cdot \gamma_2}^{tbc_{9.2}} \Bigg\} \cdot \hat{M}_{\mathrm{C,char}}(t)
\end{aligned} \tag{7.11}
$$

A linear expression for the change in the gas temperature in the burning chamber is now found.

7.3.3 Linearization of the Gas Chamber Equation

The non-linear differential equation for the gas temperature in the gas chamber (Equation (6.48)) is linearized as described in the beginning of this chapter. Equation (7.12) shows the non-linear equation whereas Equation (7.13) shows the linear equation for the gas temperature in the gas chamber.

$$
\begin{aligned}
M_{gc} \cdot c_{gc} \cdot \frac{\mathrm{d}T_{gc}(t)}{\mathrm{dt}} &= m_g(t) \cdot (c_{bc} \cdot T_{bc}(t) - c_{gc} \cdot T_{gc}(t)) \\
&\quad - \alpha_{gc} \cdot A_{gcw} \cdot (T_{gc}(t) - T_w(t))
\end{aligned} \tag{7.12}
$$

$$
\begin{aligned}
\overbrace{M_{gc} \cdot c_{gc}}^{tgc_1} \cdot \frac{\mathrm{d}\hat{T}_{gc}(t)}{\mathrm{dt}} &= \overbrace{\bar{m}_g \cdot c_{bc}}^{tgc_3} \cdot \hat{T}_{bc}(t) - \overbrace{(\bar{m}_g \cdot c_{gc} + \alpha_{gc} \cdot A_{gcw})}^{tgc_4} \cdot \hat{T}_{gc}(t) + \overbrace{\alpha_{gc} \cdot A_{gcw}}^{tgc_6} \cdot \hat{T}_w(t) \\
&\quad + \overbrace{\left(c_{bc} \cdot \bar{T}_{bc} - c_{gc} \cdot \bar{T}_{gc}\right) \cdot \tilde{m}_g}^{tgc_7} \cdot \hat{m}_{sf}(t) \\
&\quad + \overbrace{\left(\frac{(n_{\mathrm{CO_2}} - 2 \cdot n_{\mathrm{O}}) \cdot \chi \cdot \gamma_1}{n_{\mathrm{C}}} + c_{\mathrm{N}} + c_{a,\mathrm{O}}\right) \cdot \left(c_{bc} \cdot \bar{T}_{bc} - c_{gc} \cdot \bar{T}_{gc}\right)}^{tgc_8} \cdot \hat{m}_a(t) \\
&\quad + \overbrace{\left(\frac{(n_{\mathrm{CO_2}} - 2 \cdot n_{\mathrm{O}}) \cdot \gamma_2}{n_{\mathrm{C}}}\right) \cdot \left(c_{bc} \cdot \bar{T}_{bc} - c_{gc} \cdot \bar{T}_{gc}\right)}^{tgc_9} \cdot \hat{M}_{\mathrm{C,char}}(t)
\end{aligned} \tag{7.13}
$$

A linear expression for the change in the gas temperature in the gas chamber is now found.

7.3.4 Linearization of the Exhaust Gas Equation

The non-linear differential equation for the exhaust gas temperature (Equation (6.54)) is linearized as described in the beginning of this chapter. Equation (7.14) shows the non-linear equation whereas Equation (7.15) shows the linear equation for the exhaust gas temperature.

$$\begin{aligned} M_{eg} \cdot c_{eg} \cdot \frac{\mathrm{d}T_{eg}(t)}{\mathrm{dt}} &= m_g(t) \cdot (c_{gc} \cdot T_{gc}(t) - c_{eg} \cdot T_{eg}(t)) \\ &- \alpha_{eg} \cdot A_{egw} \cdot (T_{eg}(t) - T_w(t)) \end{aligned} \tag{7.14}$$

$$\begin{aligned} \overbrace{M_{eg} \cdot c_{eg}}^{teg_1} \cdot \frac{\mathrm{d}\hat{T}_{eg}(t)}{\mathrm{dt}} &= \overbrace{\bar{m}_g \cdot c_{gc}}^{teg_4} \cdot \hat{T}_{gc}(t) - \overbrace{(\bar{m}_g \cdot c_{eg} + \alpha_{eg} \cdot A_{egw})}^{teg_5} \cdot \hat{T}_{eg}(t) + \overbrace{\alpha_{eg} \cdot A_{egw}}^{teg_6} \cdot \hat{T}_w(t) \\ &+ \overbrace{\left(c_{gc} \cdot \bar{T}_{gc} - c_{eg} \cdot \bar{T}_{eg}\right) \cdot \tilde{m}_g}^{teg_7} \cdot \hat{m}_{sf}(t) \\ &+ \overbrace{\left(\frac{(n_{\mathrm{CO_2}} - 2 \cdot n_{\mathrm{O}}) \cdot \chi \cdot \gamma_1}{n_{\mathrm{C}}} + c_{\mathrm{N}} + c_{a,\mathrm{O}}\right) \cdot \left(c_{gc} \cdot \bar{T}_{gc} - c_{eg} \cdot \bar{T}_{eg}\right)}^{teg_8} \cdot \hat{m}_a(t) \\ &+ \overbrace{\left(\frac{(n_{\mathrm{CO_2}} - 2 \cdot n_{\mathrm{O}}) \cdot \gamma_2}{n_{\mathrm{C}}}\right) \cdot \left(c_{gc} \cdot \bar{T}_{gc} - c_{eg} \cdot \bar{T}_{eg}\right)}^{teg_9} \cdot \hat{M}_{\mathrm{C,char}}(t) \end{aligned} \tag{7.15}$$

A linear expression for the change in the exhaust gas temperature is now found.

7.4 Linearization of the Mass Balance Equations

In this section the last two non-linear differential equations are linearized.

7.4.1 Linearization of the Solid Fuel Equation

The non-linear differential equation for the mass of solid fuel (Equation (6.58)) is linearized as described in the beginning of this chapter. Equation (7.16) shows the non-linear equation whereas Equation (7.17) shows the linear equation for the mass of the solid fuel.

$$\frac{\mathrm{d}M_{\mathrm{C,char}}(t)}{\mathrm{dt}} = \zeta_{\mathrm{char}}(t) \cdot c_{\mathrm{C}} \cdot m_{sf}(t) - \chi \cdot m_a(t) \cdot \gamma_1 - M_{\mathrm{C,char}}(t) \cdot \gamma_2 \tag{7.16}$$

$$\frac{\mathrm{d}\hat{M}_{\mathrm{C,char}}(t)}{\mathrm{dt}} = \overbrace{(-\tilde{m}_{\mathrm{C}} + c_{\mathrm{C}})}^{mchar_7} \cdot \hat{m}_{sf}(t) - \overbrace{\chi \cdot \gamma_1}^{mchar_8} \cdot \hat{m}_a(t) - \overbrace{\gamma_2}^{mchar_9} \cdot \hat{M}_{\mathrm{C,char}} \tag{7.17}$$

A linear expression for the change in the mass of solid fuel is now found.

7.4.2 Linearization of the O_2 Equation

The non-linear differential equation for the O_2-level (Equation (6.66)) is linearized as described in the beginning of this chapter. Equation (7.18) shows the non-linear equation whereas Equation

(7.19) shows the linear equation for the O_2-level.

$$\begin{aligned} M_{\text{total}} \cdot \frac{\mathrm{dO_2}(t)}{\mathrm{dt}} &= c_{a,\mathrm{O}} \cdot m_a(t) + c_{sf,\mathrm{O}} \cdot m_{sf}(t) - 2 \cdot \frac{n_{\mathrm{O}} \cdot m_{\mathrm{C}}(t)}{n_{\mathrm{C}}} \\ &\quad -\frac{1}{2} \cdot \frac{c_{\mathrm{H}} \cdot n_{\mathrm{O}}}{n_{\mathrm{H}}} \cdot m_{sf}(t) - \mathrm{O_2}(t) \cdot m_g(t) \end{aligned} \tag{7.18}$$

$$\begin{aligned} \overbrace{M_{\text{total}}}^{o2_1} \cdot \frac{\mathrm{d\hat{O}_2}(t)}{\mathrm{dt}} &= \overbrace{\left(c_{sf,\mathrm{O}} - \frac{2 \cdot n_{\mathrm{O}} \cdot \tilde{m}_{\mathrm{C}}}{n_{\mathrm{C}}} - \frac{c_{\mathrm{H}} \cdot n_{\mathrm{O}}}{2 \cdot n_{\mathrm{H}}} - \bar{\mathrm{O}}_2 \cdot \tilde{m}_g\right)}^{o2_7} \cdot \hat{m}_{sf}(t) \\ &\quad + \overbrace{\left(c_{a,\mathrm{O}} - \frac{2 \cdot n_{\mathrm{O}} \cdot \chi \cdot \gamma_1}{n_{\mathrm{C}}} - \left(\frac{(n_{\mathrm{CO_2}} - 2 \cdot n_{\mathrm{O}}) \cdot \chi \cdot \gamma_1}{n_{\mathrm{C}}} + c_{\mathrm{N}} + c_{a,\mathrm{O}}\right) \cdot \bar{\mathrm{O}}_2\right)}^{o2_8} \cdot \hat{m}_a(t) \\ &\quad - \overbrace{\frac{\left(2 \cdot n_{\mathrm{O}} + (n_{\mathrm{CO_2}} - 2 \cdot n_{\mathrm{O}}) \cdot \bar{\mathrm{O}}_2\right) \cdot \gamma_2}{n_{\mathrm{C}}}}^{o2_9} \cdot \hat{M}_{\mathrm{C,char}}(t) - \overbrace{\bar{m}_g}^{o2_{10}} \cdot \hat{\mathrm{O}}_2(t) \end{aligned} \tag{7.19}$$

A linear expression for the change in the O_2-level is now found. The six linear differential equations needed to create a linear model of the system is now derived. This linear model has to be validated to see the accuracy of the model.

7.5 Verification of the Linear Model

The linear model is verified using the non-linear model. This is done by comparing the six states from the two models. The measurable states in the system are also compared with the linear model. This is done to show how good the linear system can simulate the plant. The linear model when wood pellets are combusted is first verified, after that is the same verification made when wheat is combusted. In the following figures is the non-linear model given by a blue line, the linear model is given by a red line and the measured states are given by a yellow line.

In Figure 7.1 the linear model output from the water temperature, exhaust gas temperature and O_2-level are shown along with the non-linear model output and the plant measurements when wood pellets are used as solid fuel.

The water temperature shown in the first graph in Figure 7.1. Here the two model outputs and the actual output are very close to each other, and the linear model for the water temperature is therefore accepted. The small difference in the two models can be explained by the chosen operation points. The linear model and the plant output is also close to each other, which is good as this is one of the variables that is desirable to control.

The exhaust gas is also simulated for the linear model. This has been compared to the non-linear model and the plant measurement, as shown in the second graph in Figure 7.1. The figure shows that the linear model has a little less dynamics compared to the non-linear model. But the linear model is still accepted, as the temperature from the two other chambers influences the exhaust gas which can explain the inaccuracy. The linear model output is also a little below the plant output but this is accepted as the exhaust gas temperature is not a critical parameter that the system has to be controlled by.

The O_2-level is shown in the third graph in Figure 7.1. The linear model has less dynamics when a step in the supply air is performed compared to the non-linear model, otherwise the two models are almost identical. The plant measurement is also shown in the figure and it can be seen that the linear model of the O_2-level is close to this value also.

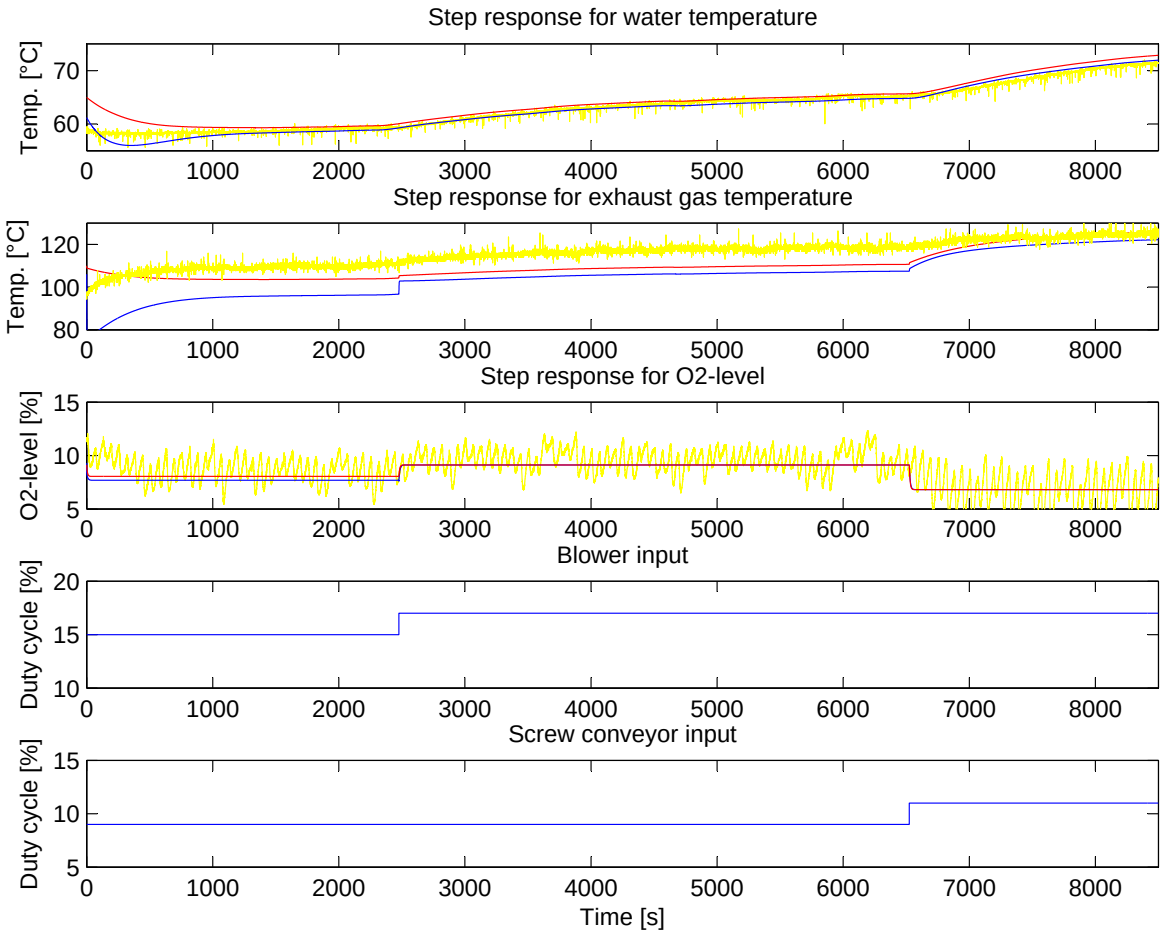

Figure 7.1: *Simulation of the linear model (red) and the non-linear model (blue) and the plant measurement (yellow) with a step response in both the solid fuel and the supply air for the water temperature, exhaust gas temperature and O_2-level.*

In Figure 7.2 the linear model output from the mass of solid fuel, burning chamber temperature and gas chamber temperature is shown along with the non-linear model output when wood pellets are used as solid fuel.

The first graph in Figure 7.2 shows the simulation of the mass of the solid fuel. The linear model and the non-linear model have an output just above 0.45 kg. The linear model output is below the non-linear model output but the dynamics fit both when a step in the supply air and in the solid fuel is performed. The linear model of the mass of the solid fuel is however accepted as the inaccuracy is only a few g and due to the operation points. The mass of the solid fuel has influence on all the other simulated states. Moreover to fit the mass of the solid fuel to the linear model, it is also fitted so the O_2-level fits as best as possible. This influences the accuracy of the temperatures inside the stoker, thus the linear model is less accurate. This is chosen as the O_2-level is assumed to be more important to be close to the plant output compared to the exhaust gas temperature.

In the second graph in Figure 7.2 it can be seen that the linear model for the burning chamber temperature has less dynamics when a step in the supply air is performed and more dynamics when a step in the solid fuel is performed compared to the non-liner model. The two models are however close to each other around the operation point as expected. The little difference appear because the mass of the solid fuel is used to calculate the temperature which is a bit inaccurate.

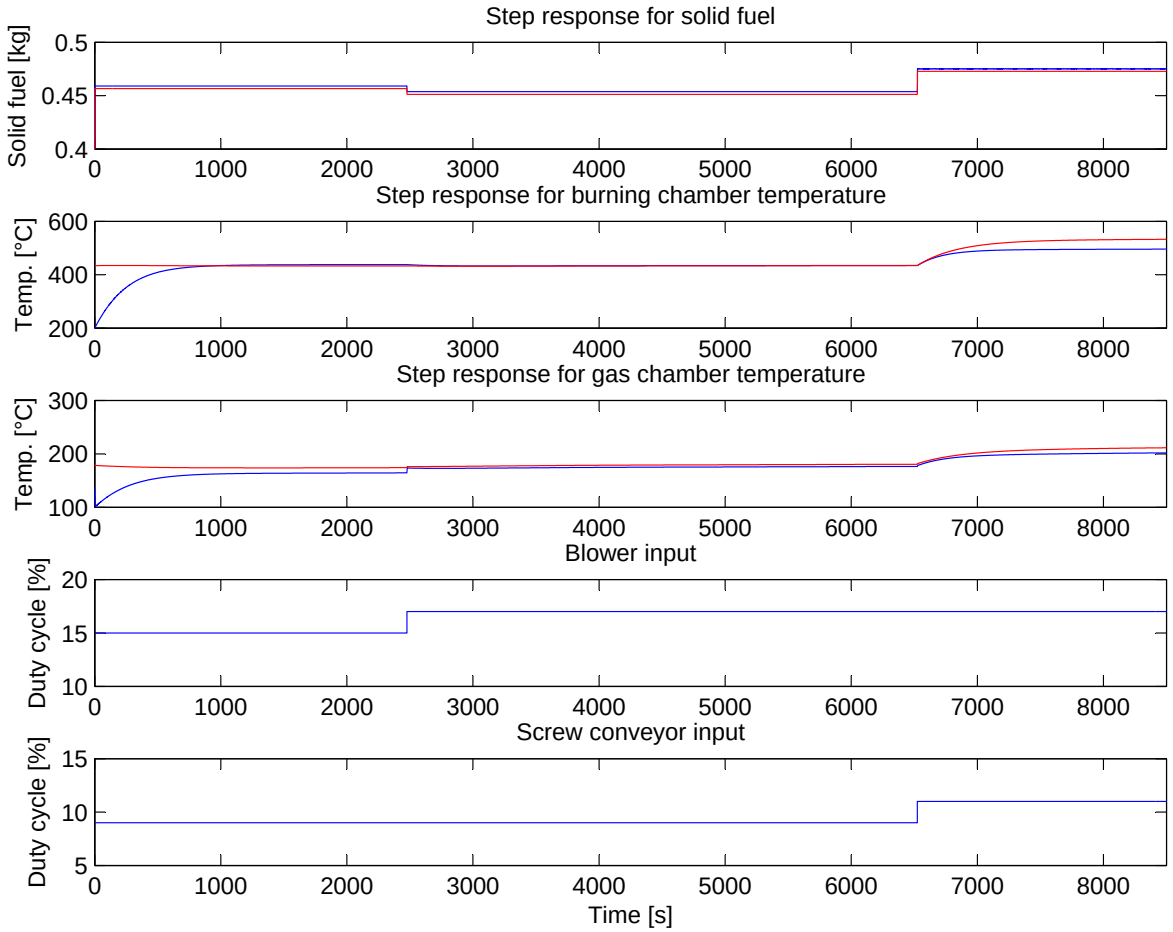

Figure 7.2: *The linear model (red) and the non-linear model (blue) simulated with a step response in both solid fuel and supply air for the mass of solid fuel, burning chamber temperature and gas chamber temperature.*

The third graph in Figure 7.2 is the temperature simulated in the gas chamber. The linear and the non-linear model are close to each other. The linear model has less dynamics when a step in the supply air is performed compared to the non-linear model. Again the mass of the solid fuel is the cause of the inaccuracy as a difference between the two models in the mass of solid fuel will influence the temperature. The linear model is however accepted although there is a inaccuracy.

In Figure 7.3 and Figure 7.4 the linear model output from the six states are seen along with the non-linear model output and measurement data from the plant when wheat is used as solid fuel. Overall can it be seen that the linear model fits the non-linear model well. The considerations made for the two previous figures (Figure 7.1 and Figure 7.2) where wood pellets where used as solid fuel is also valid when wheat is used as solid fuel, which can be seen in Figure 7.3 and Figure 7.4.

Overall the simulation of the linear models are close to the non-linear models, therefore the linear models are verified satisfactory. The operation points for the mass of the solid fuel and the supply air is chosen so the linear models of the O_2-levels fit to the measured O_2-levels as close as possible. This is chosen, as the O_2-level is one of the variables which the plant is controlled by. When the linear models moves away from the different operation points the dynamics are varying compared to the non-linear models. This is expected however as the linear models are derived around these operation points. The simulated water temperature is also very close to

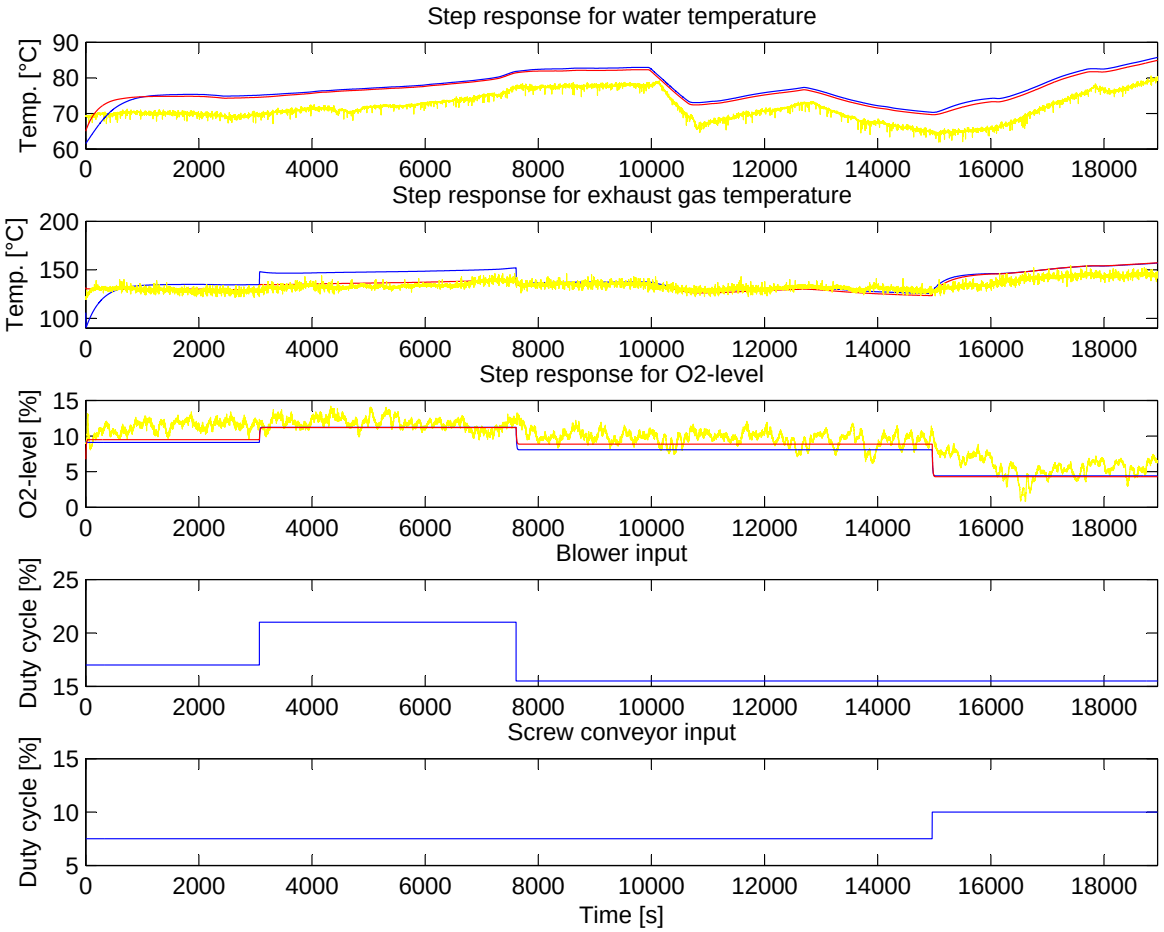

Figure 7.3: *Simulation of the linear model (red) and the non-linear model (blue) and the plant measurement (yellow) with a step response in both the solid fuel and the supply air for the water temperature, exhaust gas temperature and O_2-level.*

the measured. This is important as this is the other variable which the plant is controlled by.

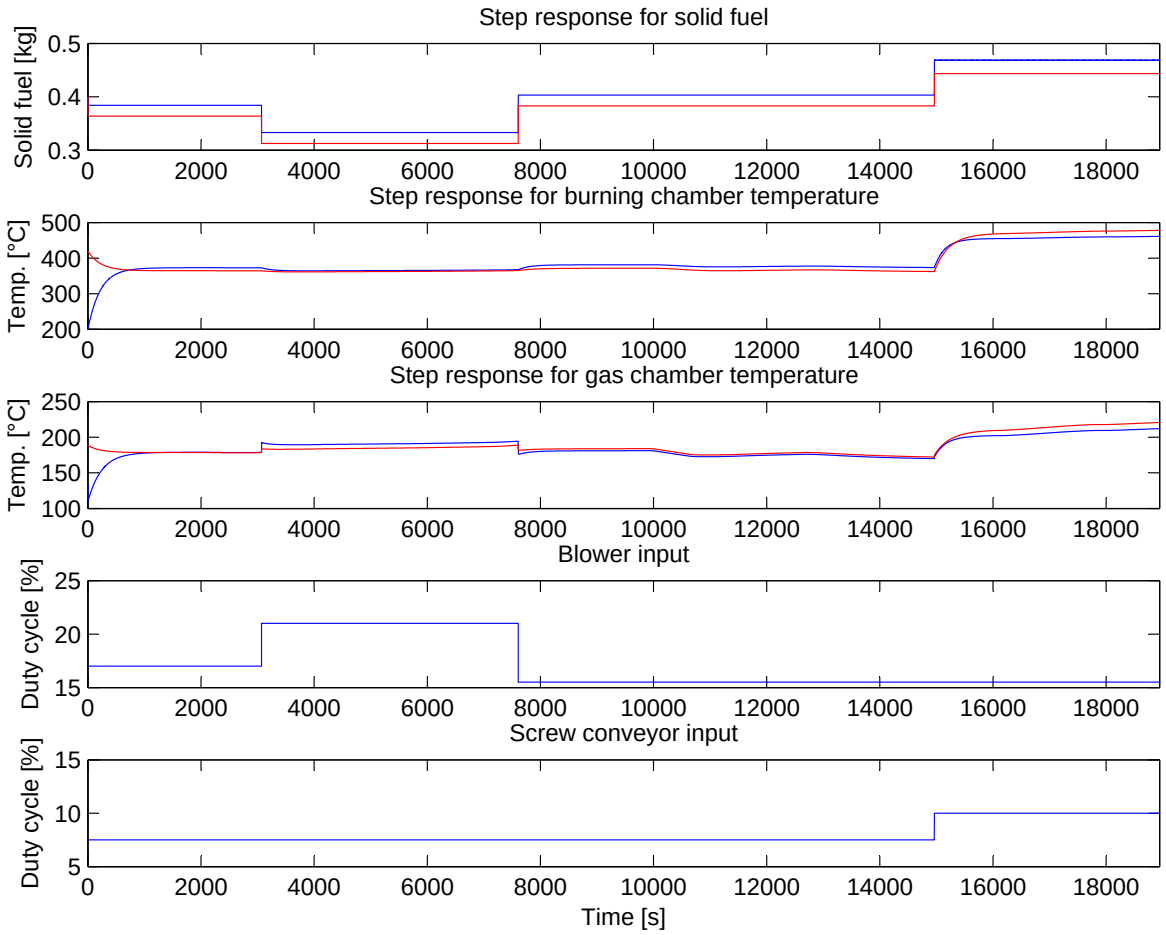

Figure 7.4: *The linear model (red) and the non-linear model (blue) simulated with a step response in both solid fuel and supply air for the mass of solid fuel, burning chamber temperature and gas chamber temperature.*

Chapter 8

State Space Model of the Stoker System

In the controller design it is advantageous with a state space model of the system. The state space model can be set up directly from the linear differential equations derived in Chapter 7. In the state space model the linear differential equations are set up in a matrix form. In the continuous time-variant case is the state space model given by Equation (8.1) including both process and measurement noise.

$$\begin{aligned} \dot{\mathbf{x}}(t) &= \mathbf{A}\mathbf{x}(t) + \mathbf{B}\mathbf{u}(t) + \mathbf{G}\mathbf{w}(t) \\ \mathbf{y}(t) &= \mathbf{C}\mathbf{x}(t) + \mathbf{D}\mathbf{u}(t) + \mathbf{H}\mathbf{v}(t) \end{aligned} \tag{8.1}$$

where matrices are given by capital letters in bold and vectors are given in small letters in bold. A function description for each matrix and vector is seen in Table 8.1 along with their dimensions.

Letter	Description	Dimension
A	System matrix	# states × # states
B	Input matrix	# states × # inputs
C	Output matrix	# outputs × # states
D	Direct matrix	# outputs × # inputs
G	Process noise coupling matrix	# states × # states
H	Measurement noise coupling matrix	# outputs × # outputs
x	State vector	# states × 1
u	Input vector	# input × 1
y	Output vector	# output × 1
w	Process noise vector	# states × 1
v	Measurement noise vector	# output × 1

Table 8.1: *Used notation in the state space model.*

A block diagram of Equation (8.1) can be seen in Figure 8.1.

In the linear model derived in Chapter 7 terms are multiplied with the derived state variables. This means that Equation (8.1) cannot be used directly, as it has to be rewritten so these terms are removed from the derived state variables. This is done as in Equation (8.2). Moreover **D** is

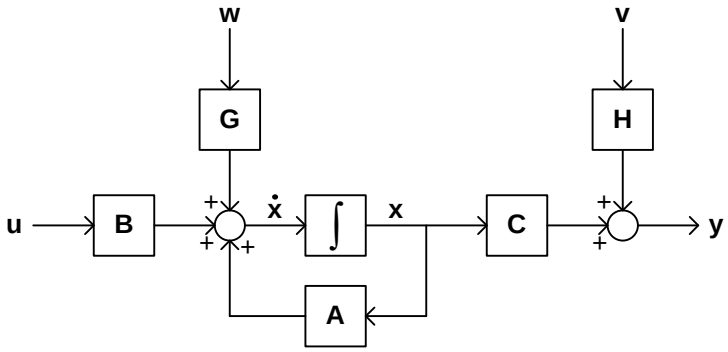

Figure 8.1: *Block diagram of a continuous time-variant state space model.*

set to zero as there are no direct controllable outputs in the system.

$$\begin{aligned} \dot{\mathbf{x}}(t) &= \mathbf{M}^{-1}\tilde{\mathbf{A}}\mathbf{x}(t) + \mathbf{M}^{-1}\tilde{\mathbf{B}}\mathbf{u}(t) + \mathbf{M}^{-1}\tilde{\mathbf{G}}\mathbf{w}(t) \\ \mathbf{y}(t) &= \mathbf{C}\mathbf{x}(t) + \mathbf{H}\mathbf{v}(t) \end{aligned} \tag{8.2}$$

where $\mathbf{M}$ contains the terms which has to be removed.

The matrices and vectors in Equation (8.2) are now set up. The shortening terms used in the following refers to the terms in the linear equations in Chapter 7. $\mathbf{x}$ is the state vector which contains the state variables.

$$\mathbf{x} = \begin{bmatrix} T_w & T_{bc} & T_{gc} & T_{eg} & M_{\mathrm{c,char}} & \mathrm{O}_2 \end{bmatrix}^\top \tag{8.3}$$

$\mathbf{M}$ contains the terms multiplied on the derived state vector.

$$\mathbf{M} = \begin{bmatrix} tw_1 & 0 & 0 & 0 & 0 & 0 \\ 0 & tbc_1 & 0 & 0 & 0 & 0 \\ 0 & 0 & tgc_1 & 0 & 0 & 0 \\ 0 & 0 & 0 & teg_1 & 0 & 0 \\ 0 & 0 & 0 & 0 & 1 & 0 \\ 0 & 0 & 0 & 0 & 0 & o2_1 \end{bmatrix} \tag{8.4}$$

$\tilde{\mathbf{A}}$ contains the constants multiplied on the state vector.

$$\tilde{\mathbf{A}} = \begin{bmatrix} -tw_6 & tw_3 & tw_4 & tw_5 & 0 & 0 \\ tbc_6 & -tbc_3 & 0 & 0 & tbc_9 & 0 \\ tgc_6 & tgc_3 & -tgc_4 & 0 & tgc_9 & 0 \\ teg_6 & 0 & teg_4 & -teg_5 & teg_9 & 0 \\ 0 & 0 & 0 & 0 & -mchar_9 & 0 \\ 0 & 0 & 0 & 0 & -o2_9 & -02_{10} \end{bmatrix} \tag{8.5}$$

$\mathbf{u}$ is the input vector which contains both the inputs and the disturbance.

$$\mathbf{u} = \begin{bmatrix} m_{sf} & m_a & T_{iw} \end{bmatrix}^\top \tag{8.6}$$

$\tilde{\mathbf{B}}$ contains the constants multiplied on the input vector.

$$\tilde{\mathbf{B}} = \begin{bmatrix} 0 & 0 & tw_2 \\ tbc_7 & tbc_8 & 0 \\ tgc_7 & tgc_8 & 0 \\ teg_7 & teg_8 & 0 \\ mchar_7 & -mchar_8 & 0 \\ 02_7 & 02_8 & 0 \end{bmatrix} \tag{8.7}$$

$\tilde{\mathbf{G}}$ is the noise coupling matrix which weight how much process noise each state influences the other states. $\tilde{\mathbf{G}}$ is set to the identity matrix which means that the process noise is uncorrelated. The following is valid for the process noise.

$$E\left\langle \mathbf{w}(t) \right\rangle = 0 \tag{8.8}$$

$$E\left\langle \mathbf{w}(t)\mathbf{w}^{\top}(s) \right\rangle = \delta(t-s)\mathbf{Q}_n(t) \tag{8.9}$$

where E is the expected value and δ is the Dirac-delta function. The diagonal in the $\mathbf{Q}_n$ matrix is the variance of the state process noise and the other elements are the cross noise between the states which is zero. The T_{bc}, T_{gc}, T_{eg} and $M_{\mathrm{c,char}}$ states are added process noise. The process noise for the three temperatures inside the stoker is set to 2°C as it is observed that the exhaust gas vary that mush when both actuators are running with fixed duty cycle. The process noise for $M_{\mathrm{c,char}}$ is set to 0.01 kg as it sounds reasonable that the molehill vary that much with fixed duty cycle on the actuators. $\mathbf{Q}_n$ is then given by:

$$\mathbf{Q}_n = \begin{bmatrix} 0 & 0 & 0 & 0 & 0 & 0 \\ 0 & 2^2 & 0 & 0 & 0 & 0 \\ 0 & 0 & 2^2 & 0 & 0 & 0 \\ 0 & 0 & 0 & 2^2 & 0 & 0 \\ 0 & 0 & 0 & 0 & 0.01^2 & 0 \\ 0 & 0 & 0 & 0 & 0 & 0 \end{bmatrix} \tag{8.10}$$

$\mathbf{y}$ is the output vector which contains the outputs.

$$\mathbf{y} = \begin{bmatrix} T_w & \mathrm{O}_2 \end{bmatrix}^{\top} \tag{8.11}$$

$\mathbf{C}$ describes which output states the system has.

$$\mathbf{C} = \begin{bmatrix} 1 & 0 & 0 & 0 & 0 & 0 \\ 0 & 0 & 0 & 0 & 0 & \upsilon \end{bmatrix} \tag{8.12}$$

where υ is a constant which transforms the O_2-level given in a decimal mass percentage value to a volume percentage value.

$\tilde{\mathbf{H}}$ is the measurement noise coupling matrix which weight how much measurement noise each output influences the other outputs. $\tilde{\mathbf{H}}$ is set to the identity matrix which means that the measurement noise is uncorrelated. The following is valid for the measurement noise.

$$E\left\langle \mathbf{v}(t) \right\rangle = 0 \tag{8.13}$$

$$E\left\langle \mathbf{v}(t)\mathbf{v}^{\top}(s) \right\rangle = \delta(t-s)\mathbf{R}_n(t) \tag{8.14}$$

where E is the expected value and δ is the Dirac-delta function. The diagonal in the $\mathbf{R}_n$ matrix is the variance of the measurement noise and the other elements are the cross noise between the measurements which is zero. From the measurements on the system the measurement noise is estimated to be 1°C for the water temperature sensor and 0.1% for the lambda oxygen sensor. $\mathbf{R}_n$ is then given by:

$$\mathbf{R}_n = \begin{bmatrix} 1^2 & 0 \\ 0 & 0.1^2 \end{bmatrix} \tag{8.15}$$

A state space model of the system is now obtained. A verification of the state space model is not necessary as the state space model is found directly from the linear model by rewriting the equations on matrix form.

Part III

Controller

In this part the controller used on the stoker system is developed. This part consists of three chapters.

In the first chapter the controller approach is presented and two different strategies are discussed. After a short analysis of the two strategies is a final controller choice made.

The actual controller is derived in the second chapter. An optimal LQR controller is designed with a full order observer and integral control. A feedback gain is found both for when wood pellets are combusted and when wheat is combusted. The two feedback gains are found through simulations. Finally is the controller tested both in simulations and on the plant.

In the third chapter of this part a solid fuel estimator is designed. The solid fuel estimator is capable of estimating the composition of the solid fuel using the linear models, Kalman filters and measurement data. Combining the optimal controllers and the solid fuel estimator is a adaptive controller designed where the control input to the actuators is found from a weighting between the two LQR controllers and the solid fuel estimator.

Chapter 9

Controller Approach

A model based controller approach as described in Chapter 3 is chosen for controlling the stoker system. This means that the controller is designed from the mathematical model of the stoker system. Only linear control methods are used in this project, meaning that only the linear model is used in the controller design.

The purpose of the controller is to make the plant capable of tracking a reference signal for the water temperature and the O_2-level. The controller must suppress any load which may affect the plant. Moreover the controller must be able to detect when the solid fuel is changed and change the controller setup to the most optimal for the concerned solid fuel.

The designed controller is verified against the non-linear model in SIMULINK before it is implemented and tested on the plant. The quality of the designed controller can afterwards be compared with the original controller from Techno-Matic A/S and any advantages and disadvantages can be found.

When a model based controller is desirable various controller strategies are present which is described in the following section. Afterwards is the choice of controller presented.

9.1 Controller Strategies

Several different control strategies can be used to control the stoker. In this report two different strategies are investigated and the most suitable control strategy for the stoker is chosen and described in more details. The control strategies which are investigated are classical and modern control, these two strategies can then be divided into several sub strategies. The different strategies can be used to solve the same control problem but with different advantages and disadvantages.

9.1.1 Classical Control Strategies

Classical control is based on transfer functions. This is normally used on systems with only single input and output (SISO) or when the coupling factor in a multiple input and output (MIMO) system is small. Classical control uses feedback to stabilize the system through three terms; a proportional term, an integral term and a derivative term (PID).

PID Control

PID control is widely used in industrial control systems. A PID controller attempts to correct the error between the measured plant output and a desired reference. Usually the PID controller does not involve any criterion of optimality. By tuning the three terms in the controller, is it possible to design a controller for a specific process requirement. Robustness of stability is ensured by the skills of the person who design the controller [Franklin et al., 2002].

9.1.2 Modern Control Strategies

Modern control is based on ordinary differential equations organized in a matrix form which is also called a state space form. The state space form is advantageous when dealing with multiple inputs and outputs. The following theories within modern control are described: Optimal control, predictive control, robust control, adaptive control and intelligent control.

Optimal Control

The optimal control is often used in problems, where a predefined trajectory or reference is known. The principle of the optimal control is based on Calculus of Variations. This involves a performance function which weights the different states, and this performance function can then be minimized, to find the optimal solution. This is often implemented by using a linear quadratic regulator (LQR) [Zhou et al., 1996].

Predictive Control

Predictive control is a control algorithm based on the predictive model of the process. The model is used to predict the future output based on the historical information of the process as well as the future input. Predictive control is an algorithm of optimal control. It calculates future control action based on a performance function. The optimization of predictive control is limited to a moving time interval and is carried on continuously on-line. This is the key difference compared to traditional optimal control that uses a performance function to judge global optimization and the ability to handle constraints in the optimization due to the finite horizon [Bemporad et al., 1997].

Robust Control

Robust control is a controller design strategy that focuses on the robustness of the control algorithm. This strategy is useful when the parameters do not change or vary within known bounds, but in return control performance is guaranteed. The robust control strategy usually assumes that the knowledge of process dynamics and its variation ranges are known. Some algorithms may not need a precise process model but then require some kind of off-line identification [Zhou & Doyle, 1997].

Adaptive Control

An adaptive control system can be defined as a feedback control system intelligent enough to adjust its characteristics in a changing environment so as to operate in an optimal manner

according to some specified criteria. It will often be filters that are used to tune the parameters on-line in the controller, so that it will be adaptive [Sastry & Bodson, 1989].

Intelligent Control

There are different definitions regarding intelligent control, but it is referring to a control paradigm that uses various artificial intelligence techniques [Tay, 2007]. In this report the following methods will be described: Hybrid control, fuzzy control, and neural network.

Hybrid systems model non-trivial interactions of continuous phenomena (i.e., describable by a set of difference or differential equations) and discrete phenomena (i.e., asynchronous systems where the state transitions are initiated by discrete events as in automata or finite state machines). This leads to a formulation with several modes of operation, whereby in each mode the behaviour of the system is given by difference or differential equations [Bak, 2007].

Fuzzy control is built on mathematical foundations with fuzzy set theory. It represents knowledge or experience in a mathematical format that process and system dynamic characteristics can be described by fuzzy sets and fuzzy relational functions. Control decisions can be generated based on the fuzzy sets and functions with rules [Jantzen, 1991].

Neural network control is a control method using artificial neural networks. It has great potential since artificial neural networks are built on a firm mathematical foundation that includes versatile and well understood mathematical tools. Artificial neural networks are also used as one of the key elements in the Model-Free Adaptive controller's [B & J, 1999].

The first four control strategies are also algorithms of feedback control. If there is a mismatch between the model and the process, or if there is a control performance problem caused by the system uncertainties, these control strategies could compensate for the error or adjust the model parameters based on on-line identification.

9.2 Controller Choice

As a model of the actual stoker system is made and verified the knowledge of the system is high. This allows choosing a control strategy, where knowledge of the system is necessary. The stoker system can use different solid fuels. These different solid fuels will not have the same characteristics, which means that the parameters in the system will change. Furthermore the system has multiple inputs and outputs.

All these aspect is in favour of using a modern control theory, the time consumption is however much larger when dealing with modern control theory. The decisive factor when choosing between classical and modern control is the cross coupling between the inputs and outputs. If the cross coupling is small or can be disregarded the classical control strategy can be used with advantage. If the cross coupling is large the modern control strategy can be used with advantage. Therefore the cross coupling is investigated in the following subsection.

9.2.1 Cross Coupling

The dynamic coupling factor is used to describe the level of influence the cross coupling has. When this factor is much smaller than one, the cross coupling is small. The dynamic coupling

factor can be calculated by equation 9.1.

$$Q(s) = \frac{P_{12}(s) \cdot P_{21}(s)}{P_{11}(s) \cdot P_{22}(s)} \tag{9.1}$$

where P is transfer functions between the respective inputs and outputs. These transfer functions can be found from the state space model with the MATLAB-function `ss2tf`. This function use the matrices from the state space model, see Chapter 8. A model of the cross coupling between the transfer functions can be seen in Figure 9.1.

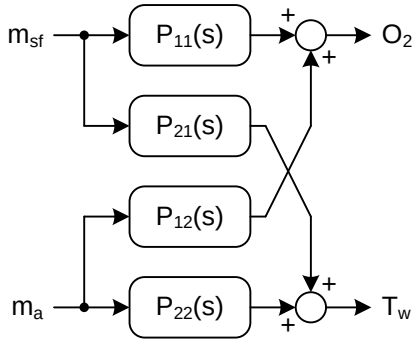

Figure 9.1: *Block diagram of the cross coupling between the transfer functions.*

A bode plot is made of the dynamic coupling factor Q(s), this is shown in Figure 9.2.

From the figure can it be seen that the decoupling between the inputs change with the frequency. When the magnitude is 0 dB, the cross coupling will have the same influence as the direct coupling. As shown in the bode plot will a controller that use the cross coupling be advantageous and it is therefore chosen for this project.

9.2.2 Modern control Choice

Both optimal and predictive control use an optimization function. This function will optimize the controller to be optimal to one set of parameters. But as the parameters change when a new solid fuel is used, this solution is not optimal for the stoker system.

The robust control strategy is also based on static parameters. This strategy is advantageous when large model uncertainties and large disturbances are present in the system. This means that the robust control strategy is based on the worst case scenario. This solution is therefore also not optimal for the stoker system.

Optimal, predictive and robust control can all three be used as a part of a solution along with some of the other strategies as intelligent or adaptive control.

Intelligent control could be implemented on the system. Especially hybrid control can be used to control the stoker system. However adaptive control is chosen as the primary controller strategy in this project. This is done as the stoker system will be able to handle changes in the solid fuels, without user input or predefined thresholds.

But what is meant by an adaptive controller? Intuitively, an adaptive controller is thus a controller that can modify its behaviour in response to changes in the dynamics of the process and the character of the disturbance [Åström & Wittenmark, 1995]. But as feedback also attempts to reduce the effects of disturbances and plant uncertainty, a clear definition of adaptive control is

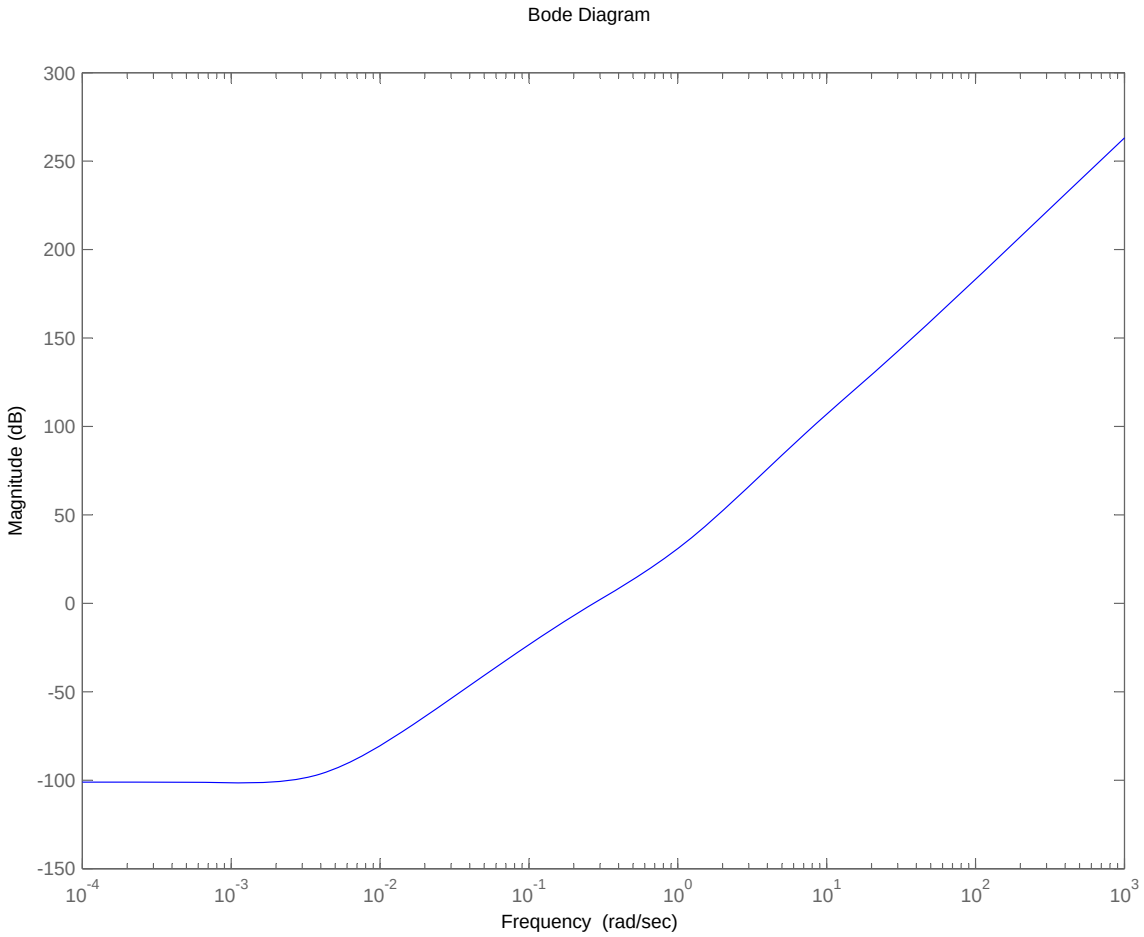

Figure 9.2: *Bode plot of the dynamic coupling factor(Q(s)).*

stated for this report. An example of a adaptive block diagram can be found in Figure 9.3. Different approaches can be taken when an adaptive controller is made. Some of these approaches are gain scheduling, model reference adaptive control, self-tuning control and dual control.

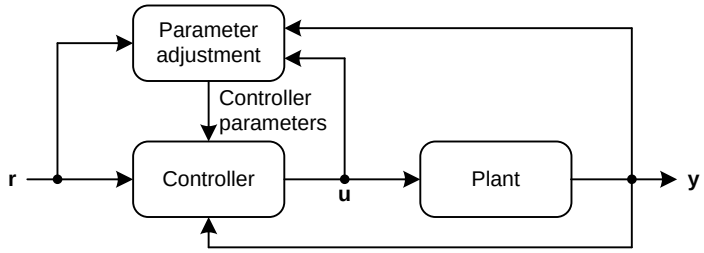

Figure 9.3: *Block diagram of an adaptive control system.*

The two former approaches are called direct methods, due to the fact, that the adjustment rules tell directly the controller how the parameters should be updated. The two latter approaches is based on a self-tuning method.

Dual control is chosen for this project as the estimated quality of the parameters is used. Moreover the knowledge of the plant is also used, this result in a model of the system, which can be

used in the controller design [Åström & Wittenmark, 1995]. A block diagram of a dual controller is given in Figure 9.4. Moreover it is chosen to use a optimal controller in the controller block.

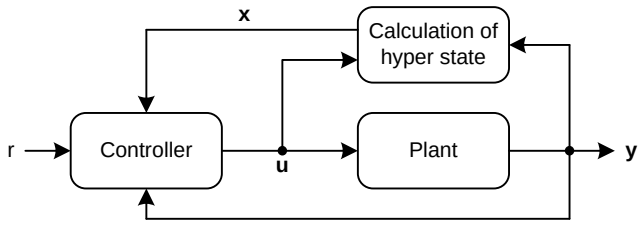

Figure 9.4: *Block diagram of dual control.*

First the controller block is designed and verified afterwards the hyper state block is designed and verified and finally is the two blocks combined, creating the controller set up seen in Figure 9.4.

Chapter 10

The Controller Block

The controller block for the controller setup seen in Figure 10.1 is designed in this chapter.

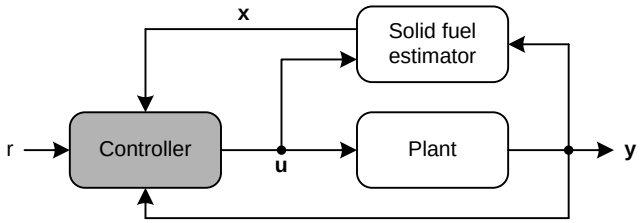

Figure 10.1: *A block diagram of the controller setup with the controller and solid fuel estimator block.*

Two different optimal controllers will be developed in this project, which are optimal for one type of solid fuel each. The optimal controller is using the cross coupling in the system to optimize the performance by weighting the inputs and states or outputs. The optimal controller is based on the linear state space model.

To ease the controller design the inlet water temperature (T_{iw}) is introduced as a disturbance ($\mathbf{d}$), and is mapped to $\dot{\mathbf{x}}_p$ using $\mathbf{E}_p$. This also means that it is no longer a part of $\mathbf{u}$. $\mathbf{u}$ now only contains the mass flow of solid fuel (m_{sf}) and the mass flow of supply air (m_a).

Looking at Figure 10.2 the following system equations can be setup.

$$\dot{\mathbf{x}}(t) = \mathbf{A}_p\mathbf{x}_p(t) + \mathbf{B}_p\mathbf{u}(t) + \mathbf{E}_p\mathbf{d}(t) + \mathbf{G}\mathbf{w}(t) \quad (10.1)$$

$$\mathbf{y}_p(t) = \mathbf{C}_p\mathbf{x}_p(t) + \mathbf{H}\mathbf{v}(t) \quad (10.2)$$

Before the actual controller can be designed the non-measurable states in the system must be estimated. This can be done by an observer.

10.1 Observer

The primary objective of an observer is to provide the values of the states inside the plant to the controller. To accomplish this it uses the model of the plant to predict/simulate the values of the states inside the plant. The same inputs are provided to the observer as to the plant, and

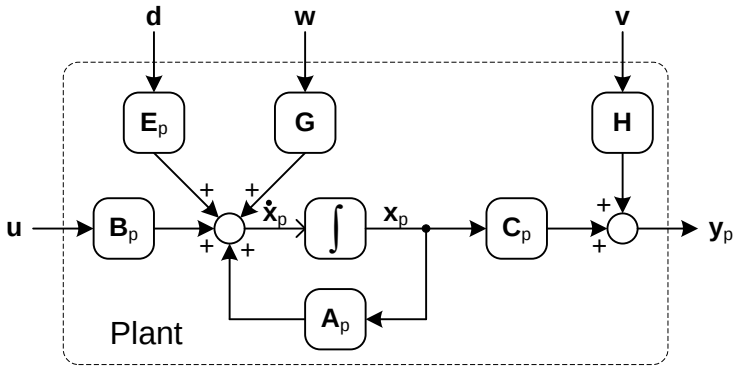

Figure 10.2: *A block diagram of the plant where the lowercase p indicates plant values.*

if these respond in the same way the states should also be the same. Before the observer can be designed the rank of the observability matrix must be calculated to insure that the plant is observable. The matrix is shown in Equation (10.3) [Franklin et al., 2002].

$$O = \begin{bmatrix} \mathbf{C} \\ \mathbf{C} \cdot \mathbf{A} \\ \vdots \\ \mathbf{C} \cdot \mathbf{A}^{n-1} \end{bmatrix} \tag{10.3}$$

where n is the number of states and the matrices $\mathbf{C}$ and $\mathbf{A}$ are found in Chapter 8.

$$\text{rank} \left(\begin{bmatrix} \mathbf{C} \\ \mathbf{C} \cdot \mathbf{A} \\ \mathbf{C} \cdot \mathbf{A}^2 \\ \mathbf{C} \cdot \mathbf{A}^3 \\ \mathbf{C} \cdot \mathbf{A}^4 \\ \mathbf{C} \cdot \mathbf{A}^5 \end{bmatrix} \right) = 6 \tag{10.4}$$

When $\mathbf{C}$ and $\mathbf{A}$ are inserted the equation equals true. This means that the matrix have full rank and therefore all the entries are independent of each other. The system is thus observable, and an observer can be designed as in Figure 10.3. As $\mathbf{d}$ is known, it is included in the observer. When the plant and the observer are connected as in Figure 10.3 the outputs $\mathbf{y}_p$ and $\mathbf{y}_o$ should be identical. Here p is used to denote plant values and o is used to denote observer values.

The matrices $\mathbf{A}_o$ and $\mathbf{C}_o$ are the matrices derived in Chapter 8. $\mathbf{B}_o$ is the first two columns of $\mathbf{B}$ and $\mathbf{E}_o$ is the last column of $\mathbf{B}$, where $\mathbf{B}$ is derived in Chapter 8.

However as all models are based on assumptions, a slight error will occur. This error will build up over time, and the outputs $\mathbf{y}_p$ and $\mathbf{y}_o$ will drift apart. The error between these outputs can be used to adjust the model using feedback through a observer gain $\mathbf{L}$ as shown in Figure 10.4.

Looking at Figure 10.4 the following observer equations can be set up.

$$\dot{\mathbf{x}}_o(t) = \mathbf{A}_o\mathbf{x}_o(t) + \mathbf{B}_o\mathbf{u}(t) + \mathbf{E}_o\mathbf{d}(t) + \mathbf{L}\left(\mathbf{y}_p(t) - \mathbf{y}_o(t)\right) \tag{10.5}$$

$$\mathbf{y}_o(t) = \mathbf{C}_o\mathbf{x}_o(t) \tag{10.6}$$

Various methods can be used to design $\mathbf{L}$, one method is pole placement, where the observer poles are chosen. The choice of poles are however a trade off between the magnitude of the

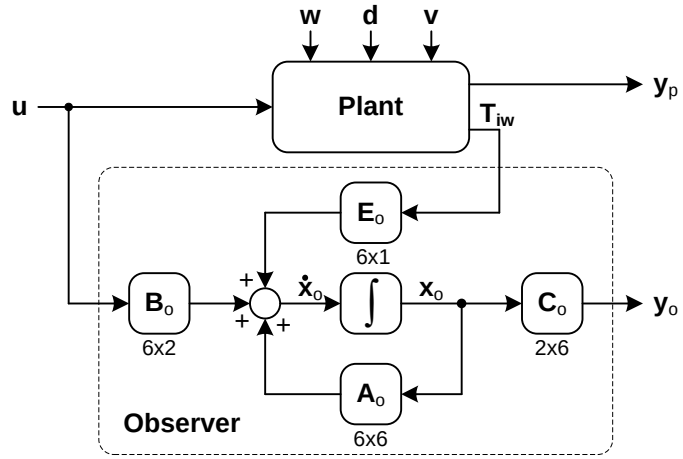

Figure 10.3: *The plant from Figure 10.2 and a block diagram of its observer where the lowercase o indicates observer values.*

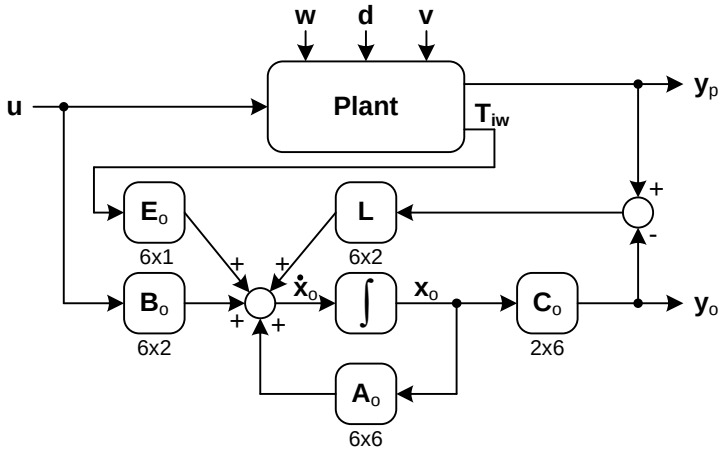

Figure 10.4: *Plant and observer with observer gain feedback included. This set up is also called a Luenberger based observer.*

estimate error and the noise suppression. The observer poles can be calculated by finding the eigenvalues of $\mathbf{A}_o - \mathbf{L} \cdot \mathbf{C}_o$.

In this project the observer gain will be calculated using the MATLAB-function `lqe`. LQE stands for Linear Quadratic Estimation which basically is a Kalman filter, and as a Kalman filter is needed in the adaptive controller this method is ideal. As input to `lqe` the $\mathbf{A}_o$, $\mathbf{G}$, $\mathbf{C}_o$, $\mathbf{Q}_n$ and $\mathbf{R}_n$ matrices are used which all are derived in Chapter 8. When these matrices are used the observer gain is calculated to:

$$\mathbf{L} = \begin{bmatrix} 9.010 \cdot 10^{-6} & -0.253 \cdot 10^{-3} \\ 0.287 \cdot 10^{-3} & -30.887 \\ 0.107 \cdot 10^{-3} & -117.725 \\ 51.160 \cdot 10^{-6} & -52.666 \\ 0.079 \cdot 10^{-9} & -0.086 \\ -15.983 \cdot 10^{-9} & 0.308 \end{bmatrix} \tag{10.7}$$

The observer poles can now be found by calculating the eigenvalues of $\mathbf{A}_o - \mathbf{L} \cdot \mathbf{C}_o$, this is done

using the `eig()`-function in MATLAB which gives:

$$\big(-26.379 + 26.226i;\ -26.379 - 26.226i;\ -4.281 \cdot 10^{-3};\ -3.093 \cdot 10^{-3};\ -0.952;\ -1.295\big) \quad (10.8)$$

As they all are in the left half plan the observer is stable.

With a full order observer, like the one described above, not only the non-monitored but also the monitored states are calculated. This may slow down the system, as calculations not needed are performed. This can be avoided by designing a reduced order observer, which only calculates the unknown states. The full order observer does however possess other qualities than just providing the unmonitored states. It also effectively filters noise from the monitored states. For this reason a full order observer is chosen for this project.

10.2 Feedback Controller

Now that a full order observer is designed, it is possible to design a full state feedback controller. Full state feedback aims at using the cross coupling in the model to optimize performance. This means that the contribution from each input is used to control the outputs.

Before a feedback controller can be designed the rank of the controllability matrix must be calculated to ensure that the plant is controllable. The matrix is shown in Equation (10.9) [Franklin et al., 2002].

$$C = \begin{bmatrix} \mathbf{B} & \mathbf{A}\cdot\mathbf{B} & \cdots & \mathbf{A}^{n-1}\cdot\mathbf{B} \end{bmatrix} \quad (10.9)$$

where n is the number of states and the matrices $\mathbf{A}$ and $\mathbf{B}$ are derived in Chapter 8.

$$\operatorname{rank}\left(\begin{bmatrix} \mathbf{B} & \mathbf{A}\cdot\mathbf{B} & \mathbf{A}^2\cdot\mathbf{B} & \mathbf{A}^3\cdot\mathbf{B} & \cdot\mathbf{A}^4\cdot\mathbf{B} & \mathbf{A}^5\cdot\mathbf{B} \end{bmatrix}\right) = 6 \quad (10.10)$$

When $\mathbf{A}$ and $\mathbf{B}$ are inserted the equation equals true. Thus the system is controllable and a feedback gain can be designed.

The feedback gain ($\mathbf{F}$) is used to control the system according to Figure 10.5.

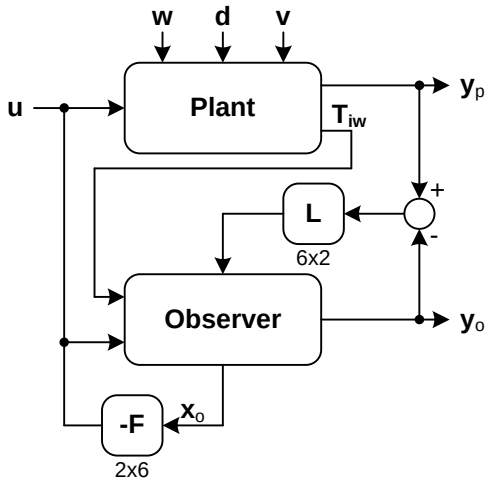

Figure 10.5: *Block diagram of the state space model with full state feedback.*

The feedback equation or the control law can from figure 10.5 be expressed as:

$$\mathbf{u}(t) \quad = \quad -\mathbf{F}\mathbf{x}_o(t) \quad (10.11)$$

Given a properly designed feedback gain $\mathbf{F}$, the closed loop system in figure 10.5 will converge towards a steady state where the outputs are zero. To enable other values of $\mathbf{y}$ in steady state, a reference is needed which is designed before the feedback gain is calculated.

10.3 Reference Signal

The reference signal ($\mathbf{r}$) is introduced, by subtracting it from the plant output ($\mathbf{y}_p$). This can however contribute to a steady state error which can be eliminated by introducing integral control. The setup including the integral control can be seen in Figure 10.6

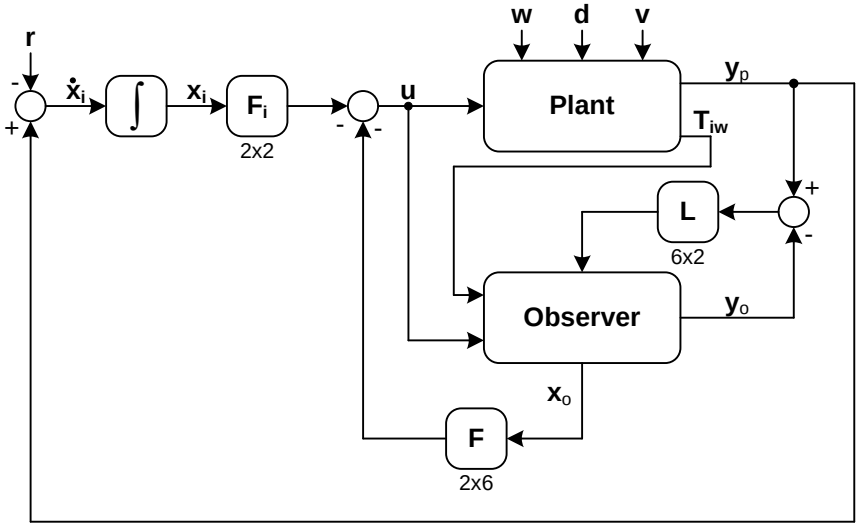

Figure 10.6: *Block diagram of the controller including observer, feedback, reference signal and integral control.*

When the integral control is included, two new states are added to the system. It is therefore necessary to extend the state space matrices before the feedback gains ($\mathbf{F}$ and $\mathbf{F}_i$) can be calculated. The new system and output equations including the contribution from the integral control can be seen in Equation (10.12) and Equation (10.13).

$$\dot{\mathbf{x}}_e(t) = \mathbf{A}_i\mathbf{x}_e(t) + \mathbf{B}_i\mathbf{u}(t) + \mathbf{E}\mathbf{d}(t) \tag{10.12}$$

$$\mathbf{y}_i = \mathbf{C}_i\mathbf{x}_e(t) \tag{10.13}$$

where

$$\mathbf{x}_e(t) = \begin{bmatrix} \mathbf{x}_o \\ \mathbf{x}_i \end{bmatrix} \quad , \quad \mathbf{x}_i = \begin{bmatrix} T_w - \mathrm{ref}(T_w) \\ \mathrm{O}_2 - \mathrm{ref}(\mathrm{O}_2) \end{bmatrix} \quad , \quad \mathbf{y}_i = \begin{bmatrix} T_w \\ \mathrm{O}_2 \\ T_w - \mathrm{ref}(T_w) \\ \mathrm{O}_2 - \mathrm{ref}(\mathrm{O}_2) \end{bmatrix}$$

$$\mathbf{A}_i = \begin{bmatrix} \mathbf{A}_o & \mathbf{0}_{6\times2} \\ \mathbf{C}_o & \mathbf{0}_{2\times2} \end{bmatrix} \quad , \quad \mathbf{B}_i = \begin{bmatrix} \mathbf{B}_o \\ \mathbf{0}_{2\times2} \end{bmatrix} \quad , \quad \mathbf{C}_i = \begin{bmatrix} \mathbf{C}_o & \mathbf{0}_{2\times2} \\ \mathbf{0}_{2\times6} & \mathbf{I}_{2\times2} \end{bmatrix}$$

where $\mathbf{0}$ is a matrix only consisting of zeros with the dimension specified in the index and $\mathbf{I}$ is the identity matrix with the dimension specified in the index. Using Equation (10.3) and Equation (10.9) it can be seen that the extended system also is observable and controllable.

Using the extended feedback matrix $\mathbf{F}_e$ given by Equation (10.14)

$$\mathbf{F}_e = \begin{bmatrix} \mathbf{F} & \mathbf{F}_i \end{bmatrix} \tag{10.14}$$

is it possible to move the poles of the system such the system obtains the desired dynamic. From Figure 10.6 can the new control law be found to:

$$\begin{aligned} \mathbf{u}(t) &= -\mathbf{F}\mathbf{x}_o(t) - \mathbf{F}_i\mathbf{x}_i(t) \\ &= -\mathbf{F}_e\mathbf{x}_e(t) \end{aligned} \tag{10.15}$$

Equation (10.15) is then inserted in Equation (10.12)

$$\dot{\mathbf{x}}_e(t) = \mathbf{A}_i\mathbf{x}_e(t) - \mathbf{B}_i\mathbf{F}_e\mathbf{x}_e(t) + \mathbf{E}_i\mathbf{d}(t) \tag{10.16}$$

The closed-loop poles can now be found by Equation (10.17).

$$\det\left[\lambda I - (\mathbf{A}_i - \mathbf{B}_i\mathbf{F}_e)\right] = 0 \tag{10.17}$$

which is equal to finding the eigenvalues of $\mathbf{A}_i - \mathbf{B}_i\mathbf{F}_e$. This can be done using the MATLAB-function `eig()`. But first it is necessary to calculate $\mathbf{F}_e$.

10.4 Feedback Gain Matrix

The feedback gain $\mathbf{F}_e$ is designed using optimal control. This method is used to obtain an optimal result in ratio to the relation between control precision and control performance. This method uses a cost function (J), see Equation (10.18).

$$J = \int_0^\infty \left(\mathbf{x}^\top \cdot \mathbf{Q} \cdot \mathbf{x} + \mathbf{u}^\top \cdot \mathbf{R} \cdot \mathbf{u}\right) \mathrm{dt} \tag{10.18}$$

By minimizing this cost function is it possible to obtain an optimal control. By selecting suitable weighting matrices ($\mathbf{Q}$ and $\mathbf{R}$), acceptable values for the states and inputs are obtained. $\mathbf{Q}$ and $\mathbf{R}$ are found iterative to obtain satisfying results, the iteration process takes its starting point in Bryson's rule which yields [Franklin et al., 2002]:

$$\mathbf{Q}_{ii} = \frac{1}{\text{max value of } ({x_i}^2)} \tag{10.19}$$

$$\mathbf{R}_{ii} = \frac{1}{\text{max value of } ({u_i}^2)} \tag{10.20}$$

This means that $\mathbf{Q}$ and $\mathbf{R}$ only contains non-zero values in the diagonal. To obtain optimal control $\mathbf{Q}$ must be positive semi-definite and $\mathbf{R}$ positive definite. As the state space model is based on small signal values, the maximum acceptable value correspond to the maximum acceptable change of the value. $\mathbf{F}_e$ can be found using the MATLAB-function `lqr`. This function takes the system matrix $\mathbf{A}_i$, the input matrix $\mathbf{B}_i$, and the two weighting matrices $\mathbf{Q}$ and $\mathbf{R}$ as input.

It is however not relevant to limit the states which are not output. The first term in the cost function is therefore rewritten to:

$${\mathbf{y}_i}^\top \cdot \mathbf{Q}_r \cdot \mathbf{y}_i = (\mathbf{C}_i \cdot \mathbf{x}_e)^\top \cdot \mathbf{Q}_r \cdot \mathbf{C}_i \cdot \mathbf{x}_e = {\mathbf{x}_e}^\top \cdot {\mathbf{C}_i}^\top \cdot \mathbf{Q}_r \cdot \mathbf{C}_i \cdot \mathbf{x} \tag{10.21}$$

where the two first values in the diagonal of $\mathbf{Q}_r$ weigh the outputs whereas the last two values weigh the integral states. The outputs and the integral states are related through the response time of the system, $\mathbf{Q}_r$ can then be written as in Equation (10.22).

$$\mathbf{Q}_r = \begin{bmatrix} \frac{1}{\text{max value of } {T_w}^2} & 0 & 0 & 0 \\ 0 & \frac{1}{\text{max value of } {O_2}^2} & 0 & 0 \\ 0 & 0 & \frac{1/\text{max value of } {T_w}^2}{Ti^2} & 0 \\ 0 & 0 & 0 & \frac{1/\text{max value of } {O_2}^2}{Ti^2} \end{bmatrix} \tag{10.22}$$

where Ti is the response time of the system.

When the `lqr` function is used in MATLAB the original weighting matrix $\mathbf{Q}$ is replaced with ${\mathbf{C}_i}^\top \cdot \mathbf{Q}_r \cdot \mathbf{C}_i$ which weights the output instead of the states. The variations in output and input are chosen to be:

$$\begin{aligned} T_w &= \pm 5^\circ\text{C} \\ \text{O}_2 &= \pm 2\% \\ m_{sf} &= \pm 100\% \\ m_a &= \pm 100\% \end{aligned}$$

Using these values in $\mathbf{Q}_r$ and $\mathbf{R}$ will not give an acceptable result, so both $\mathbf{Q}_r$ and $\mathbf{R}$ must be fitted iterative until a satisfying result is found. All the inputs to the `lqr` function is now found and $\mathbf{F}_e$ can be calculated. With the calculated $\mathbf{F}_e$ will the plant converge towards a desired reference signal.

Before the controller is implemented on the plant it has to be discretized.

10.5 Discretization of the State Space Model

The controllers are implemented in a digital environment. To realize this, the controllers must be digitalized. This is done with zero order hold. The transformation may change the response of the system, and care must therefore be taken when performing this transformation to avoid this. The sample frequency is the major factor which determines the digital controller's likeness to the designed analogue one. A fast frequency will ensure interchangeability between the analogue and the digital version of the controller. How fast is relative to the time constants of the system. These are above 1 Hz so a sample frequency of 1 Hz should be sufficient, and is therefore chosen. Moreover the measurements are used from the sensors with a frequency of 1 Hz.

The matrices derived in Chapter 8 are discretized using the function `c2dm`-function in MATLAB. The observer gain and feedback gain in the discrete version is found using `dlqe` and `dlqr` in MATLAB. When the discrete version of $\mathbf{A}_i$ is found the zero matrix in the right lower corner must be replaced with the identity matrix as seen in Equation (10.23).

$$\mathbf{A}_i = \begin{bmatrix} \mathbf{A}_o & \mathbf{0}_{6\times 2} \\ \mathbf{C}_o & \mathbf{0}_{2\times 2} \end{bmatrix} \quad , \quad \mathbf{A}d_i = \begin{bmatrix} \mathbf{A}_o & \mathbf{0}_{6\times 2} \\ \mathbf{C}_o & \mathbf{I}_{2\times 2} \end{bmatrix} \tag{10.23}$$

10.6 Delay in the O_2-level

Preliminary test of the discrete controller has shown that there is a delay in the O_2-level from the model. This is because the O_2-level found in the modelling phase is for the exhaust gas and

the one needed is for the burning chamber where the combustion takes place. Through test the delay is found to approximately 15 s.

To deal with this delay of 15 s 15 new states are included in the model, where the seventh state is the O_2-level delayed with one sample, the eighth state is the O_2-level delayed two samples and so on. This means that all the matrices derived in Chapter 8 are extended so they match 21 states instead of 6 states. This is done by including 15 ones in the diagonal of $\mathbf{M}$, including 15 ones in the $\tilde{\mathbf{A}}$ matrix so the seventh state becomes equal to the sixth state one sample ago and so on until a delay of 15 s is reached, and extending $\tilde{\mathbf{B}}$ and $\mathbf{C}$ so they match a system of 21 states, as seen in the four next equations.

$$\mathbf{M} = \begin{bmatrix} tw_1 & 0 & 0 & 0 & 0 & 0 & 0 & 0 & 0 \\ 0 & tbc_1 & 0 & 0 & 0 & 0 & 0 & 0 & 0 \\ 0 & 0 & tgc_1 & 0 & 0 & 0 & 0 & 0 & 0 \\ 0 & 0 & 0 & teg_1 & 0 & 0 & 0 & 0 & 0 \\ 0 & 0 & 0 & 0 & 1 & 0 & 0 & 0 & 0 \\ 0 & 0 & 0 & 0 & 0 & o2_1 & 0 & 0 & 0 \\ 0 & 0 & 0 & 0 & 0 & 0 & 1 & 0 & 0 \\ 0 & 0 & 0 & 0 & 0 & 0 & 0 & \ddots & 0 \\ 0 & 0 & 0 & 0 & 0 & 0 & 0 & 0 & 1 \end{bmatrix} \tag{10.24}$$

$$\tilde{\mathbf{A}} = \begin{bmatrix} -tw_6 & tw_3 & tw_4 & tw_5 & 0 & 0 & \cdots & 0 & 0 \\ tbc_6 & -tbc_3 & 0 & 0 & tbc_9 & 0 & \cdots & 0 & 0 \\ tgc_6 & tgc_3 & -tgc_4 & 0 & tgc_9 & 0 & \cdots & 0 & 0 \\ teg_6 & 0 & teg_4 & -teg_5 & teg_9 & 0 & \cdots & 0 & 0 \\ 0 & 0 & 0 & 0 & -mchar_9 & 0 & \cdots & 0 & 0 \\ 0 & 0 & 0 & 0 & -o2_9 & -02_{10} & \cdots & 0 & 0 \\ 0 & 0 & 0 & 0 & 0 & 1 & \cdots & 0 & 0 \\ 0 & 0 & 0 & 0 & 0 & 0 & \ddots & 0 & 0 \\ 0 & 0 & 0 & 0 & 0 & 0 & \cdots & 1 & 0 \end{bmatrix} \tag{10.25}$$

$$\tilde{\mathbf{B}} = \begin{bmatrix} 0 & 0 & tw_2 \\ tbc_7 & tbc_8 & 0 \\ tgc_7 & tgc_8 & 0 \\ teg_7 & teg_8 & 0 \\ mchar_7 & -mchar_8 & 0 \\ 02_7 & 02_8 & 0 \\ 0 & 0 & 0 \\ \vdots & \vdots & \vdots \\ 0 & 0 & 0 \end{bmatrix} \tag{10.26}$$

$$\mathbf{C} = \begin{bmatrix} 1 & 0 & 0 & 0 & 0 & \cdots & 0 \\ 0 & 0 & 0 & 0 & 0 & \cdots & v \end{bmatrix} \tag{10.27}$$

These extended matrices are then used in the controller design described in this chapter. The new controller is now verified through simulations.

10.7 Verification of the Optimal Controller

The optimal controller is implemented in SIMULINK from Figure 10.6. In the verification phase the plant is replaced by the non-linear model. As the output from the control law (Equation (10.15)) can be negative the input to the non-linear model/plant can be negative. This is however not desirable so a saturation block is inserted to ensure an allowable input. The saturation block is made such that the minimum input is equal to zero and the maximum input is equal to $\beta_{\text{motor}} \cdot 100$ and $\beta_{\text{blower}} \cdot 100$ respectively.

In this verification section two optimal controllers are found one when wood pellets are combusted and one when wheat is combusted. The two controllers are found by fitting $\mathbf{Q}_r$ and $\mathbf{R}$ iterative until a satisfying result is obtained for each solid fuel. These two parameters are fitted from the non-linear model which is controlled by the optimal controller.

Figure 10.7 shows a simulation of the optimal controller where the reference is set to 60°C and 8% respectively (red lines) and the non-linear model for wood pellets is used. The simulation lasts for 7200 s and after 3600 s a step is made in the load where the inlet water is decreased to 50°C. It can be seen that the output from the non-linear model tracks the reference signal satisfactory with no steady state error.

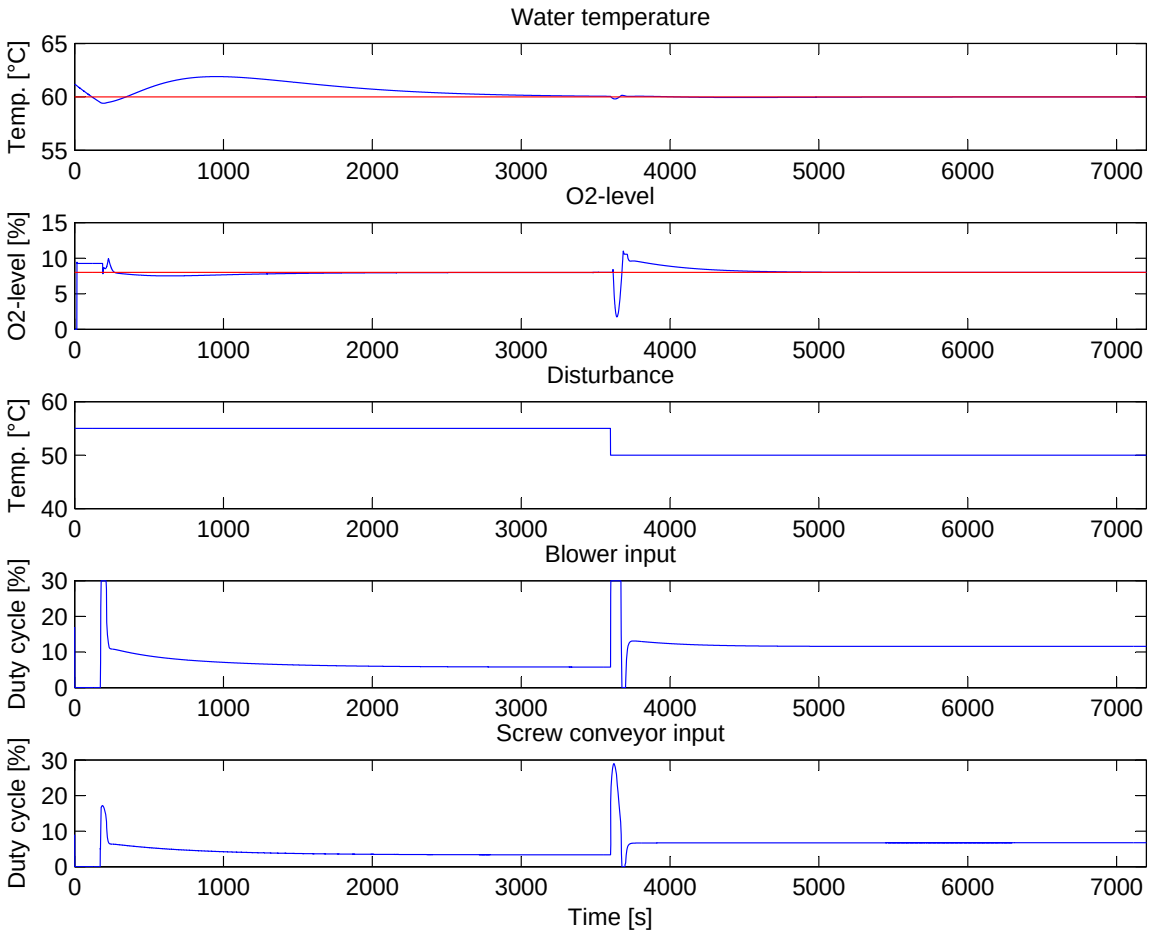

Figure 10.7: *Output from the non-linear model controlled by a LQR controller where the reference s set to 60°C and 8%. The load and input to the actuators are also seen in this figure.*

The first graph in Figure 10.7 is the water temperature, it can be seen that it tracks the reference of 60°C satisfactory. It takes rather long time before the water temperature settles at 60°C but this is expected as the water temperature has a large time constant. Moreover is the water temperature inside the requirements set in Chapter 3. When the step in the load is made the water temperature decreases short.

From the second graph it can be seen that the O_2-level also tracks the reference which is 8%. The O_2-level settles to the reference much faster as the time constant for the O_2-level is much shorter then for the water temperature. The O_2-level reacts heavy on the step in the load as it first drops fast and then raises shortly after to settle at the reference again. This is however accepted as the requirements set to the controller in Chapter 3 is fulfilled.

The third graph shows the load on the system given by the inlet water temperature. As mentioned it can be seen that the load is increased after 3600 s which means that the water temperature and the O_2-level decrease. To avoid a permanent decrement in the water temperature and the O_2-level both the inputs to the actuators are increased as seen in the fourth and fifth graph in Figure 10.7.

As just mentioned the controller input to the actuators is seen in the fourth graph for the supply air and in the fifth graph for the solid fuel. It can be seen that the inputs go to steady state values when the reference is reached. These steady state values are enough to keep the system at the reference signal as long as the load is steady. When the load is changed the inputs will also change. It can also be seen that the blower reaches its maximum when the load is made as the PWM signal to the blower is linearized the maximum input to the blower is 30%.

Figure 10.8 shows a simulation of the optimal controller where the reference is set to 70°C and 12% respectively and the non-linear model for wheat is used. The simulation lasts for 7200 s and after 3600 s a step is made in the load where the inlet water is decreased to 60°C. It can be seen that the output from the non-linear model tracks the reference signal satisfactory with no steady state error.

The first graph in Figure 10.8 is the water temperature, it can be seen that it tracks the reference of 70°C satisfactory. It takes rather long time before the water temperature settles at 70°C but this is expected as the water temperature has a large time constant. Moreover the water temperature is inside the requirements set in Chapter 3. When the step in the load is made the water temperature decreases but it reaches the reference again after some time.

From the second graph it can be seen that the O_2-level also tracks the reference which is 12%. The O_2-level settles to the reference faster as the time constant for the O_2-level is shorter then for the water temperature. The O_2-level reacts on the step in the load as it increases a bit before it settles to the reference again. This is accepted however as the requirements set to the controller in Chapter 3 is fulfilled.

The third graph shows the load on the system given by the inlet water temperature. As mentioned it can be seen that the load is increased after 3600 s which means that the water temperature decreases and the O_2-level increases. To avoid a permanent change in the water temperature and the O_2-level both the inputs to the actuators are changed as seen in the fourth and fifth graph in Figure 10.7.

As just mentioned the controller input to the actuators is seen in the fourth graph for the supply air and in the fifth graph for the solid fuel. It can be seen that the inputs go to steady state values when the reference is reached. These steady state values are enough to keep the system at the reference signal as long as the load is steady. When the load is changed will the inputs also change.

Two controllers are now designed and verified, they are now ready to be tested on the plant.

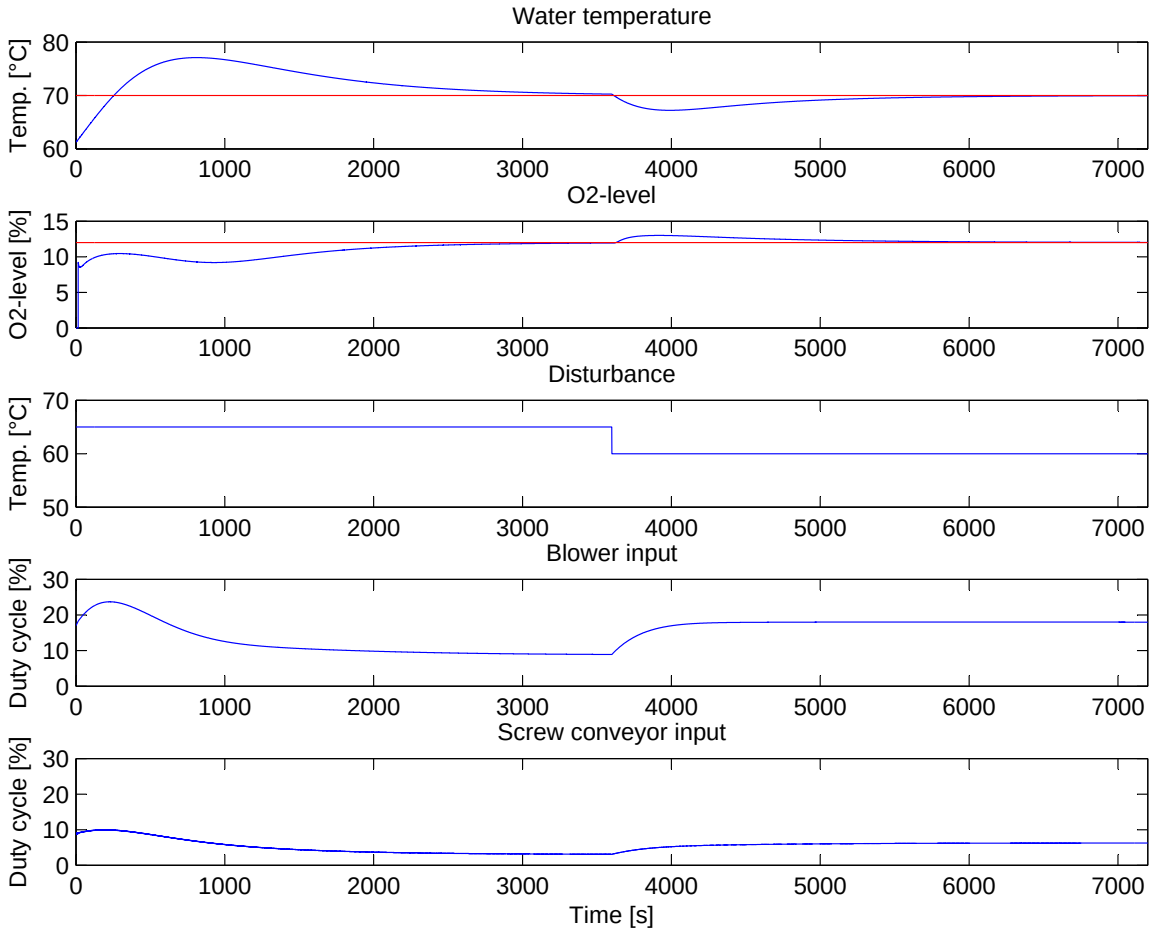

Figure 10.8: *Output from the non-linear model controlled by a LQR controller where the reference s set to 70°C and 12%. The load and input to the actuators are also seen in this figure.*

Before this is done is it investigated how well the controller designed for wood pellets combustion controls the plant when wheat is combusted and vice versa. This is done by controlling the non-linear model for wheat with the controller designed for wood pellets combustion and vice versa.

Figure 10.9 shows a simulation of the optimal controller designed for wood pellets combustion where the reference is set to 70°C and 12% respectively and the non-linear model for wheat is used. The simulation lasts for 7200 s and after 3600 s a step is made in the load where the inlet water is decreased to 60°C.

From Figure 10.9 it can be seen that the controller designed for wood pellets is capable of reaching the references within the requirements set to the controller in Chapter 3. There is however one critical point when a step in the load is made will the O_2-level drop to nearly 0% and the input to the blower actuator reaches its maximum. This is not desirable as a bigger step in the load would cause the O_2-level to drop to 0%. Even though this conroller can control the system as desired is it not optimal.

Figure 10.10 shows a simulation of the optimal controller designed for wheat combustion where the reference is set to 60°C and 8% respectively and the non-linear model for wood pellets are used. The simulation lasts for 7200 s and after 3600 s a step is made in the load where the inlet water is decreased to 50°C.

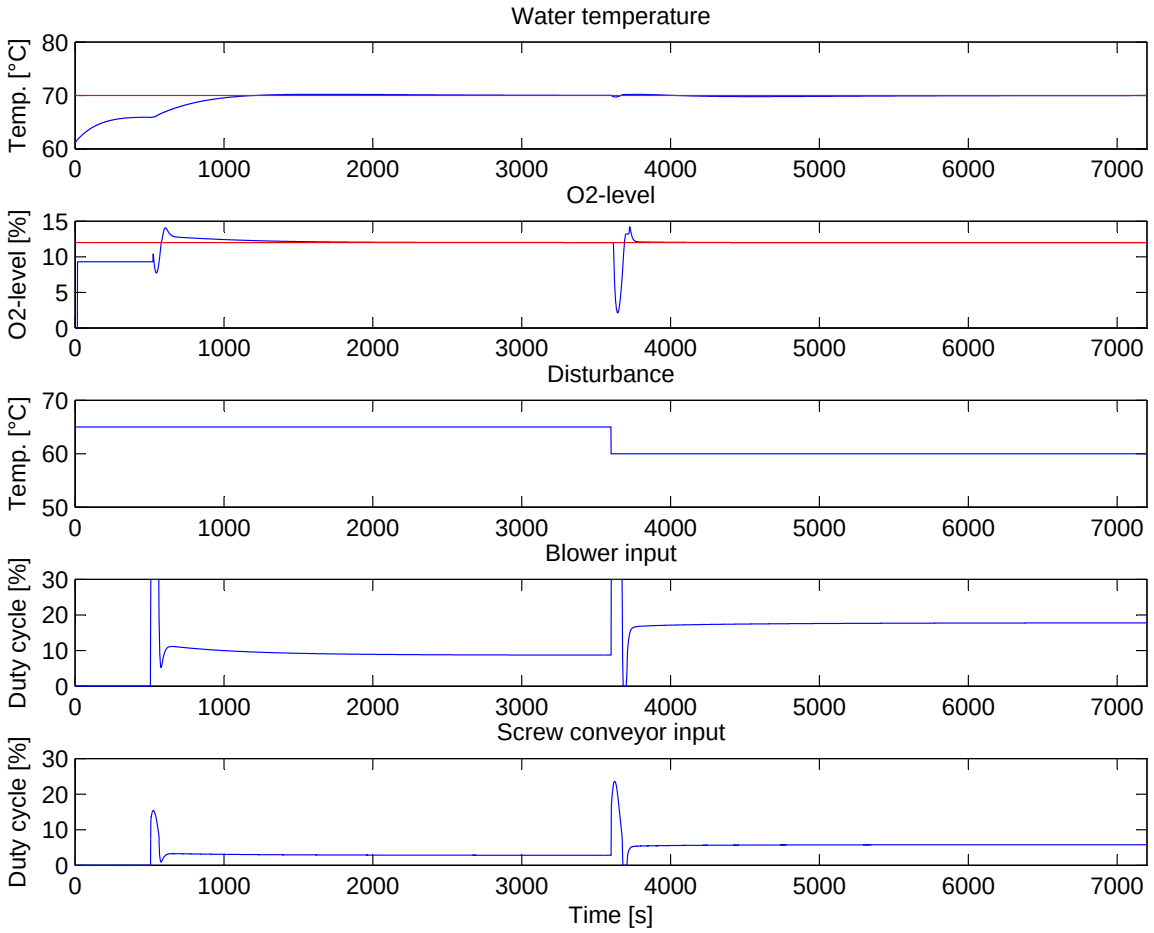

Figure 10.9: *Output from the non-linear model for wheat controlled by a LQR controller designed for wood pellets combustion where the reference s set to 70°C and 12%. The load and input to the actuators are also seen in this figure.*

From Figure 10.10 can it be seen that the controller designed for wheat is capable of reaching the references within the requirements set to the controller in Chapter 3. There is however some critical points. First of all the water temperature is slow to reach the reference and the water temperature raises 10°C before it drops down towards the reference. The O_2-level drops close to 0% before it raises towards the reference. The most critical point is that the O_2-level begins to oscillate this is due to the input to both the actuators which oscillates. The oscillation is due to the observer gain which is not capable of minimizing the error between the measured output and the model output. So the controller designed for wheat can not control the system optimal when wood pellets are combusted.

It is now shown that a controller for one solid fuel is optimal when only this solid fuel is combusted, meaning that the controller for the wood pellets is not capable of controlling the system optimal when wheat is combusted and vice versa.

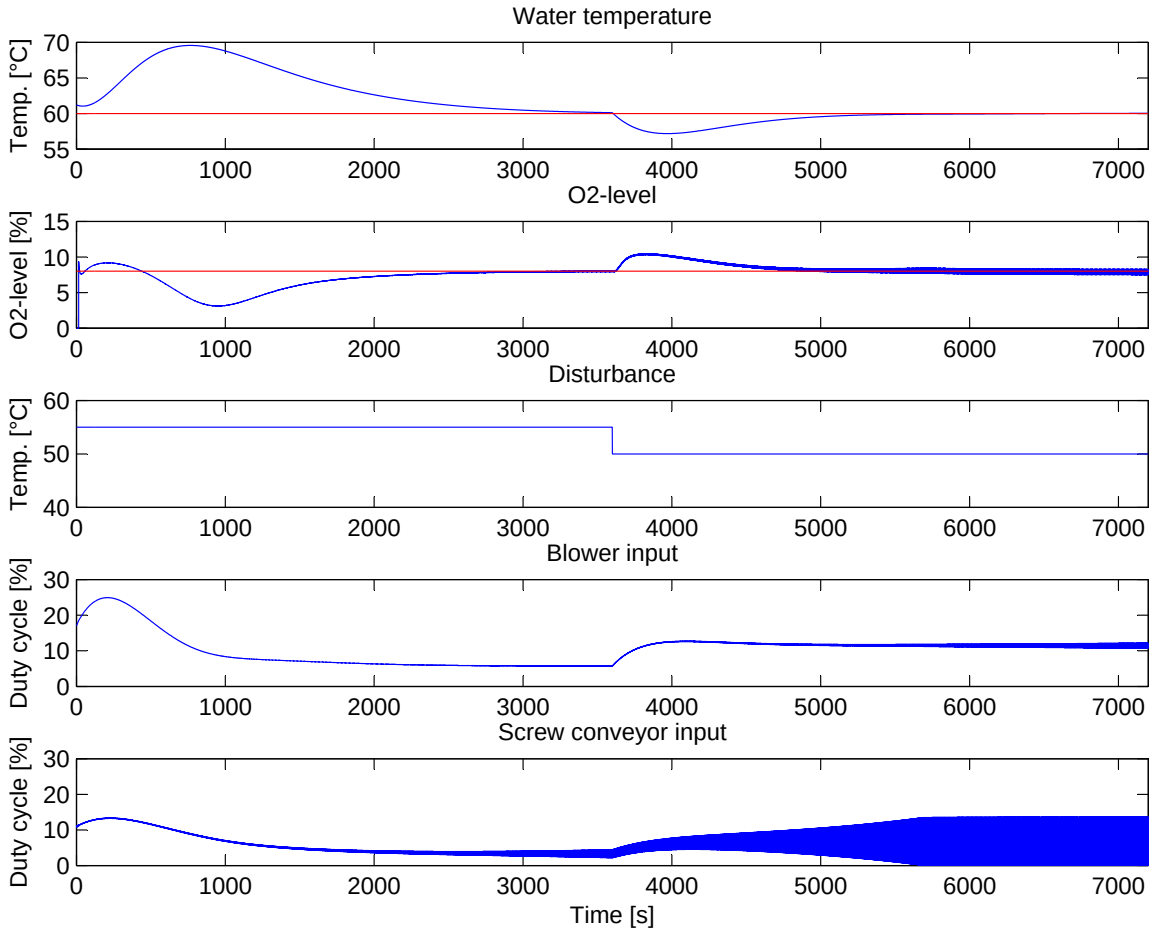

Figure 10.10: *Output from the non-linear model for wood pellets controlled by a LQR controller designed for wheat combustion where the reference s set to 60°C and 8%. The load and input to the actuators are also seen in this figure.*

Chapter 11

The Solid Fuel Estimator Block

The solid fuel estimator for the controller see Figure 11.1 is designed in this chapter and afterward is it connected to the two controllers found in the previous chapter, to complete the controller. The solid fuel estimator block uses the linear models in combination with filters to find the desired parameters to the controller.

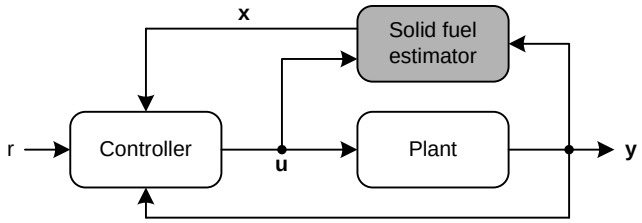

Figure 11.1: *A block diagram of the controller setup with the controller and solid fuel estimator block.*

Different methods can be used to construct the solid fuel estimator. Some of these methods are model switching, model detection and multiple hypothesis testing. The model switching method decides which model to use, from a probability calculation. This indicates that a controller must be designed for every case, which means that a controller for each solid fuel and for each operation point must be designed. The model detection method calculates which model is the most simple to a given situation, an example is a car, that uses one model when it drive forward and another when it turns. This method is not suitable for this project, as the stoker system does not shift between different behaviours. The multiple hypothesis testing calculates the possibility for each model, and weight the accuracy of the different models. This allows choosing a controller setup which is optimal in the end points of the operation space. This means that only models for solid fuels, which is at the end points of the operation space is needed. The multiple hypotheses method is illustrated in Figure 11.2.

The multiple hypotheses testing method gives the advantage that the models do not need to fit all mixtures of different solid fuels. This is because the span of the models will cover the whole operation space, and a combined result of the model will therefore give a good estimate of the current parameters of the system.

In multiple hypotheses testing it is assumed that the correct model is proposed, which means the whole operation space of interest is covered by the models. A hypothesis is checked, one for

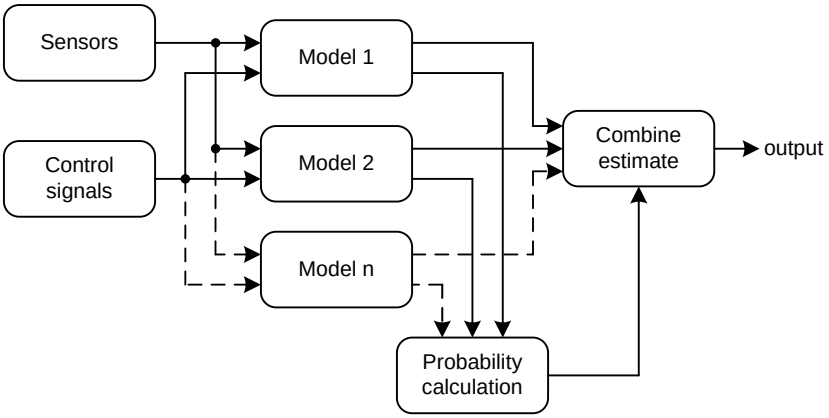

Figure 11.2: *Block diagram of solid fuel estimator.*

each model, the hypothesis is:

$$H_i = \text{Model } M_i \text{ is correct.} \tag{11.1}$$

By the assumption that the correct model is present, the null hypothesis id not present.

The probability that the model M_i is correct to time t_k with measurement Z_k up to time t_k is given by:

$$\mu_i(k) \equiv p(M_i|Z_k) \tag{11.2}$$

The initial probability that M_j is correct is given by $\mu(0)$, which according to the assumption sum up to unity over all the models.

The probability assigned to each model changes through time as more information becomes available. Considering the evolution of μ_j from k-1 to k using Bayes rule gives:

$$\begin{aligned} \mu_i(k) &\equiv p(M_i|Z_k) \\ &= p(M_i|z(k), Z_{k-1}) \\ &= \frac{p(z(k)|Z_{k-1}, M_i) \cdot p(M_j|Z_{k-1})}{p(z(k)|Z_{k-1})} \\ &= \frac{p(z(k)|Z_{k-1}, M_j) \cdot \mu_i(k-1)}{\sum_{j=1}^{n} p(z(k)|Z_{k-1}, M_j) \cdot p(Mj|Z_{k-1})} \end{aligned} \tag{11.3}$$

The $p(z(k)|Z_{k-1}, M_i)$ is the probability that the observation $z(k)$ would be made given that the model M_j is valid. This probability may be calculated directly from the innovations $r_j(k) \equiv z(k) - \hat{z}(k|k-1)$. Assuming that the innovation is Gaussian, zero mean and has covariance matrix $\mathbf{S}(k|k-1)$ the likelihood is:

$$\lambda_i(k) = \frac{e^{-1/2 \cdot {r_i}^\top(k) \cdot {\mathbf{S}_i}^{-1}(k|K-1) \cdot r_i(k)}}{(2 \cdot \pi)^{m/2} \cdot \det(\mathbf{S}_i(k|k-1))^{1/2}} \tag{11.4}$$

Where m is the dimension of the output vector and r_i is the residual found from the Kalman filter and measurements. A Kalman filter is used to estimate the covariance matrix $\mathbf{S}(k)$ which is found from Equation (11.5).

$$\mathbf{S}_i(k|k-1) = \mathbf{C}_i(k) \cdot \mathbf{P}_i(k) \cdot {\mathbf{C}_i}^\top(k) + \mathbf{R}_i(k) \tag{11.5}$$

The matrix **C** is the output matrix from the state space model. Small diagonal values in the **R** matrix means that the output from the state space model is trustworthy, while larger values means the output is given with some uncertainty [Knudsen, 2000]. The **R** matrix is set to 0.1 in the diagonal as the output from the models are accurate. The **P** matrix are found from the following equation, see Equation (11.6).

$$\begin{aligned} \mathbf{P}(0) &= \mathbf{Q} \\ \mathbf{P}(k+1) &= \mathbf{A} \cdot \mathbf{P}(k) \cdot \mathbf{A}^\top + \mathbf{Q} \end{aligned} \tag{11.6}$$

Where **Q** decides the variance of the states. Small eigenvalues in **Q** gives a small variance on the states, while values close to one gives a large variance on the states [Knudsen, 2000]. **Q** is chosen to have small values as the variance on the states is supposed to be small. When the covariance matrix **S** is calculated with help from **P**, the likelihood can be found from Equation (11.4).

The probabilities for each model can now be found from Equation (11.7).

$$\mu_i(k) = \frac{\lambda_i(k) \cdot \mu_i(k-1)}{\Sigma_{j=1}^{n} \lambda_j(k) \cdot \mu_j(k-1)} \tag{11.7}$$

The initial probability for each model at the starting point is given by $\mu(0)$ and sums up to unity over all the models. The possibility for each model is then calculated for every measurement. The output of the combine block can then be found from Equation (11.8).

$$\hat{y}(k|k) = \sum_{i=1}^{n} \hat{y}_i \mu_i(k) \tag{11.8}$$

Where $\hat{y}(k|k)$ is the combined estimate to time t_k, and $\hat{y}_i$ is the output from one model and $\mu_i(k)$ is the possibility that it is the right model to time t_k [Bak, 2000].

The solid fuel estimator is now designed it must however be verified before it can be implemented on the plant. This is done by verifying it against measurements. After the verification the controller block and the solid fuel estimator block are assembled to an adaptive controller.

11.1 Verification of the Solid Fuel Estimator

The solid fuel estimator is verified with wood pellets, wheat and a mixture of both solid fuels. First is it tested in simulations using plant measurements. Secondly is it tested on-line on the plant. The last test is also made to see how the water temperature and O_2-level influence the output from the solid fuel estimator.

11.1.1 Verification Using Measurements

In the following the test is performed on measurements from the plant. In Figure 11.3 the test with wood pellets is shown. The figure shows that the solid fuel estimator determines that the solid fuel is wood pellets. It takes around 300 s before the solid fuel estimator has settled. In the end of the test the water temperature is increased to around 70°C, this result in higher temperatures in the burning chamber, but still the estimator is able to determine that wood pellets are combusted.

The test with wheat can be seen in figure Figure 11.4. The solid fuel estimator finds after a short time period that wheat is used as solid fuel. A step in the blower does not interrupt the solid fuel estimator. However after 10000 s when the load is increased the solid fuel estimator gives a

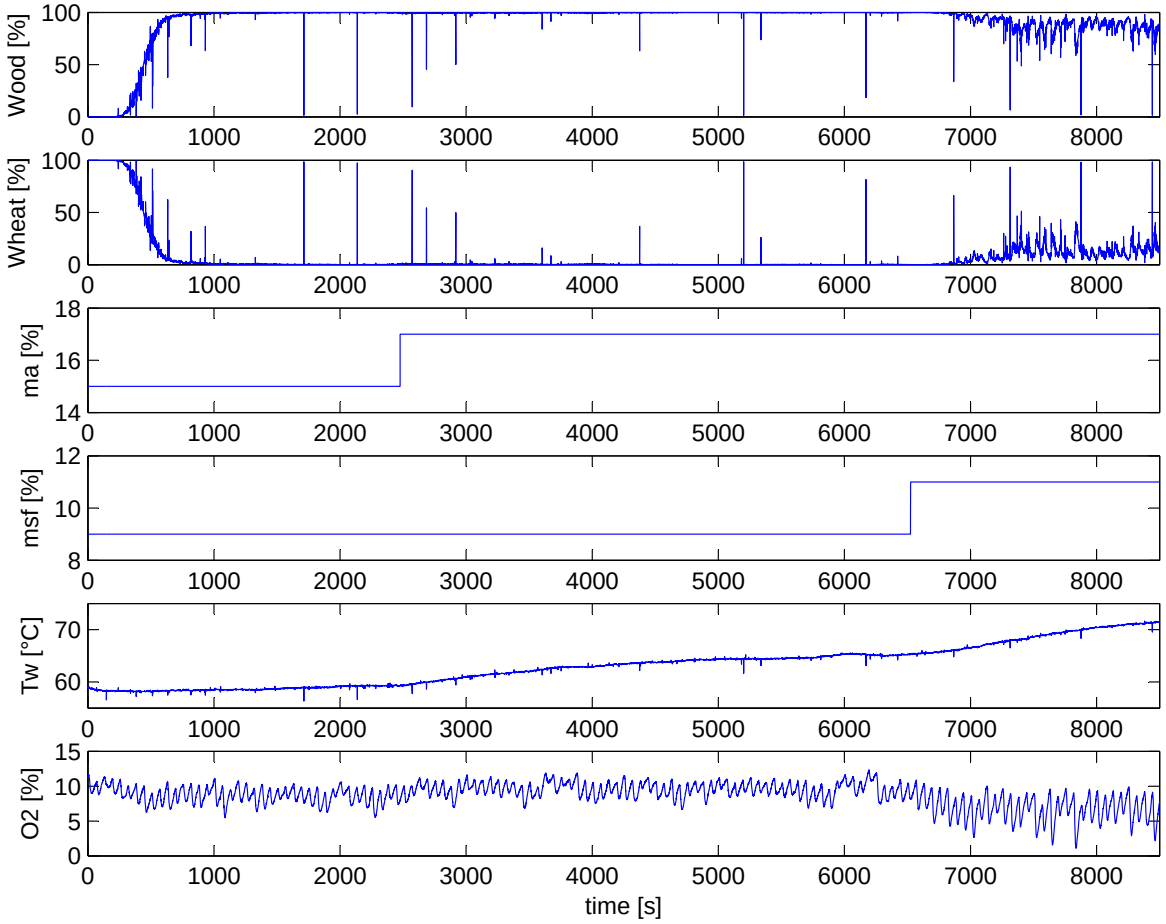

Figure 11.3: *Test with wood pellets as solid fuel.*

wrong estimate. When a small step in the load is performed again at around 13000 s the solid fuel estimator gives a wrong estimate again. Even when the O_2-level is lowered so it become close to the operation point of wood pellets the solid fuel estimator is still capable to find that wheat is the actual solid fuel.

The next test is made with a mixture of solid fuels. The mixture of the solid fuels is hard to make accurate, as the wheat is much smaller than the wood pellets. The mixture has tried to be made 1:1 of the solid fuels. The result of the test can be seen in Figure 11.5. The solid fuel estimator uses around 300 s to find the mixture of the solid fuels. The change around 10000 s is due to the uncertainty about the current solid fuel mixture. The temperature during the test is between 60°C and 70°C. The solid fuel estimator estimates that there is more wheat present after 1500 s. This can actual be the case as the wood pellets burns faster than the wheat and therefore there will be more wheat than wood pellets in the burning chamber after some time. The solid fuel estimator does as expected, when mixed solid fuel are tested.

11.1.2 On-line Verification on the Plant

This test has been made to investigate what influence the water temperature and the O_2-level has on the output of the solid fuel estimator. In the beginning of the test a mixture of solid fuels of 1:1 between wood pellets and wheat is used. In the end of the test around 5000 s the solid fuel only consist of wheat. As it is shown in Figure 11.6 the mixture is around 1:1 in the

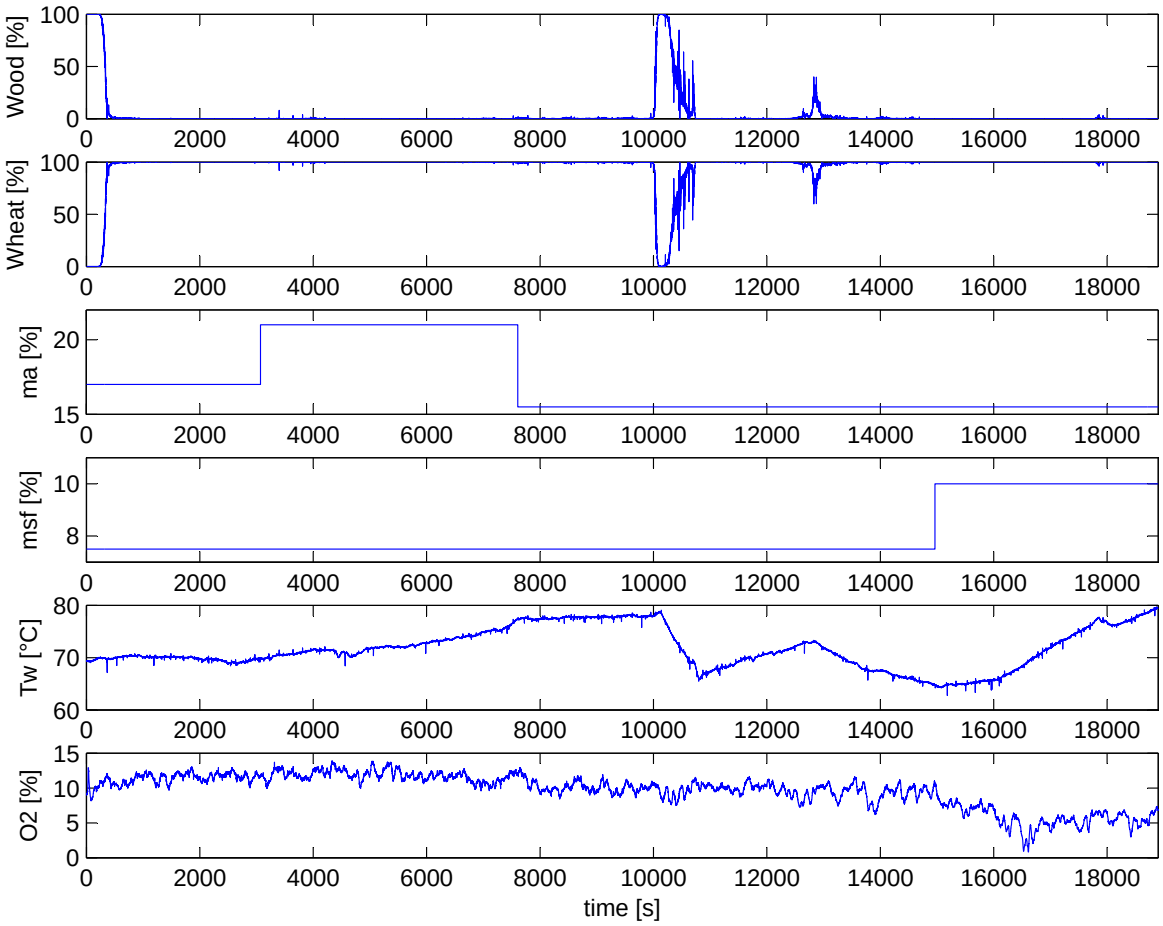

Figure 11.4: *Test with wheat as solid fuel.*

beginning of the test. When more solid fuel is put into the stoker the temperature will raise and the O_2-level drop. This means that the O_2-level indicate that wood pellets are used and the raising temperature indicate that wheat is used. But this does not change the behaviour of the solid fuel estimator. The possibility of wood pellets begins to rise as expected just around 1000 s. However a low O_2-level will result in wood pellets as output of the solid fuel estimator and when the O_2-level is raised the solid fuel estimator will assume that wheat is used as solid fuel. This can be seen from the figure in the time span from 2000 s to 4000 s as the possibility for the different solid fuels react on the change in O_2-level. After 5000 s the solid fuel only consist of wheat. Here the O_2-level is low again which indicates that wood pellets should be the actual fuel. But the solid fuel estimator can still determine that wheat is the current solid fuel.

This verification shows that the solid fuel estimator is capable of deciding which solid fuel is in use. In normal operating, the user will only use one solid fuel at a time. In this case the solid fuel estimator can estimate which solid fuel is used almost without any errors. In the test with mixed solid fuels and when the water temperature or the O_2-level is closer to the operating point of another solid fuel the solid fuel estimator is less accurate. This problem could however be solved by using extra models for the same solid fuels, but with different operation points. In this report only two different models are used as this is enough to differ between the two solid fuels used.

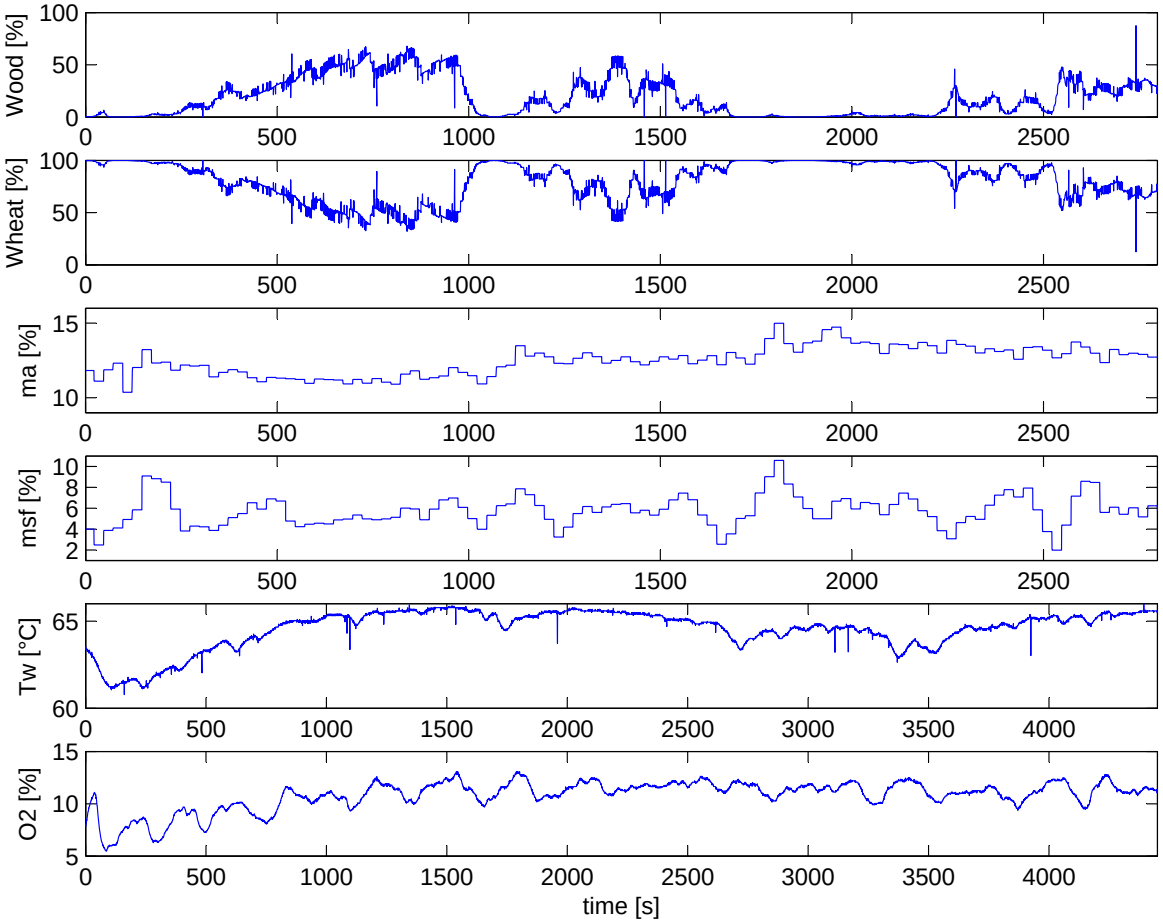

Figure 11.5: *Test with mixed solid fuel.*

11.2 Implementation of the Adaptive Controller

As both the controllers and the solid fuel estimator are designed and tested individually the two blocks are assembled. This is done by using the control signals from the two LQR controllers and the possibility from the solid fuel estimator to weight the output from the controllers. When this is done the output from the controllers is added to give the control signals to the plant. The main idea of this is illustrated in Figure 11.7.

The solid fuel estimator gives the output corresponding to the solid fuel that are used in the simulation. The simulated adaptive controller will then give the same output as the two LQR controllers individual. These simulations can been found in Chapter 10. The finally test with the adaptive controller implemented on the plant is found in the acceptance test (see Chapter 12).

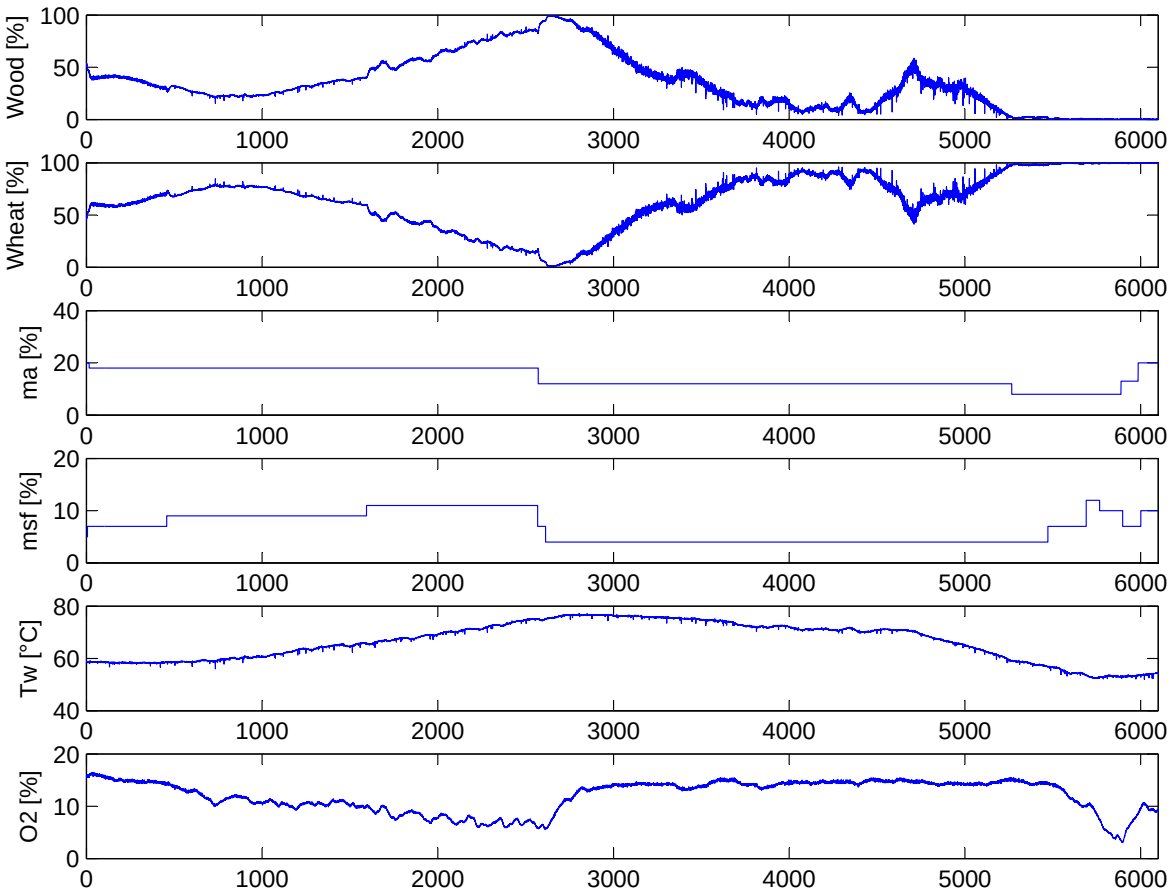

Figure 11.6: *Real system test with mixed and wheat as solid fuel.*

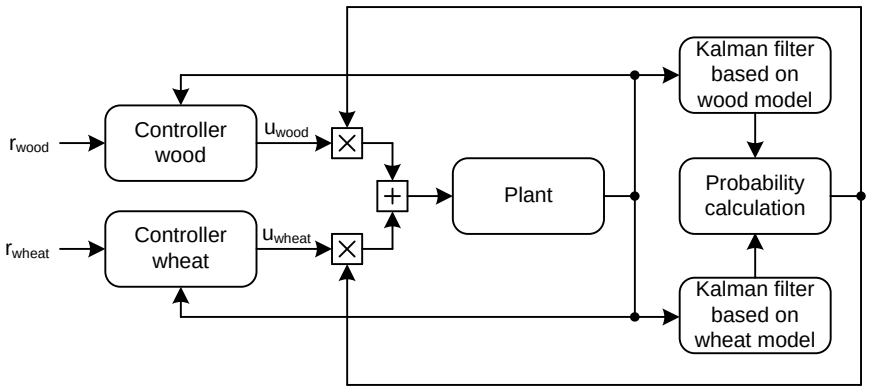

Figure 11.7: *A block diagram of the controller setup with the controller and solid fuel estimator block.*

Part IV

Conclusion

In this closing part of the main report the results from the tests which are described in Chapter 3 are presented. This part include three chapters.

First the obtained test results are presented and discussed in the acceptance test.

In the conclusion the main results in this report are emphasized.

Finally a closing statement is given to discuss the project as a whole.

Chapter 12

Acceptance Test

In this chapter the controller is tested against the requirements specified in Chapter 3. In order to test if the controller reacts as expected a comparison is made to the simulations made in SIMULINK on the non-linear model.

The tests presented in this section are divided into three separate test. The tests are discussed one by one and the results are shown in figures.

Test One

This test is done, to verify the performance of the LQR controller designed for wood pellets. A test on the plant has been made and the result is shown in Figure 12.1

The controller is compared to the requirements to the water temperature. When the water temperate fist is decreased to the reference on 60°C is the controller capable of keeping the water temperature close to the reference. Even when a large change in the disturbance is present is the controller capable of keeping the water temperature inside ±5°C from the reference.

The requirements to the O_2-level is that the controller should be able to keep the reference with ±2%. From Figure 12.1 can it be seen that this is not case as the O_2-level vary with ±3% from the reference on 6%. This is not acceptable as the requirements are not fulfilled. An explanation on why the O_2-level vary that much, can be found in the combustion of the wood pellets. When they are combusted they will form a crust. When this crust cracks, the O_2 consumption will increase, as unburned wood pellets are available.

As the requirements to the water temperature are fulfilled, will it be possible to weight the O_2-level more compared to the water temperature which may cause that the O_2-level does not vary so much.

The controller just tested is compared to the existing controller at Techno-Matic A/S, where the references are set to 60°C and 6% respectively. The results for the Techno-Matic controller are shown in Figure 12.2.

The Techno-Matic controller also keep the temperature of the water inside the ±5°C margin that has been specified. It varies however more than the controller designed in this project. There are also large variations on the O_2-level and it will sometimes reach zero. That can also be seen on the disturbance, as the inlet water temperature sensor gives an invalid output when this happens.

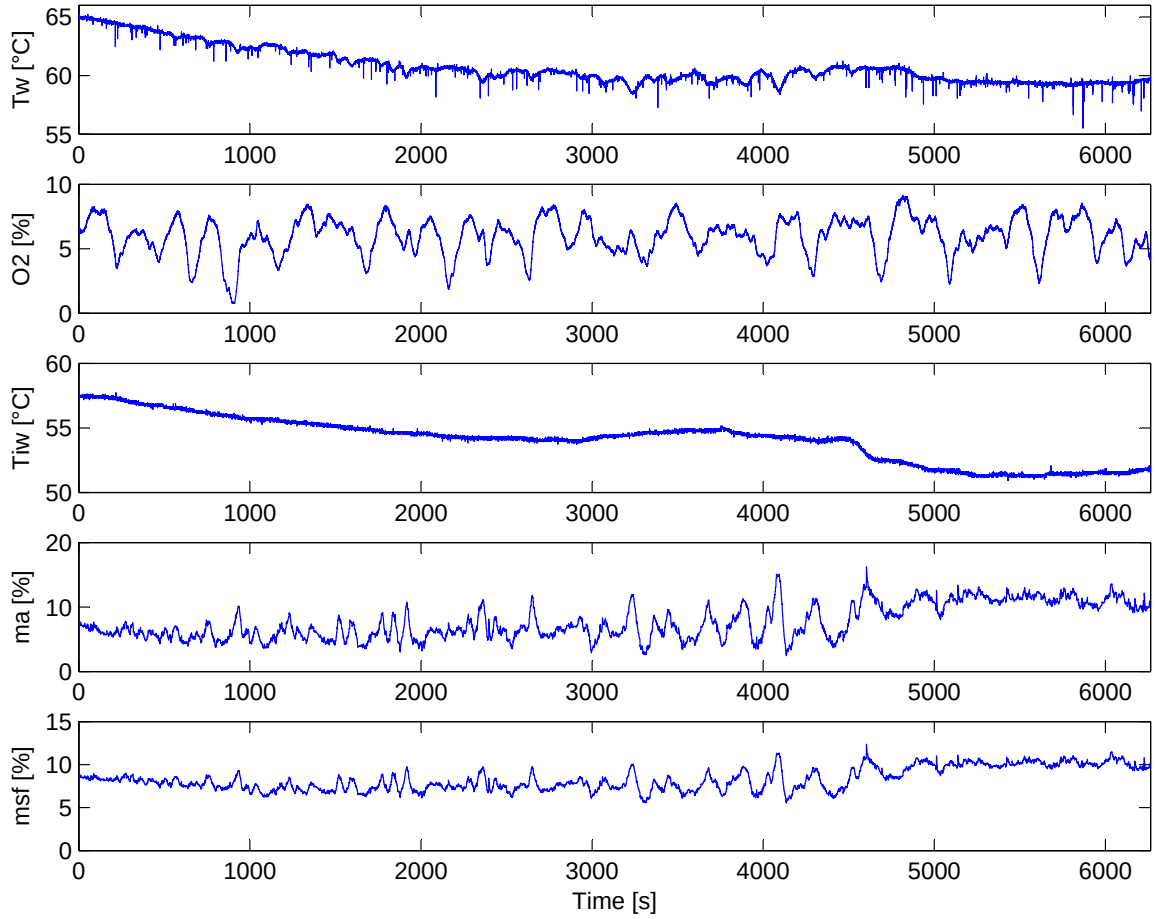

Figure 12.1: *Test of the LQR controller designed for wood pellets combustion.*

Compared to the LQR controller designed for wood pellets the Techno-Matic controller has inferior performance on both the water temperature and the O_2-level. Even though the LQR controller performs better than the Techno-Matic controller, it still does not pass the first test, as the O_2-level vary too much.

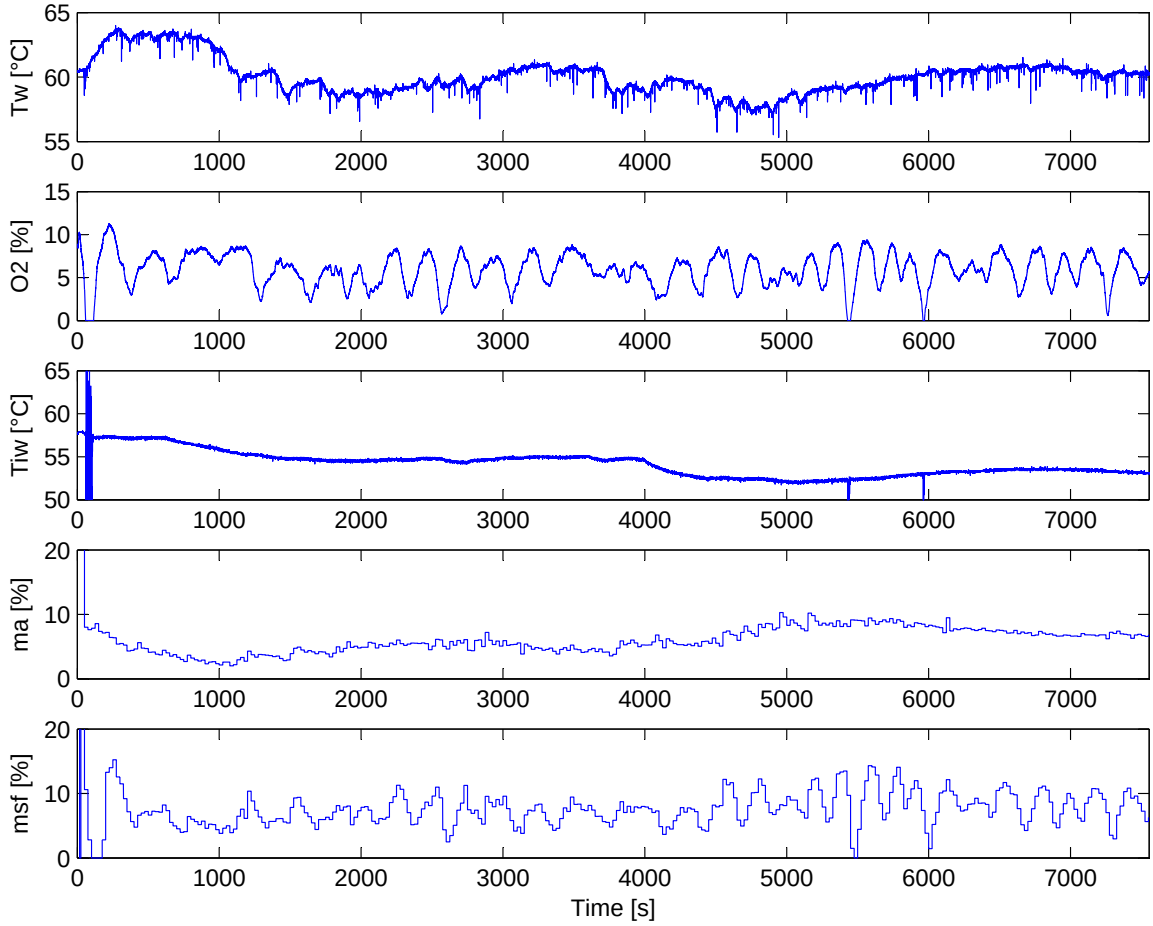

Figure 12.2: *Test of the Techno-Matic controller with wood pellets.*

Test Two

This test is done to verify the performance of the LQR controller designed for wheat. A test on the plant has been made, the results are shown in Figure 12.3.

The water temperature differ more from the reference at 70°C compared to the LQR controller designed to wood pellets. The water temperature vary around ±5°C. This is however accepted, as the requirements are fulfilled. The O_2-level is also varying from the reference on 12%. The variation is however lower than the one seen for wood pellets but it is still to large, as it very around ±3%. This controller has a more desired behaviour, compared to the LQR controller designed for wood pellets. The O_2-level also has a higher priority in this controller but not enough to pass the test.

This controller is also compared to the Techno-Matic controller, where the O_2-level reference is set to 12% and the water temperature reference to 70°C. The test of the Techno-Matic controller is shown in Figure 12.4.

The Techno-Matic controller handles the task well. The water temperature is close to the reference and the O_2-level differ not as much as the case with the other controllers. This test is however the one, where the disturbance have been closest to be constant, this can have a positive influence on the result compared to the other controllers.

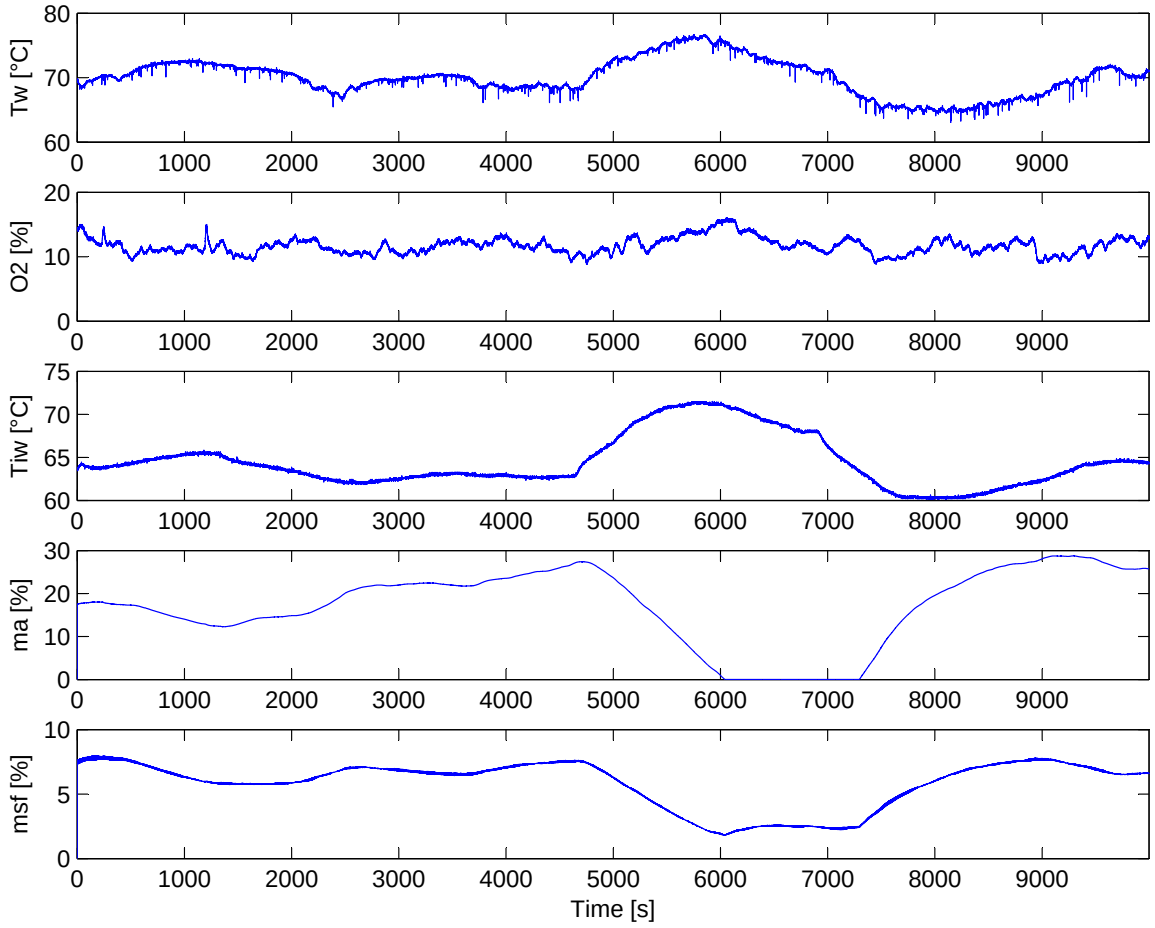

Figure 12.3: *Test of the LQR controller designed for wheat combustion.*

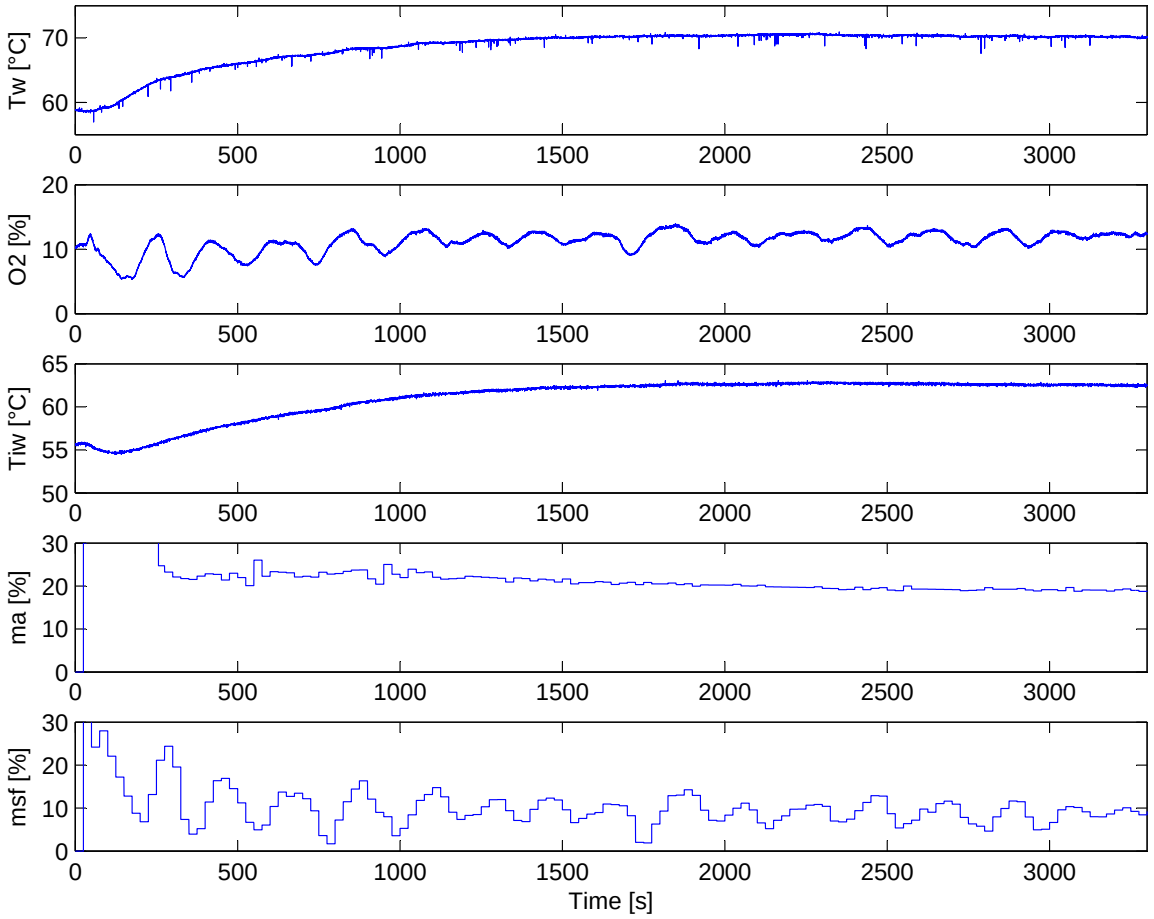

Figure 12.4: *Test of the Techno-Matic controller with wheat.*

Test Three

The two controllers are assembled as described in Chapter 11.2. The calculation of the solid fuel has been tested in Chapter 11 with satisfying result. In Figure 12.5 is the test results for the adaptive controller shown. In the beginning of the test is clean wheat used as solid fuel (first 2000 s), a mixture of 1:1 with wheat and wood pellets are afterwards used as solid fuel.

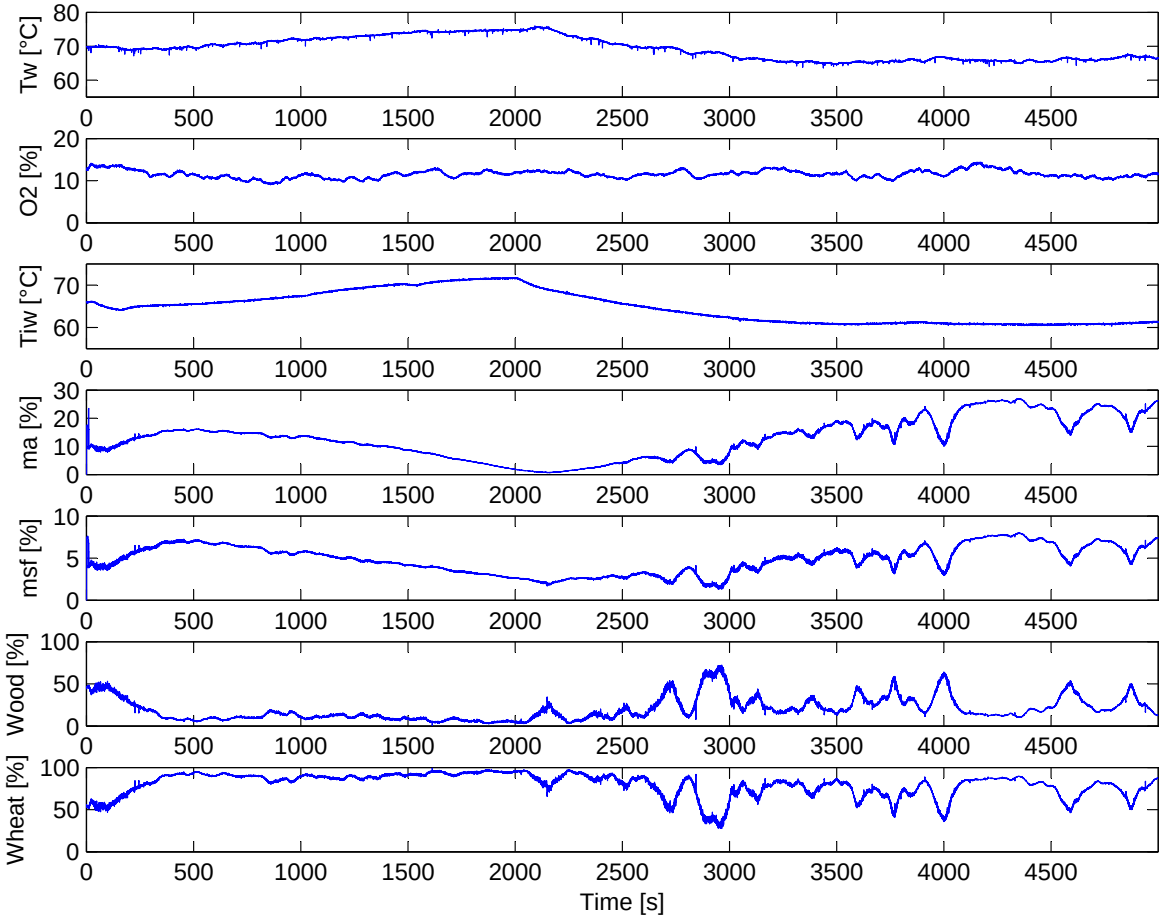

Figure 12.5: *Test of the adaptive controller.*

The controller determines that wheat is the actual solid fuel after 300 s. It is also seen that the LQR controller designed for wheat is in use for the first 2000 s, as the water temperature and O_2-level are close to 70°C and 12%. When the solid fuels are mixed, after 2000 s, is the water temperature decreased. This is as expected as the reference for the LQR controller designed for wood pellets is 60°C. The solid fuel mix is about 75% wheat and 25% wood pellets seen over the rest of the period after 2000 s. This should result in a water temperature around 67.5°C and a O_2-level around 10.5%. It can be seen that the water temperature is approximately 67.5°C and that the O_2-level is varying between 10% and 15%. This means that the weight of the O_2-level is larger for the LQR controller designed for wheat than it is for the one designed for wood pellets. Therefore is the water temperature reference for the LQR controller designed for wheat the dominating factor which gives a higher O_2-level then 10.5%.

Chapter 13

Conclusion

The main purpose of this project was to control the stoker system. This goal was accomplished through modelling the stoker system and using the model to design a controller.

As the setup was supplied by Techno-Matic A/S, some hardware improvements was made, to verify the model and obtain a better control of the stoker system. This included a flow meter, an inlet water temperature sensor, and a smaller period time for the actuators. The filters, used by Techno-Matic A/S, on the sensors have also been removed.

The main improvements were to make a model based controller and an estimator so the actual solid fuel could be determined. The non-linear and linear models of the system are satisfactory verified for both wood pellets and wheat using measurements from the plant.

This allows designing two LQR controllers based on the linear model, one for wood pellets and one for wheat. The linear models are also used in a Kalman filter to make the solid fuel estimator. This estimator is verified satisfactory using measurements from the plant, even though measurement noise was able to confuse the estimator.

The acceptance test revealed that the controller was able to control the stoker system. The predefined requirements to the controller were however not fulfilled. But the controller was able to keep the operation area around the desired reference and in most cases, the performance was better than the controller used by Techno-Matic A/S.

Even though the controller does not achieve the desired performance, the project is seen as a success as the models are verified and used in the controller and estimator design. The principle with a controller for each solid fuel worked, and based on the individual simulations made on the two controllers further improvements to the controller is seen as a possibility.

Chapter 14

Discussion

This chapter will discuss the results given in the conclusion by evaluating whether the methods used in this report are applicable for modelling and controlling the stoker system. It will provide a brief summary of the main problems encountered during the development. Further improvements to the stoker system will also be discussed here.

Due to the importance of the control aspects, the hardware of primary concern is the period time of the actuators. As the period time used in the original Techno-Matic controller was so slow, that it could be seen on the O_2 measurements. This has been improved by changing the period time from 20 s to 5 s on the actuator output.

The water temperature sensors occasionally make a faulty measurement. This could be filtered out, as the sample time for the sensor is hundred times faster than the input to the controller. This will make the measurements more trustworthy. The measurement from the lambda oxygen sensor could also be filtered in order to help the controller, as more accurate measurements would be available.

Both non-linear and linear models of the system have been developed. The non-linear models in this project are used to find the linear models and simulate the plant. The models have only been created for two different solid fuels, it is however not seen as a problem to derive models for other solid fuels as well.

The controller is based on a linear quadratic regulator algorithm. This approach yields an optimal controller according to a performance function. This method is both efficient in the sense that it optimizes the burning of solid fuel, and flexible in the sense that different aspects can be considered for optimality by designing the performance function accordingly for the water temperature and the O_2-level. Thus, this report concerns the feasibility of the application of the linear quadratic regulator algorithm. However some tuning is necessary to obtain the performance specified in the main objective. This has resulted in the design of two discrete LQR controllers one for each solid fuel.

A 15 s delay has been found between the modelled O_2-level and the O_2-level in the burning chamber. This has caused some problems in the controller design. But a solution is found by adding 15 new states to the model, where the seventh state is delayed with one sample compared to the sixth state and so on. The optimal controllers based on this assumption are less aggressive to variations in the O_2-level.

The solid fuel estimator is based on Kalman filters, which use the linear models, and Bayer's probability rule. It can be advantageous however to use the non-linear models in an extended or

unscented Kalman filter, so a linear model can be found on-line for the current operation point at each sample.

The final controller consists of the two LQR controllers and the solid fuel estimator creating an adaptive controller. This is assembled by weighting the output from the two LQR controllers by the solid fuel estimator. This setup works in some sense. However some tuning of the two LQR controllers is necessary to obtain a satisfying result for the adaptive controller.

Chapter 15

Closing Statement

The reason for this project is that Techno-Matic A/S would like a new controller for a Benekov/Liagro R 25 stoker. Today Techno-Matic A/S has a PID controller on the stoker system as mentioned in this report. A model based controller and a model of the stoker system was however wanted, to get an understanding of the system and a model from which controllers could be designed. The main objectives for this group were to model and control the stoker system and make an adaptive controller to the stoker system. Furthermore the controller concepts will probably also be used in later projects at Techno-Matic A/S, so the results from this project make up the foundation for an even better control and a more clean combustion in the stoker system.

The methods used to find the models for the two solid fuels, that are present in this report, can also be used on other fuels, so an adaptive controller for all possible solid fuels to the R 25 stoker system can be obtained. Also the knowledge from the model and controller development is useful when dealing with other stoker systems. Although the controller did not improve the performance of the stoker system to a great extent, the principle and design strategy was found suitable. However Improvements are possible with a better fitted controller to the O_2-level and more accurate or filtered measurements.

To summarize, the knowledge and experience gained from this project is a sound foundation for the development of controllers to stoker systems and in particular stoker systems from Benekov/Liagro.

Bibliography

Andersen, Palle & Pedersen, Tom S., *"Modeldannelse"* (2007). Lecture note for the course "Modeldannelse og simulering" at 6th semester at the section of Automation and Control, Aalborg University. `http://www.control.aau.dk/~pa/kurser/PR6model/modelnote.pdf`.

Annamalai, Kalyan & Puri, Ishwar K., *"Combustion Science And Engineering"* (CRC Press, 2007), first edition.

B, Martin E & J, Morris A (1999). *"neural networks"*. Newcastle University. `http://www.ncl.ac.uk/cpact/neural_networks.html`.

Bak, Thomas, *"Lecture Notes - Estimation and Sensor Information Fusion"* (2000). Lecture note for the course "Estimation and Sensor Fusion" at 9th semester at the section of Automation and Control, Aalborg University. `http://www.control.aau.dk/~tb/Teaching/Courses/Estimation/sensfusion.pdf`.

Bak, Thomas (2007). *"http://www.control.aau.dk/~tb/teaching/courses/hybrid-systems/"*. Aalborg University. Course description for the course "Introduction to hybrid systems I" at 9th semester at the section of Automation and Control, Aalborg University.

Bemporad, Alberto, Casavola, Alessandro & Mosca, Edoardo (1997). *"nonlinear control of constrained linear systems via predictive reference management"*. IEEE Transactions on Automatic Control, Vol. 42, No. 3.

Bosch (2002). *"sensors"*. Sensor catalogue from Bosch.

Cengel, Yunus A., *"Heat Transfer: A Practical Approach"* (The McGraw-Hill Companies, 2003), second edition.

COWI, *"Optimering af brændselsvalg og driftsformer - Virkningsgrader og driftsøkonomi for biomassefyrede kedler"* (COWI A/S, 2004).

Energistyrelsen, *"Varmeforsyning i Danmark - Hvem Hvad Hvor og Hvorfor"* (Energistyrelsen, 2004). `http://www.ens.dk/graphics/Publikationer/Forsyning/Varmeforsyning_pixibog/pdf/Varmeforsyning_pixibog.pdf`.

Fraden, Jacob, *"Handbook of Modern Sensors: Physics, Designs and Applications"* (Springer-Verlag, 2004), third edition.

Franklin, Gene F., Powell, J. David & Emami-Naeini, Abbas, *"Feedback Control of Dynamic Systems"* (Prentice-Hall, 2002), fourth edition.

Jantzen, Jan (1991). *"fyzzy control"*. Electric Power Engineering Department - Technical University of Danmark. Lecture notes for the course "Soft Computing" at 8th semester at the section of Automation and Control, Aalborg University. http://www.control.aau.dk/~dimon/edu/nnfl/lecture1/jantzen1.pdf.

Jensen, Søren Kildedal (2007). *"development engineer at techno-matic a/s"*. From several conversations through the fall of 2007 and spring of 2008.

Knudsen, Torben, *"Lecture Notes - Kalmanfilteret - en kort introduktion"* (2000). Lecture note for the course "Estimation and Sensor Fusion" at 9th semester at the section of Automation and Control, Aalborg University. http://www.control.aau.dk/~tk/undervisning/estimation/kf.pdf.

MathWorks, *"xPC Target Selecting Hardware Guide"* (The MathWorks, 2007). https://tagteamdbserver.mathworks.com/ttserverroot/Download/37937_xpc_target_selecting_hardware_guide.pdf.

Sastry, Shankar & Bodson, Marc, *"Adaptive Control Stability, Convergence, and Robustness"* (Prentice-Hall, Inc., 1989), first edition.

Åström, Karl J. & Wittenmark, Björn, *"Adaptive Control"* (Addison-Wesley Publishing Company, 1995), second edition.

Tay, Arthur (2007). *"http://msc2007.nus.edu.sg/isic2007.htm"*. National University of Singapore.

Dansk Fjernvarme, *"Fjernvarmepriserne i Danmark - Resultat af prisundersøgelsen 2007"* (Dansk Fjernvarme, 2007). http://www.losningfjernvarme.dk/gfx/brugerupload/documents/bilag_-_fjernvarmepriserne_i_danmark_2007.pdf.

Zhou, Kemin & Doyle, John C., *"Essentials Of Robust Control"* (Prentice-Hall, Inc., 1997), first edition.

Zhou, Kemin, Glover, Keith & Doyle, John C., *"Robust and Optimal Control"* (Prentice-Hall, Inc., 1996), first edition.

Part V

Appendix

Appendix A

SIMULINK Interface Description

This appendix describe the SIMULINK interface to the stoker system. In the interface the PLC-812PG I/O card is set up and the signals are adjusted. The description is made with a top down approach. This is chosen to give an overview of the system, before the specific details about how it is implemented is given. Notice that input on the I/O card is output in the SIMULINK-block and vice versa.

The Interface

The total interface is collected in one SIMULINK-block as show in Figure A.1, where the inputs are the fan speed in Hz, the screw conveyor, and the blower in PWM. These three inputs are outputs on the I/O card which connects SIMULINK to the actual hardware. The I/O card has two analogue outputs and five digital outputs. The screw conveyor and the blower are both controlled by a PWM signal and therefore using a digital output. The calorifier is using an analogue output.

The I/O card has both digital and analogue inputs. In the SIMULINK-block only analogue outputs are used. The analogue outputs are used to adjust the signals from the sensors.

The I/O Card

The contents of the I/O card SIMULINK-block can be seen in Figure A.2.

The two analogue output is connected to the analogue out box. The signal to the calorifier is scaled ten times down, because an output of four will give a frequency for the calorifier on 40 Hz. The other output is not used and is connected directly to the analogue out SIMULINK-block.

The screw conveyor and the blower inputs are both set into a block that calculates the needed PWM signal on the output corresponding to the given input signal. Furthermore a switch is implemented, so it is possible to manually set a constant or pulse signal directly on the I/O card. The PWM signals are then sent into the PCL-812PG digital output block, this block set up the parameters to the I/O card. The PCL-812PG block takes a channel vector, sample time, and base address as input. The channel vector specifies the channel number on the I/O card. The base address input is the address the I/O card has in the computer it is connected to. The PCL-812PG-block is made by a S-function and is using the standard `doadvpcl812`

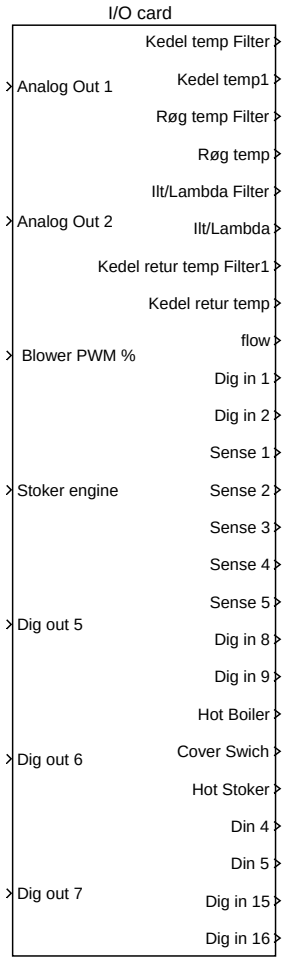

Figure A.1: *Block diagram of the I/O card* SIMULINK*-block.*

MATLAB-function.

The PCL-812PG digital input block is used to communicate with the digital inputs on the I/O card. This block is not used in this setup.

The input/sensor adjustment blocks give the analogue inputs to the I/O card. These can be taken with or without filter on the different sensors, the filters are described in Appendix B.

The Analog Out SIMULINK Block

This block connects the two analogue outputs in SIMULINK to the I/O card. This is done using the PCL-812PG-block. This block takes a channel vector, range vector, sample times and base address as inputs. The channel vector specify the channel number on the I/O card, the range vector specify the range of the signal values. The base address is the address the I/O card has on the computer. The block is working using a s-function which calls the function `daadvpcl812` that is standard in MATLAB.

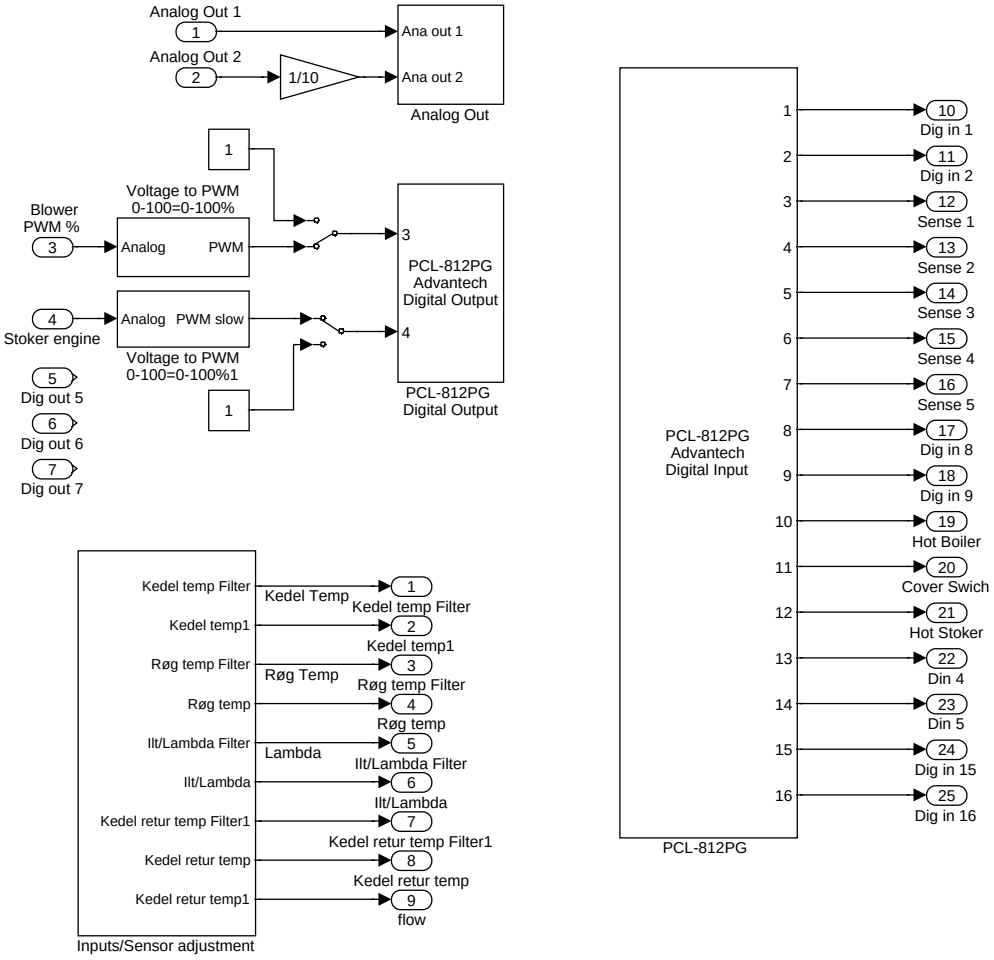

Figure A.2: *Block diagram inside the I/O board* SIMULINK*-block.*

The Voltage to PWM Blower Block

The voltage to PWM blower block can be seen in Figure A.3.

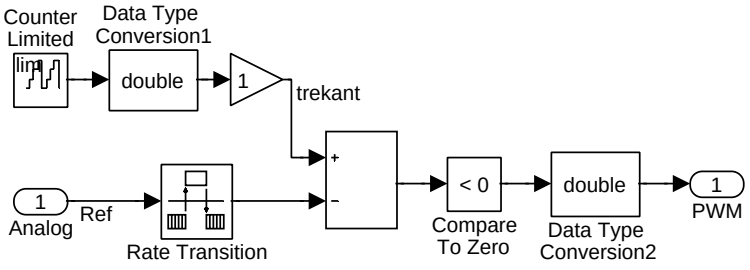

Figure A.3: *Block diagram of the voltage to PWM blower block.*

The counter limited block is counting from 0 to 99 this is then made to a double data type in the data type conversion block this gives the limitation that it always will jump with 1%. The rate transition block ensures that the input signal gain the sample time that are desired for the PWM output. This signal is then sent into a subtract block. The input signal is subtracted form the result of the counter block. The result is then compared to zero. The time where the

output from the subtract block is negative, the PWM will give a high output on the I/O card. The output signal is then converted to a double of type before it is used as an output. This means the output sample time, is found from the counter and the sample time given in the rate transition block. For the blower block, the sample time is found to:

$$\text{sample time rate transition} \cdot \text{counter interval} = 0.01 \text{ s} \cdot 100 = 1 \text{ s} \tag{A.1}$$

A duty circle on 1 s with a resolution of 1% is a good trade off. While it is assumed that the air flow inside the system, will be close to constant over a one second period. Thus the resolution on 1% is satisfying for the blower.

The Voltage to PWM Screw conveyor Block

The voltage to PWM screw conveyor block can be seen in Figure A.4.

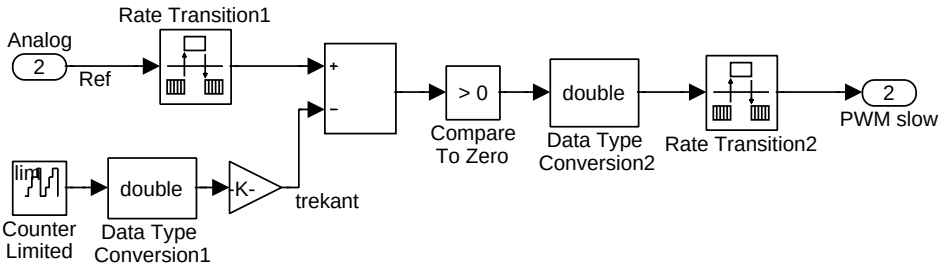

Figure A.4: *Block diagram of the voltage to PWM screw conveyor block.*

This block is working as the voltage to PWM blower block in general. But the rate transition on the input is using the TsStoker variable as sample output, but this is changed to the PWM sample output in the rate transition just before the output. So the output has the same sample time as the voltage to PWM blower block. The counter is made by the variable stokerstep. The output from this block is then divided with the number of times the stokerstep variable goes up into one hundred. This makes it possible to set the resolution on the PWM, by using the stokerstep variable. E.g. if stokerstep is set to 1000, the resolution will be 0.1%, is it set to 10000 is the resolution 0.01%. The subtraction and compare block is inverted compared to the voltage to PWM blower block but works the same way. But it is a trade off between revolution and sample time, as the sample time out of the I/O card is found from the counter and the sample time in the rate transition. For the screw conveyor the sample time is set to:

$$\text{sample time rate transition} \cdot \text{counter interval} = 0.01 \text{ s} \cdot 250 = 2.5 \text{ s} \tag{A.2}$$

A duty circle on 2.5 s with a resolution of 0.25% is a good trade off for the screw conveyor. The precision of solid fuel added to the system is assumed to be more important than the air, therefore a higher resolution is chosen. This means the duty circle is 2.5 second, but as the solid fuel is burned slower, than the air is moving, will this also not be a problem. A faster duty circle with a better resolution down to 0.1 second can also be constructed; this will however change some of the setup done by Techno-Matic A/S. And if a resolution better than 0.1 s is necessary, the solid state relay must be substituted.

The Inputs/Sensor Adjustments Block

The inputs/sensor adjustments block can be seen in Figure A.5.

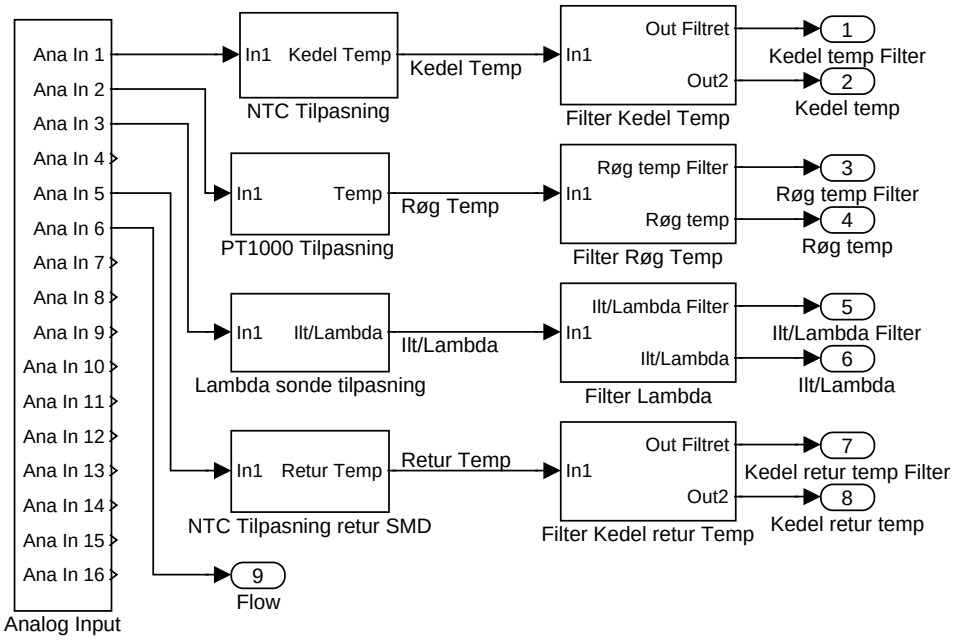

Figure A.5: *I/O card block of the input/sensor adjustments block.*

It consists of adjustments of the different sensors, so they output the desired variable instead of a voltage. The output variable can then be chosen to be taken when it has been through a filter. The filter is only used in the controller implemented on the system by Techno-Matic A/S (see Appendix B). The analogue input block gives the output measured by the I/O card from the sensors.

The Analogue Input Block

The analogue input block can be seen in Figure A.6.

This block consists of several PCL-912PG-blocks, which are communicating with the I/O card. The block takes a channel vector, range vector, sample time, and base address as parameters. The channel vector specifies the number of analogue input on the I/O card. The range vector specifies the max voltage range that can be set on the I/O input, and the base address is the address the I/O card has in the computer. The PLC-812PG-block is made with an S-function. It is using the standard MATLAB-function `adadvpc1812`.

The NTC adjustments Block

The NTC adjustments block receives the voltage from the I/O card as input and calculates the temperature of the water. It is made as shown in Figure A.7.

The NTC sensor is non-linear and the relation between temperature and resistance is given by Arrhenius Equation as:

$$t = \frac{\beta}{\frac{\beta}{t_0} - \log(\frac{R_0}{R})} - 273.15 \tag{A.3}$$

Where β is a material constant. The gain block is used to convert the voltage, to a bit value,

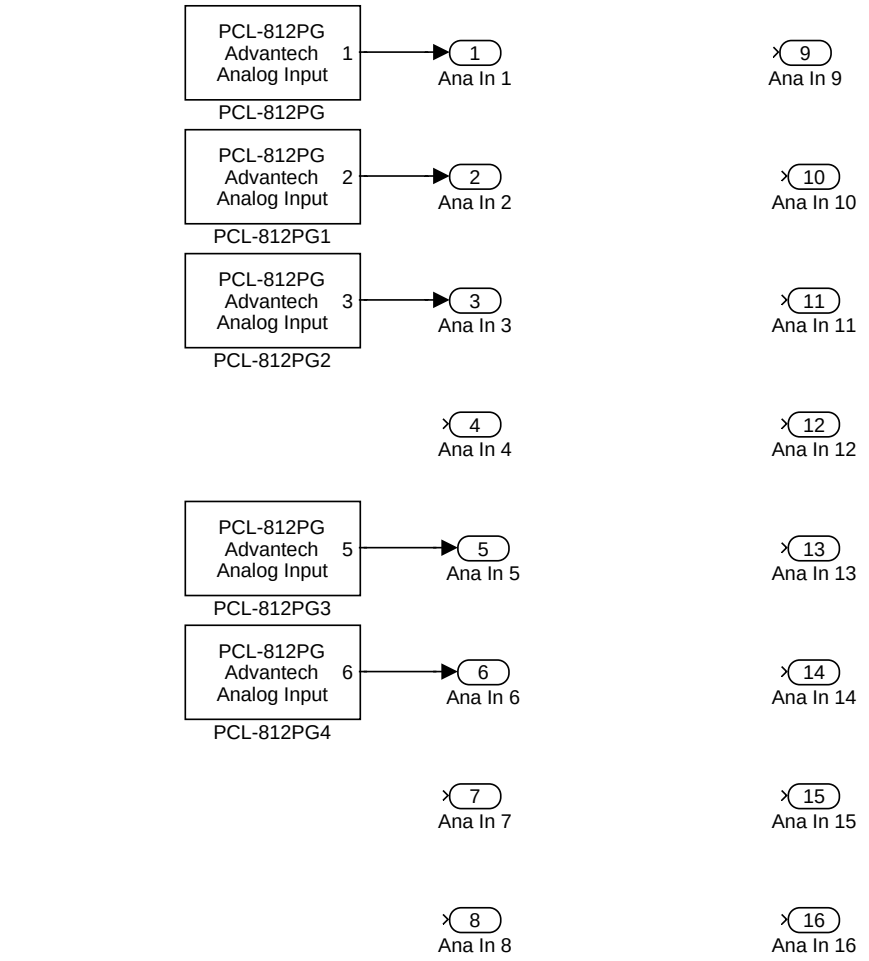

Figure A.6: *I/O board block of the analogue input block.*

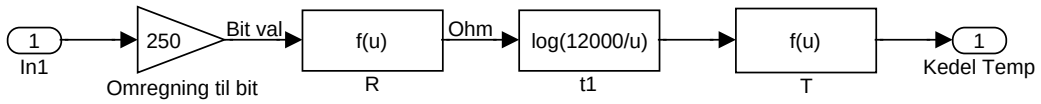

Figure A.7: *Block diagram of the NTC adjustment.*

that can be used for the equation for the NTC sensor. The next block calculates the resistance of the sensor, this is then calculated in two steps to a temperature in degrees. This is done in the blocks t1 and T. The values in the blocks are found from datasheet values [Bosch, 2002].

The PT1000 Adjustment Block

The PT1000 adjustment block receives the measured voltage as input and calculates the temperature of the exhaust gas. The block is made as shown in Figure A.8.

The PTC sensor is linear and the relation between temperature and resistance is given by:

$$t = \frac{R - R_0 + \alpha R_0 t_0}{\alpha R_0} \tag{A.4}$$

Where t is the temperature, R is the resistance, R_0 is the initial resistance at the initial temper-

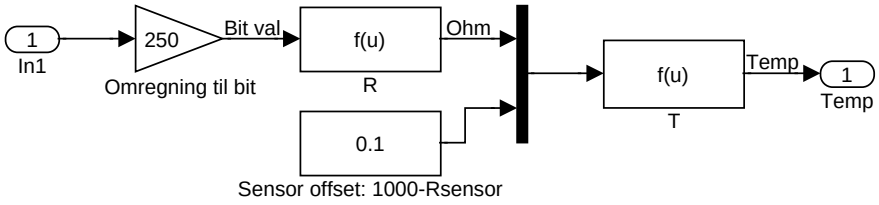

Figure A.8: *Block diagram of the PT1000 adjustment.*

ature t_0, and α is the temperature coefficient [Fraden, 2004]. The input voltage goes into a gain and the resistance of the sensor is then found, by using the R block. This and a sensor offset are then taken as input to a function that converts the resistance to a temperature in Celsius. The values are found from datasheet values [Bosch, 2002].

The Lambda sonde Adjustment Block

The block receives the signal from the I/O card as input and calculates the O_2-level. The relationship between the voltage and the O_2-level is given by Nernst Equation as:

$$O_2 - \text{ level} = \exp\left(\frac{U}{\frac{R \cdot T}{F}}\right) \tag{A.5}$$

Where U is the output voltage, R is the universal gas constant, T is the temperature of the exhaust gas in Kelvin, and F is the Faraday constant. This is implemented by using four blocks as shown in Figure A.9. First is the measured signal on the I/O card converted to mV in the two first blocks and then calculated to an O_2-level in two steps, by the last two blocks. The values inside the blocks are found from datasheet values [Bosch, 2002].

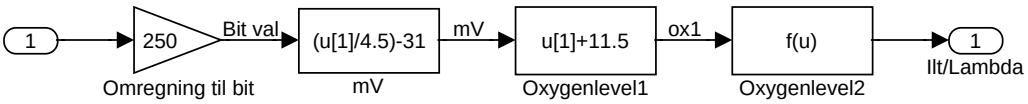

Figure A.9: *Block diagram of the lambda sonde adjustment.*

The NTC Adjustments Inlet Water Block

This block receives the measured result from the sensor that measures the temperature of the inlet water and calculates the temperature in Celsius. The NTC sensor is non-linear and the relation between temperature and resistance is given by Arrhenius Equation as:

$$t = \frac{\beta}{\frac{\beta}{t_0} - \log(\frac{R_0}{R})} - 273.15 \tag{A.6}$$

Where β is a material constant. This is implemented by using four blocks as shown in Figure A.10. First is the input signal calculated to a resistance and then is the resistance calculated to a temperature in Celsius.

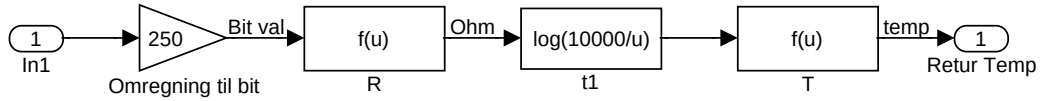

Figure A.10: *Block diagram of the return water NTC adjustment.*

The Water Flow Adjustment Block

This block receives the measured voltage as input and calculates the flow in m^3/s. The sensor is linear and 2 V equals a flow on 0 m/s and 10 volt equals a flow on 3 m/s. The implemented block is shown in Figure A.11.

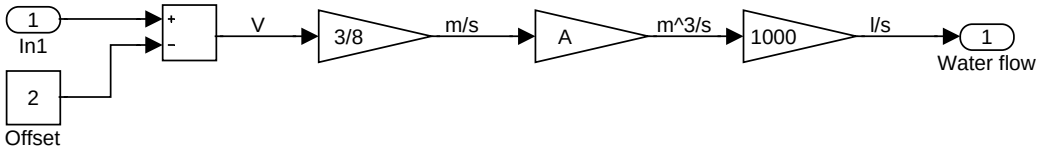

Figure A.11: *Block diagram of the water flow adjustment.*

First is a constant of 2 subtracted from the input voltage, due to the bias. The voltage is then calculated to a flow in m/s in the first gain block. In the next block the flow is found in m^3/s and finally is the last gain used to calculate the flow in L/s. This is also the output of the block.

Appendix B

Techno-Matic Controller

This appendix describes the controller which is designed and implemented on the plant by Techno-Matic A/S. The performance of the Techno-Matic controller is compared with the controller derived in this project in Chapter 12.

Implementation of the Techno-Matic Controller

The controller made by Techno-Matic A/S is implemented as shown on Figure B.1. The temperature reference is set by the user. This reference is then set into a PID controller that gives the output to the blower. The signal is sent through a rate transition to get the desired sample time on the output signal before the signal is sent into the I/O card block. Furthermore is it sent through a look up table to linearize it so the controller output is from 0 to 100%. The output from the controller is also used to control the screw conveyor directly with a feed screw gain and through a PID controller where the reference is found through an O_2-reference calculation. This is then feed into a screw conveyor PID controller that is multiplied with the output from the feed screw gain and through a gain and a look-up table is the input to the screw conveyor found. The screw conveyor PID controller also gets the O_2-level as input. This means that the water temperature and O_2-level is controlled by the blower and the screw conveyor. The setup with the I/O card and SIMULINK is described in Appendix A, but the filters that are implemented in the I/O card block is described in this appendix, because the filters only are used in the Techno-Matic controller.

PID Blower Block

The PID blower block takes the temperature reference and the temperature of the water as input and gives a signal from 0 to 100% to the blower. This is implemented as shown in Figure B.2. The difference on the measured and desired temperature is found. This is then sent into a saturation block that allows a maximal difference of 40°C on the temperature measurement and the desired temperature. The difference is then sent through a proportional gain on 3, with a saturation on 100. The controller also has an integral coupling with a gain on 0.3 this is added to the proportion gain. An anti wind-up gain is added with a value of 0.3. The rest of the controller blocks are multiplied with a gain on 0 and therefore have these no influence.

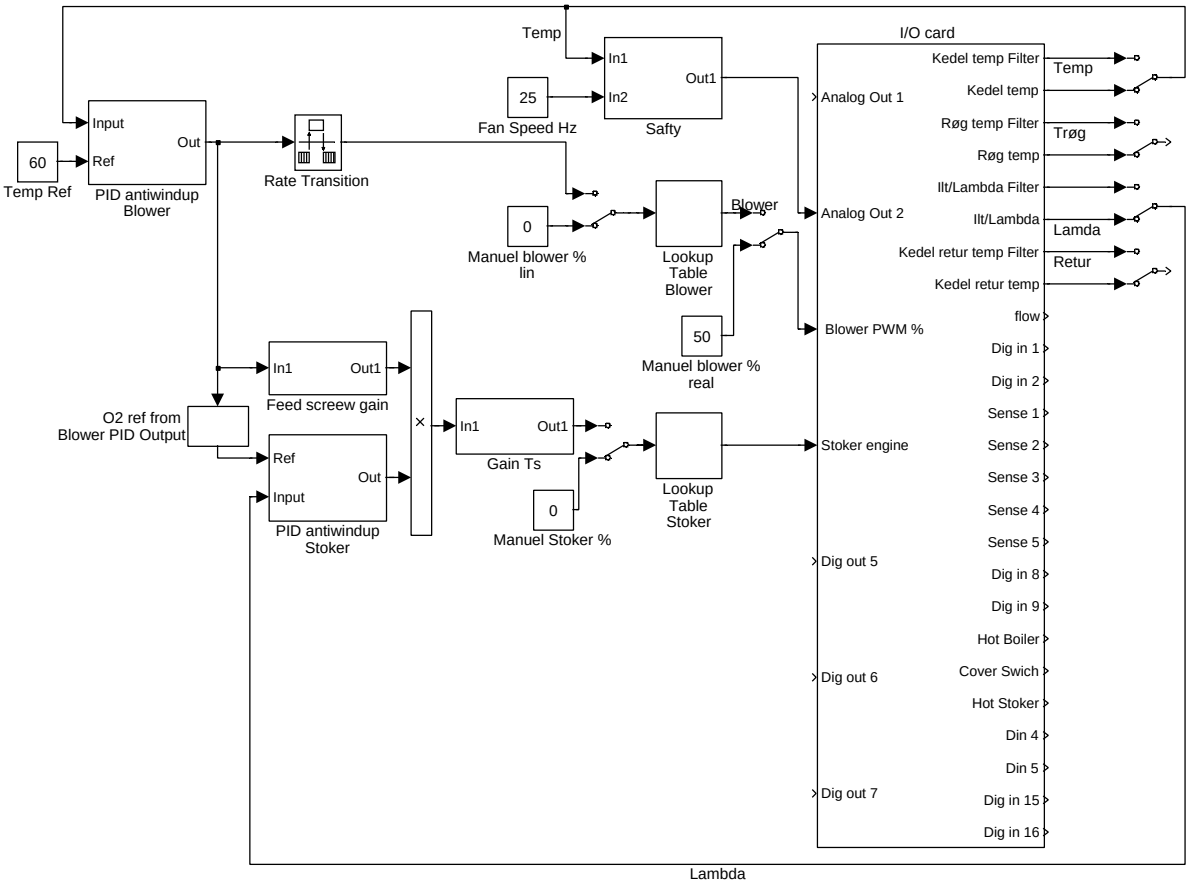

Figure B.1: *Diagram of the Techno-Matic controller.*

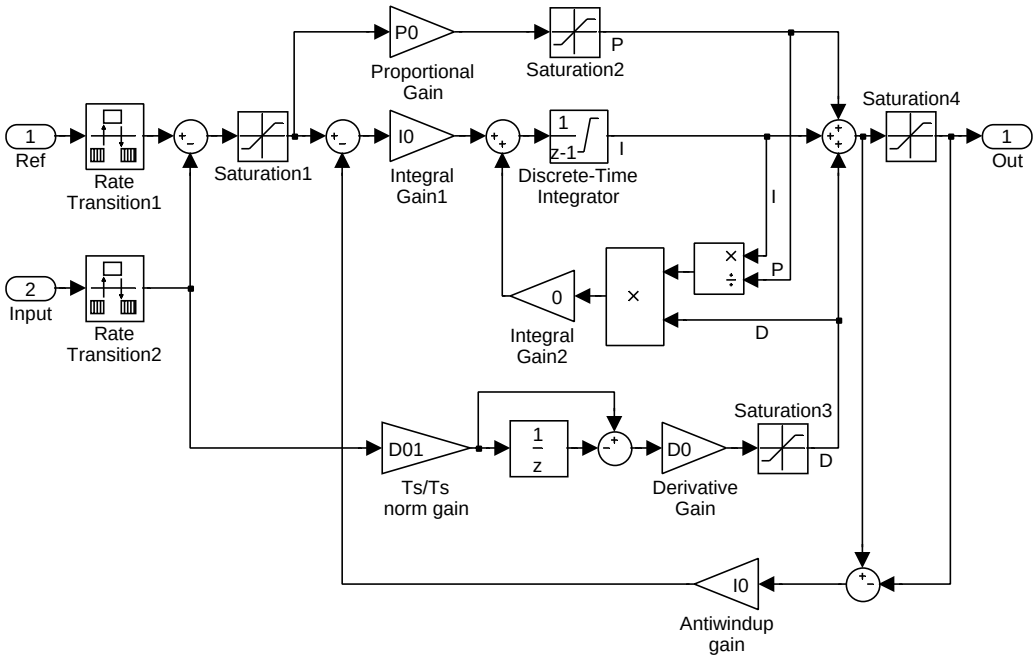

Figure B.2: *Diagram of the blower PID controller made by Techno-Matic A/S.*

PID Screw Conveyor Block

The PID screw conveyor block takes the O_2-reference from the block that calculates the O_2-reference from the stoker controller output as input and the O_2-level measured by the lambda oxygen sensor. The controller finds the difference between the two inputs. It is then sent through a PI controller, with a propagation gain on 3 and an integral gain on 0.3. The derivative gain and the added integral gain are multiplied by zero and have therefore no influence in the controller. The controller is implemented with anti wind-up with a gain on 0.3. For the implementation of the controller, see Figure B.3.

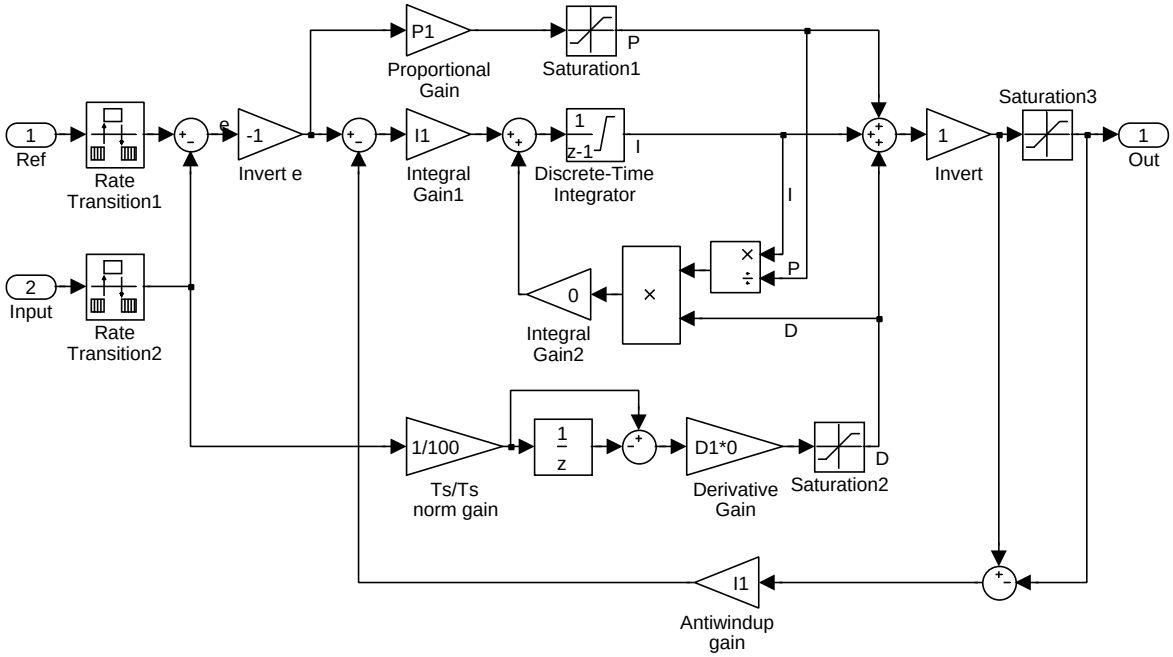

Figure B.3: *Diagram of the screw conveyor PID controller made by Techo-Matic A/S.*

Filters in the I/O Card Block

The measurements are filtered before they are sent into the controller in the solution that Techno-Matic A/S uses today. The filters used to the outlet water temperature, the exhaust gas temperature, and the inlet water temperature are implemented as shown in Figure B.4.

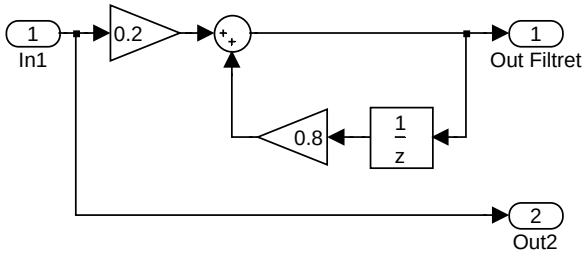

Figure B.4: *Temperature filters made by Techno-Matic A/S.*

This filter works as a low pass filter where it uses 80% from earlier measurements and 20% from

the new measurements. The lambda oxygen sensor output is also filtered this is made as shown in Figure B.5.

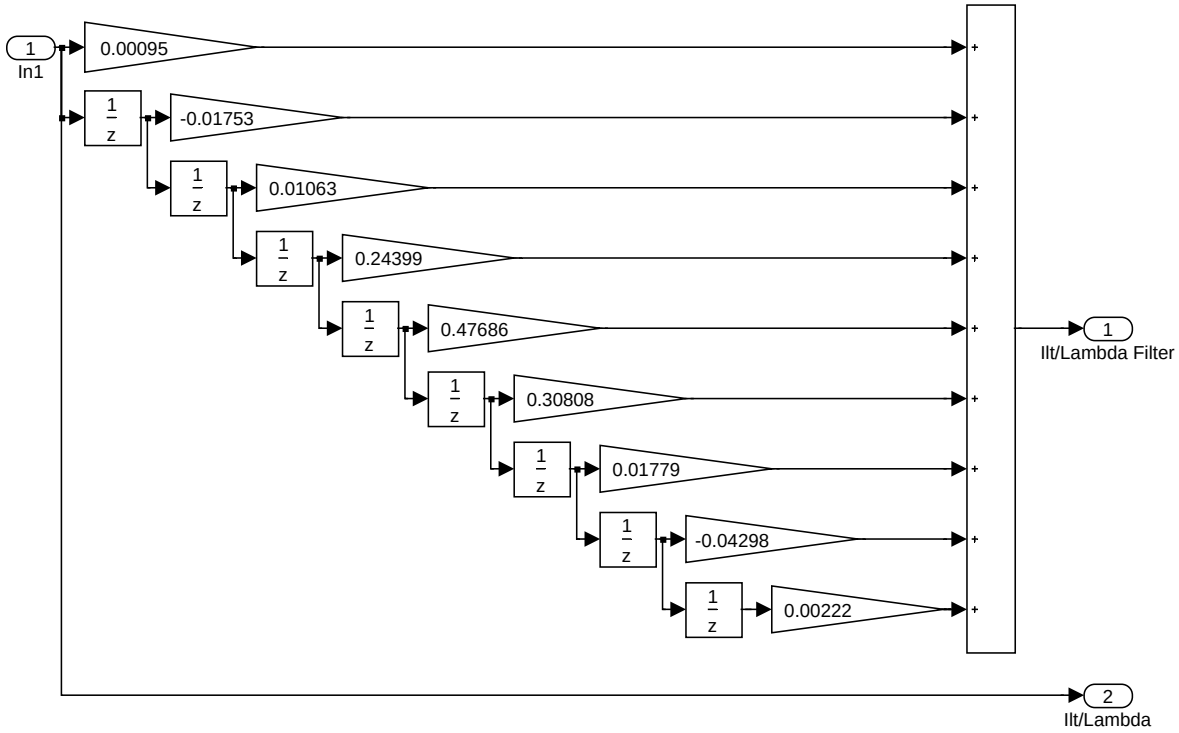

Figure B.5: *Lambda oxygen sensor filter made by Techno-Matic A/S.*

As the filter looks a little strange a step response is made. This can be seen in Figure B.6. As shown in the step response the filter gives a delay on 40 s. This is not optimal as the O_2-level is one of the fastest changing variables in the plant. The response of the filter shows it first damps the actual output whereafter it has an overshoot before it settle to the new value. The reason for implementing this filter can be a remain from an old controller where the solid fuel was feed from the top of the fireplace. The solid fuel will then temporary lower the fire and the O_2-level will decrease, the start of the step can then balance this. When the fire then get reach in the new solid fuel the O_2-level will increase and that can explain the reason for making the overshoot in the filter. So it could have been used to hide the system behaviour for the controller.

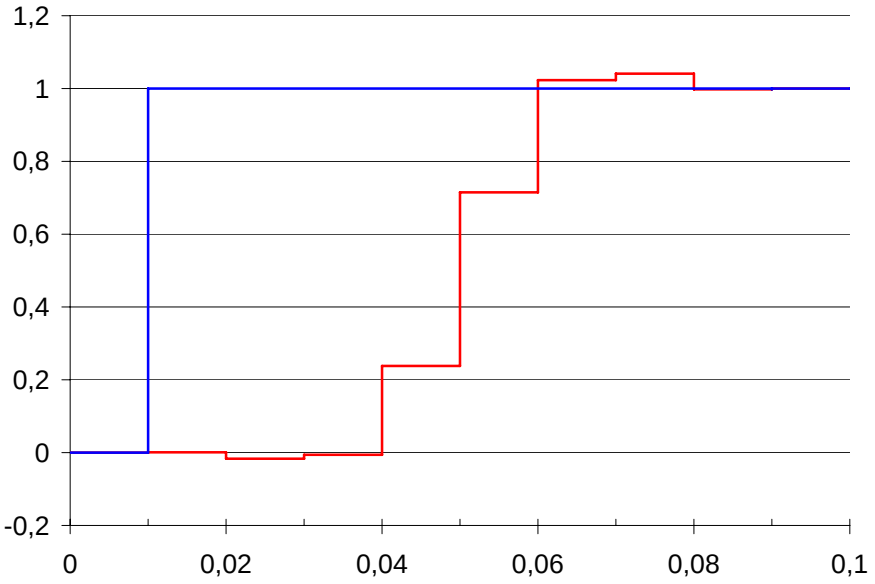

Figure B.6: *Step responce for lambda filter used by Techno-Matic A/S.*

Appendix C

Modelling Terms

In this appendix the terms which is depended on the composition of the solid fuel and the supply air are derived afterwards ζ_{char} is derived.

Derivation of c-terms

The c-terms is used to find the mass flow of a certain atom in the solid fuel and supply air. This can be done as the composition of the solid fuel and supply air is known using the standard atomic weights for the atoms (n) which has the unit [kg/mol]. The standard atomic weights for the atoms are given in Table C.1.

Atom	Standard atomic weight
H	$n_{\text{H}} = 1.00797 \cdot 10^{-3}$
C	$n_{\text{C}} = 12.011 \cdot 10^{-3}$
N	$n_{\text{N}} = 14.007 \cdot 10^{-3}$
O	$n_{\text{O}} = 15.999 \cdot 10^{-3}$

Table C.1: *Standard atomic weights for the atoms in the solid fuel and the supply air.*

The c-terms used in the modelling chapter can now be found. c_{C} is the fraction of C in the solid fuel given by:

$$c_{\text{C}} = \frac{\eta_{\text{CHO}} \cdot n_{\text{C}}}{n_{\text{C}} + \kappa_{\text{H}} \cdot n_{\text{H}} + \kappa_{\text{O}} \cdot n_{\text{O}}} \tag{C.1}$$

where η_{CHO} is the fraction of $\text{CH}_{\kappa_{\text{H}}}\text{O}_{\kappa_{\text{O}}}$ in the solid fuel and κ is the fraction of H or O proportional to C in the solid fuel depended on the composition of the solid fuel. c_{H} is the fraction of H in the solid fuel given by:

$$c_{\text{H}} = \frac{\eta_{\text{CHO}} \cdot \kappa_{\text{H}} \cdot n_{\text{H}}}{n_{\text{C}} + \kappa_{\text{H}} \cdot n_{\text{H}} + \kappa_{\text{O}} \cdot n_{\text{O}}} \tag{C.2}$$

$c_{sf,\text{O}}$ is the fraction of O in the solid fuel given by:

$$c_{sf,\text{O}} = \frac{\eta_{\text{CHO}} \cdot \kappa_{\text{O}} \cdot n_{\text{O}}}{n_{\text{C}} + \kappa_{\text{H}} \cdot n_{\text{H}} + \kappa_{\text{O}} \cdot n_{\text{O}}} \tag{C.3}$$

c_{N} is the fraction of N in the supply air given by:

$$c_{\mathrm{N}} = \frac{\kappa_{\mathrm{N}} \cdot n_{\mathrm{N}}}{2 \cdot \kappa_{\mathrm{N}} \cdot n_{\mathrm{N}} + 2 \cdot n_{\mathrm{O}}} \tag{C.4}$$

where κ_{N} is the fraction of N_2 proportional to O_2 in the supply air and it is equal to 79/21. $c_{a,\mathrm{O}}$ is the fraction of O in the supply air given by:

$$c_{a,\mathrm{O}} = \frac{n_{\mathrm{O}}}{2 \cdot \kappa_{\mathrm{N}} \cdot n_{\mathrm{N}} + 2 \cdot n_{\mathrm{O}}} \tag{C.5}$$

All the c-terms are now derived.

Derivation of $\zeta_{\mathbf{char}}$

ζ_{char} is the the fraction of the solid fuel which is converted to charcoal. Charcoal is degassed solid fuel which only consists of C. ζ_{char} is best found by looking at the amount of C which is not converted to charcoal. The amount of C not converted is only depended on the amount of H in the solid fuel. The amount of H indicates how much C that can react with the H forming a highly flammable gas which is ignited and combusted instantly. Each C atom can bind four H atoms but if the C atoms are in a chain the following apply:

$$\text{amount of H} = 2 \cdot \text{amount of C} + 2 \tag{C.6}$$

From Equation (C.6) the total amount of H needed to ignite all the C can be found. The amount of C ignited can be found from the ratio between the actual amount of H in the solid fuel and the amount of H needed to ignite all the C in the solid fuel and the actual amount of C in the solid fuel.

$$\begin{aligned} \mathrm{C}_{\mathrm{ignited}}(t) &= \frac{\overbrace{\frac{c_{\mathrm{H}} \cdot m_{sf}(t)}{n_{\mathrm{H}}}}^{\text{amount of H in the solid fuel}}}{\underbrace{2 \cdot \frac{c_{\mathrm{C}} \cdot m_{sf}(t)}{n_{\mathrm{C}}} + 2}_{\text{amount of H needed to ignite all the C}}} \cdot \underbrace{\frac{c_{\mathrm{C}} \cdot m_{sf}(t)}{n_{\mathrm{C}}}}_{\text{amount of C in the solid fuel}} \\ &= \frac{c_{\mathrm{C}} \cdot c_{\mathrm{H}} \cdot m_{sf}(t)^2}{n_{\mathrm{C}} \cdot n_{\mathrm{H}} \cdot \left(\frac{2 \cdot c_{\mathrm{C}} \cdot m_{sf}(t)}{n_{\mathrm{C}}} + 2 \right)} \end{aligned} \tag{C.7}$$

The amount of solid fuel which is converted to charcoal is found by subtracting the value in Equation (C.7) from the amount of C in the solid fuel.

$$\begin{aligned} \mathrm{C}_{\mathrm{charcoal}}(t) &= \frac{c_{\mathrm{C}} \cdot m_{sf}(t)}{n_{\mathrm{C}}} - \mathrm{C}_{\mathrm{ignited}}(t) \\ &= \frac{c_{\mathrm{C}} \cdot m_{sf}(t)}{n_{\mathrm{C}}} - \frac{c_{\mathrm{C}} \cdot c_{\mathrm{H}} \cdot m_{sf}(t)^2}{n_{\mathrm{C}} \cdot n_{\mathrm{H}} \cdot \left(\frac{2 \cdot c_{\mathrm{C}} \cdot m_{sf}(t)}{n_{\mathrm{C}}} + 2 \right)} \end{aligned} \tag{C.8}$$

ζ_{char} is now found by dividing the amount of C which is converted to charcoal with he total amount of C in the solid fuel.

$$\begin{aligned}
\zeta_{\text{char}}(t) &= \frac{\text{C}_{\text{charcoal}}(t)}{\frac{c_{\text{C}} \cdot m_{sf}(t)}{n_{\text{C}}}} \\
&= \frac{\left(\frac{c_{\text{C}} \cdot m_{sf}(t)}{n_{\text{C}}} - \frac{c_{\text{C}} \cdot c_{\text{H}} \cdot m_{sf}(t)^2}{n_{\text{C}} \cdot n_{\text{H}} \cdot \left(\frac{2 \cdot c_{\text{C}} \cdot m_{sf}(t)}{n_{\text{C}}} + 2 \right)} \right) \cdot n_{\text{C}}}{c_{\text{C}} \cdot m_{sf}(t)} \\
&= 1 - \frac{c_{\text{H}} \cdot m_{sf}(t)}{n_{\text{H}} \cdot \left(\frac{2 \cdot c_{\text{C}} \cdot m_{sf}(t)}{n_{\text{C}}} + 2 \right)}
\end{aligned} \tag{C.9}$$

Appendix D

Actuator Input

The relationships between the duty cycle and the mass flow per second are found in this appendix. First the relation is found for the screw conveyor motor for the two different solid fuels. Afterward the relation is found for the air blower moreover the relation between primary and secondary supply air is found.

Screw Conveyor

The relation between the duty cycle of the motor signal and the mass flow of solid fuel per second is found by conducting a experiment. The motor is given five different duty cycles and the mass is measured each test last for 300 s. The results for the two different solid fuels can be seen in the following.

Test Results

The test results can be seen in Table D.1 and Table D.2 for respectively wood pellets and wheat.

Duty cycle %	Time [s]	Mass [kg]	Mass flow [kg/s]
99	297	2.831	0.00944
75	225	2.127	0.00709
50	150	1.483	0.00494
25	75	0.697	0.00432
0	0	0	0.00000

Table D.1: *Test results for the wood pellets.*

The relation between duty cycle and mass flow is now found by taking the mass flow as a function of the duty cycle, as seen in Figure D.1.

As it can be seen from Figure D.1 the relationship is linear for both solid fuels. Wood pellets has the function $y = 95.48 \cdot 10^{-6} \cdot x$ and wheat has the function $y = 117.07 \cdot 10^{-6} \cdot x$. It is the slope rate that is used in the modelling phase as β_{motor}.

Duty cycle %	Time [s]	Mass [kg]	Mass flow [kg/s]
100	300	3.505	0.01168
75	225	2.628	0.00876
50	150	1.803	0.00601
25	75	0.831	0.00277
0	0	0	0.00000

Table D.2: *Test results for the wheat.*

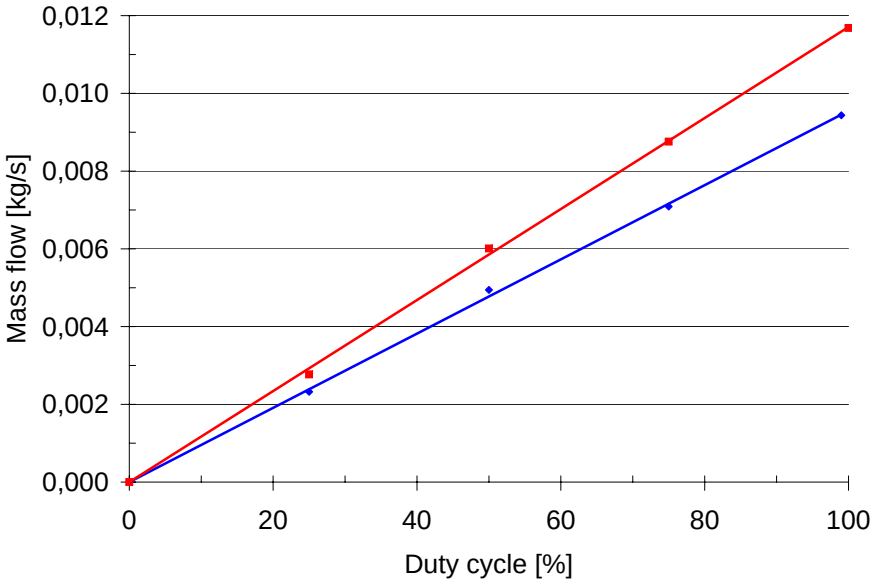

Figure D.1: *The relation between mass flow and duty cycle. The blue line is for wood pellets and it has a slope rate of* $95.48 \cdot 10^{-6}$. *The red line is for wheat and it has a slope rate of* $117.07 \cdot 10^{-6}$.

Blower

The relation between the duty cycle of the blower and mass flow of air per second is found by conducting an experiment. The motor is given 14 different duty cycles and the mass flow is measured with a handhold flow meter. The measured flow value is a average value taken over one minute moreover the test is done three times for each duty cycle and the average value is found. The measurement is taken at the intake of the blower and it is assumed that the air flow is equalled distributed over the whole intake area of the blower. The test results can be seen in Table D.3.

The velocity is measured by the flow meter. The air flow is found by multiplying the velocity with the intake area and the density of air.

The relation is now found by taking the mass flow as a function of the duty cycle, as seen in Figure D.2.

As it can be seen this relation is non-linear. But as the blower is oversized to the system the whole spectra is not need. The operating area for the blower is therefore set from 0% to 30% duty cycle [Jensen, 2007]. The blower can now be linearized in this operating area by finding a function for

Duty cycle %	Velocity [m/s]	Air flow [kg/s]
100	2.70	0.0304
90	2.67	0.0301
80	2.57	0.0289
70	2.57	0.0289
60	2.53	0.0286
50	2.43	0.0274
40	2.33	0.0263
30	2.10	0.0237
25	2.07	0.0233
20	1.87	0.0210
15	1.57	0.0177
10	1.23	0.0139
5	0.73	0.0083
0	0.00	0.0000

Table D.3: *Test results for the blower.*

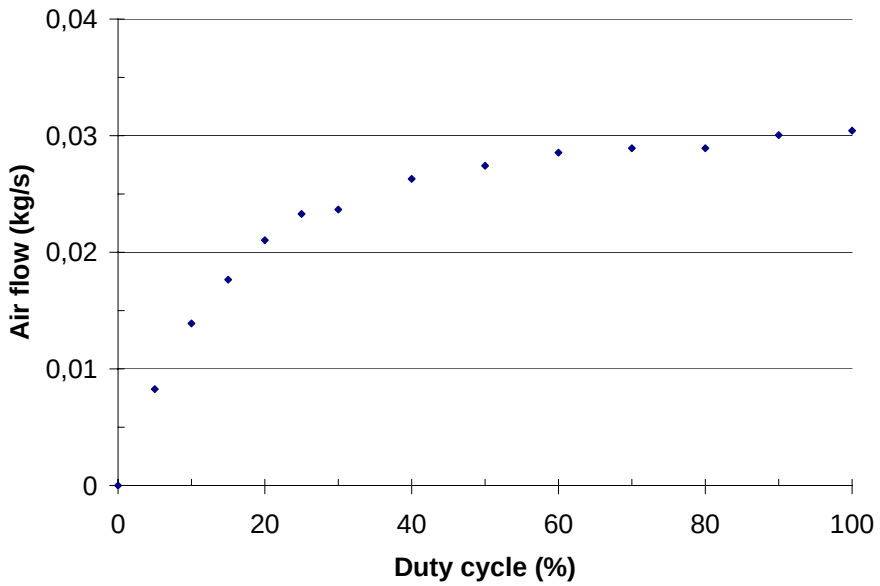

Figure D.2: *The relation between the air flow and the duty cycle.*

the relationship between air flow and duty cycle in this operating area. The function is found in MATLAB to: $y = -54.36 \cdot 10^{-9} \cdot x^4 + 3.59 \cdot 10^{-6} \cdot x^3 - 102.47 \cdot 10^{-6} \cdot x^2 + 2.10 \cdot 10^{-3} \cdot x - 15.93 \cdot 10^{-6}$. The actual duty cycle is inserted instead of x and this expresion is poltted as a function of the linearized duty cycle. The actual duty cycle, the linearized duty cyle and the solution set of the function can be seen in Table D.4

The plot of the solution set of the function as a function of the linearized duty cycle can be seen in Figure D.3.

It can be seen that the relation approximately is linear with the function $y = 266.56 \cdot 10^{-6} \cdot x$ and it is the slope rate that is used in the modelling phase as β_{blower}.

Actual duty cycle	Linearised duty cycle	Solution set
0.0	0	0.0000
2.2	10	0.0041
4.0	20	0.0070
6.0	30	0.0096
8.0	40	0.0118
12.0	50	0.0155
14.0	60	0.0170
17.0	70	0.0191
21.0	80	0.0215
25.0	90	0.0233
30.0	100	0.0237

Table D.4: *Actual duty cycle, linearized duty cycle and solution set of the function used in the linearization of the blower.*

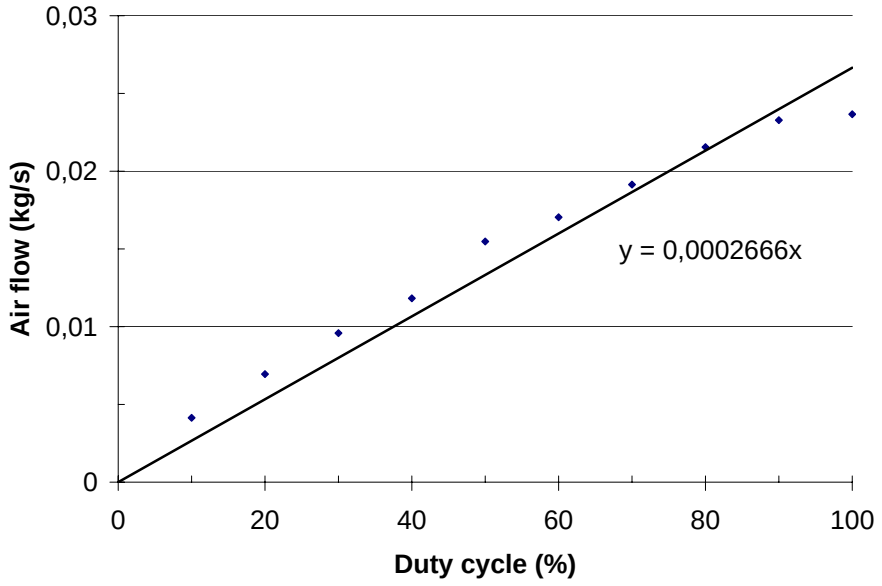

Figure D.3: *The linear relation between the air flow and the duty cycle.*

The relation between primary and secondary supply air is also needed in the modelling phase. Only the secondary supply air can be measured by the flow meter but some modifications on the stoker must be done first. The upper ceramic plate in the burning chamber must be removed which removes the pressure on the secondary air supply. To compensate for this the solid fuel is removed so the pressure on primary air is also removed. Do to these modifications this test only gives a indication of the relationship between the primary and secondary supply air.

The test is done similar to that when the entire air flow was found. The test results can be seen in Table D.5.

Duty cycle %	Velocity [m/s]	Air flow [kg/s]	Percent of entire supply air
30	6.20	0.005259	22%
25	5.85	0.004962	21%
20	5.25	0.004453	21%
15	4.35	0.003690	21%
10	3.35	0.002842	20%
5	1.85	0.001569	19%
0	0.00	0.000000	0%

Table D.5: *Test results for the test of the secondary supply air.*

From Table D.5 it can be seen that approximately 21% of the entire supply air goes to the secondary part. This means that approximately 79% of the supply air goes to the primary part. χ used in the modelling phase is therefore set to 0.79.

Appendix E

Model of the Exhaust Gas Temperature Sensor

In this appendix a model of the exhaust gas temperature sensor mounted on the test setup is found. First a stationary model is found after which the dynamic model is derived.

Stationary Model

The stationary model can be found from the relation between the exhaust gas temperature and the corresponding voltage. A sufficient test is however difficult to conduct as air with different constant temperatures are needed and the air flow around the sensor must be equal to that inside the stoker. Such a test can however be done with two measurements; one when the combustion is extinguished and one when the stoker has reached its steady state. Two measurements are not enough to give a sufficient description of the characteristic of the sensor.

In the interface to the sensor a function is used two convert the voltage measurement to a temperature measurement ($T = f(U)$). Taking the inverse of this function ($T^{-1} = f^{-1}(U) \Leftrightarrow U = f(t)$) and inserting different temperature values a relation between voltage and temperature is found. This relation is however not based on measurements but it can be used as a good indication for the dynamic model. Figure E.1 shows the voltage as a function of the exhaust gas temperature.

It can be seen that the relation is of second order (blue line) but when looking at the operation area of the stoker (70-180°C) the relation is approximately of first order (red line) given by the following equation.

$$U = 5.148 \cdot 10^{-3} \cdot T + 0.141 \tag{E.1}$$

A approximated stationary transfer function is now found for the exhaust gas temperature sensor.

Dynamic Model

The dynamic of the exhaust gas temperature sensor can be found from a step response. This step response is made by bringing the stoker in steady state without the sensor plugged in when steady state is reached the sensor is plugged in. The step is made from 23-79°C and it can be seen in Figure E.2.

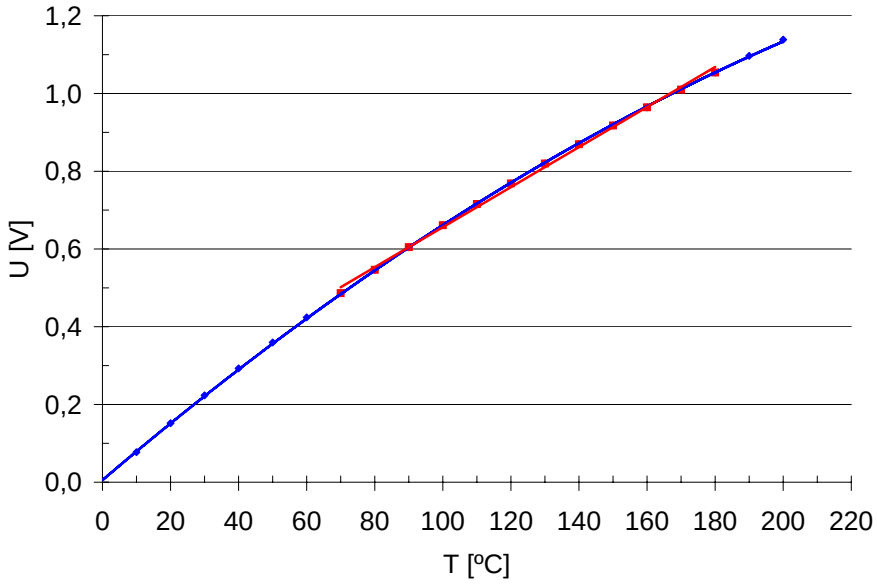

Figure E.1: *Relation between the voltage and the temperature. The blue line is a second order function fitted to all the points where as the red line is a first order function fitted to the points in the operating area.*

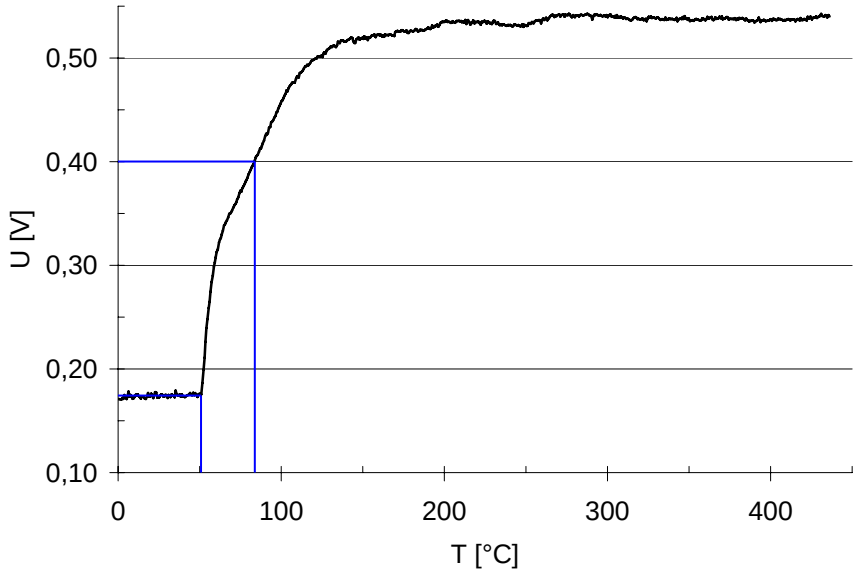

Figure E.2: *Step response for the exhaust gas temperature sensor.*

It is assumed that the temperature sensor is of first order and that it does not contain any time delays. The time constant can be read to 33.5 s in Figure E.2. The time constant is found where the step response is increased 63%. The transfer function for the temperature sensor is then found to:

$$H_{TS}(s) = \frac{1}{33.5 \cdot s + 1} \tag{E.2}$$

The model is given as the transfer function multiplied with the stationary gain.

$$T(s) = 5.148 \cdot 10^{-3} \cdot \frac{1}{33.5 \cdot s + 1} \tag{E.3}$$

Figure E.3 shows the step response (blue line) and the model (green line). As it can be seen is the gain to small this is because the step response on the sensor is taken outside the operating area (20-70°C). If the gain was found from this operating area the sensor model would fit as seen by the red line in Figure E.3. It is therefore assumed that the derived model in Equation (E.3) is sufficient.

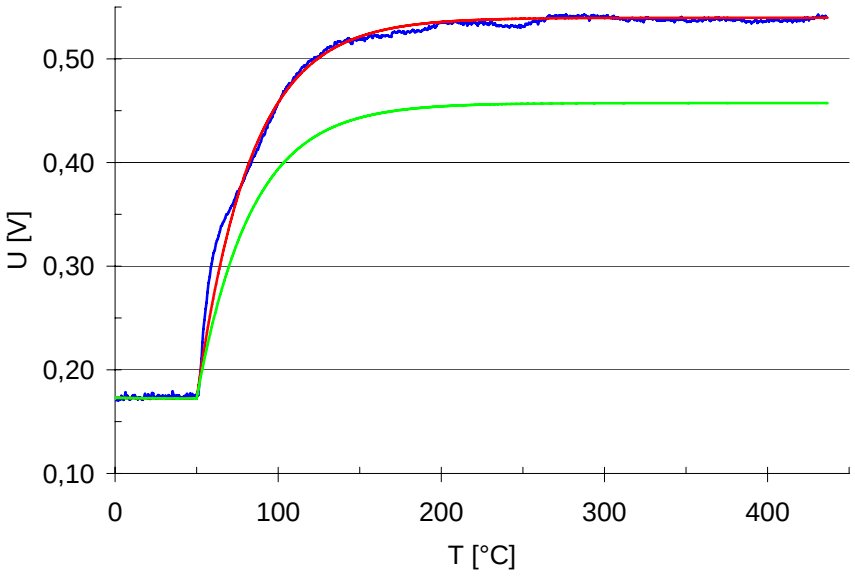

Figure E.3: *The blue line is shows the step response, the green line shows the model with a gain of* $5.148 \cdot 10^{-3}$ *and the red line shows the model with a gain of* $6.690 \cdot 10^{-3}$.

Appendix F

Real Photos of the Stoker System

This appendix presented real photos of the plant. Figure F.1 shows the whole test set up. Figure F.2 shows the two actuator on the system. Figure F.3 shows the two PCB's from Techno-Matic A/S along with the connection board. Figure F.4 shows the burning chamber where the burning head and the catalyst can be seen. Figure F.5 shows the load with the calorifier and the frequency converter.

Figure F.1: *The whole test set up. The load can be seen to the left and the target PC is just above the load. The lowest chamber in the middle is the burning chamber and the one above is the gas chamber. Just above the gas chamber can the original controller from Techno-Matic A/S be seen. Behind the white plate to the right are the two actuators located and above them is the solid fuel chamber.*

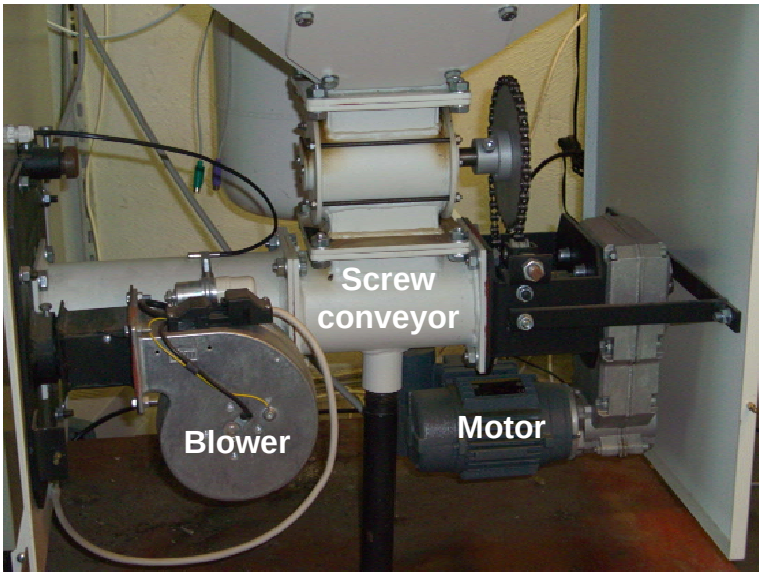

Figure F.2: *The two actuators. The blower and the screw conveyor along with motor which drives the screw conveyor.*

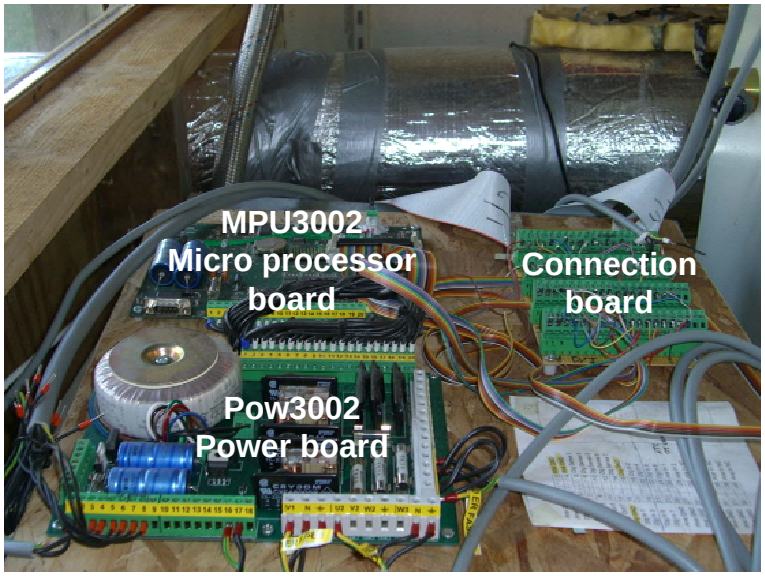

Figure F.3: *The MPU3002 PCB and the Pow3002 PCB from Techno-Matic A/S, anlong with the connection board.*

Figure F.4: *The burning chamber with the burning head and the catalyst. The pipe going up to the catalyst is the secondary air. The ash trash in the bottom collects the ash from the solid fuel.*

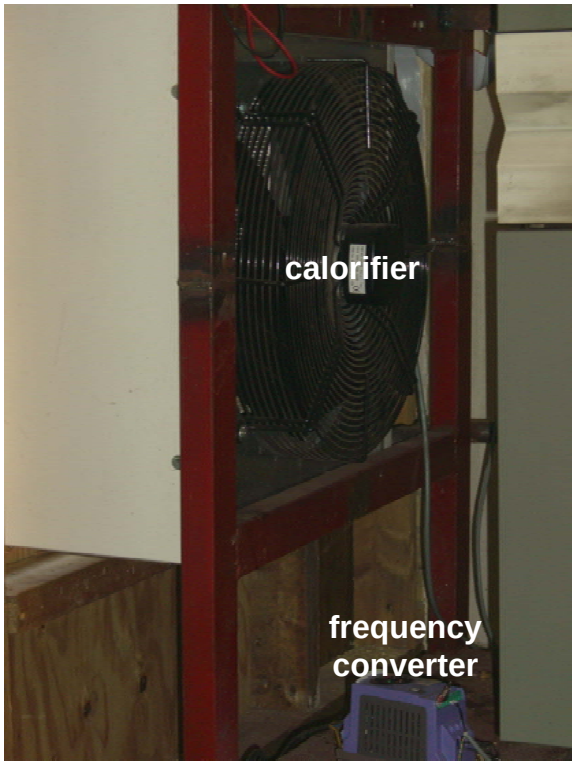

Figure F.5: *The consisting of the calorifier and the frequency converter. It is the back of the calorifier that is shown and the axial fan can be glimpsed through the black safety case.*

Appendix G

Calculation of Constants

Some of the constants in the model can not be found in look-up tables and books, they must therefore be calculated which is done in this appendix. First the physical constants on the stoker are found, secondly the heat transfer coefficients are calculated and finally the mass of the gas in the chambers is found.

Physical Constants on the Stoker

To determine the physical constants on the plant such as areas and volumes Figure G.1 to Figure G.3 are used. These figures are made from a sketch of a Benekov-Liagro R 15 stoker which Liagro has provided, measurements made on the R 25 at Techno-Matic A/S and assumptions.

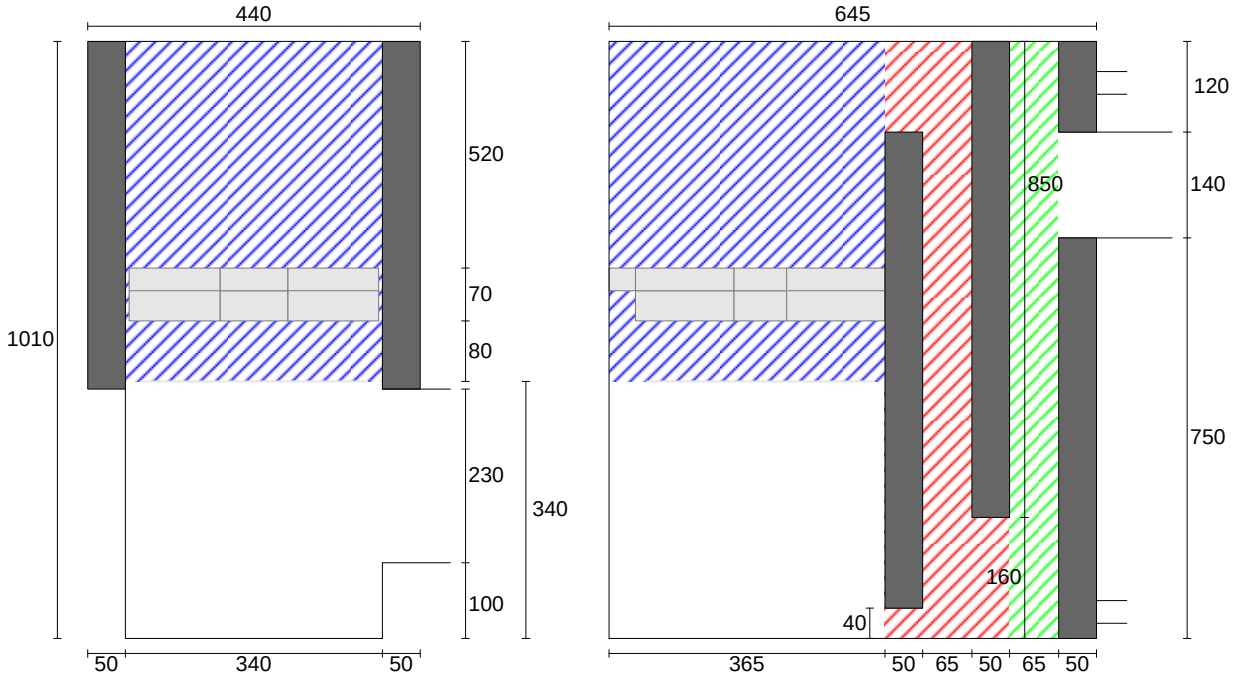

Figure G.1: *Sketch of the stoker seen from the front (left) and from the side (right). All measures are in [mm].*

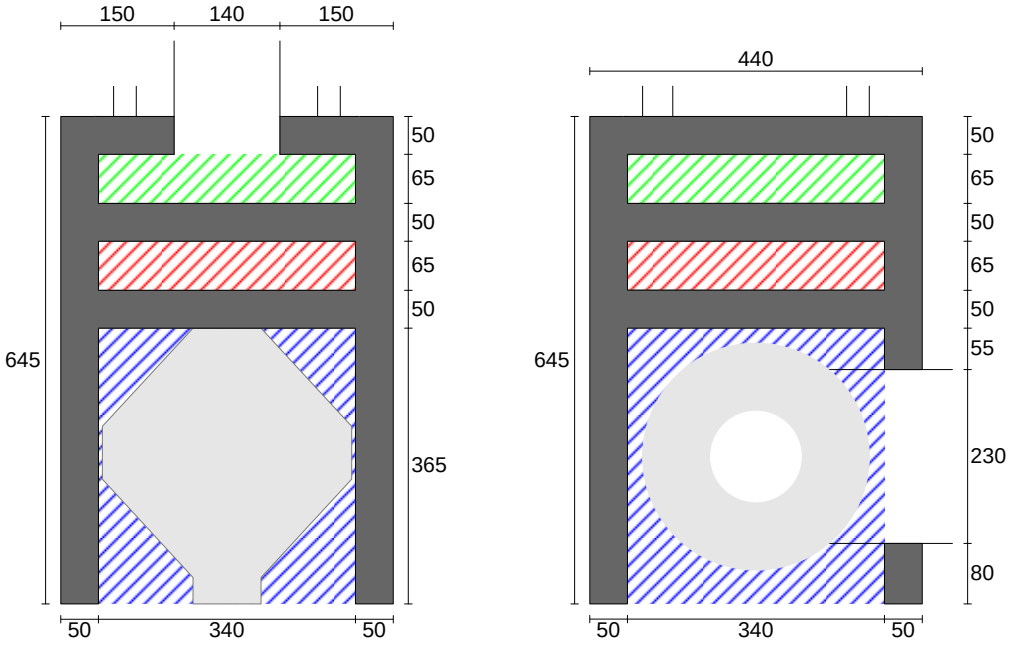

Figure G.2: *Sketch of the stoker seen from the top. The right sketch is a higher top view where as the left sketch is a lower top view. All measures are in [mm].*

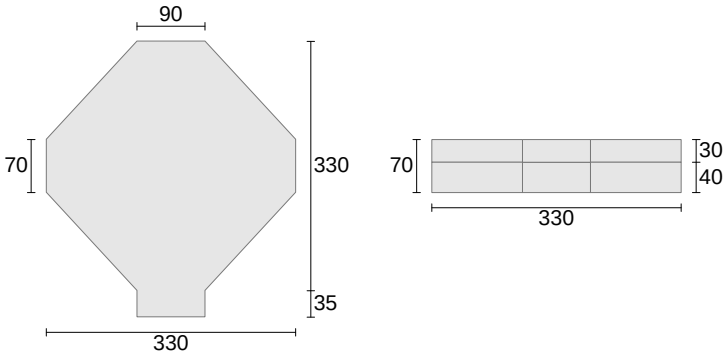

Figure G.3: *Sketch of the ceramic plate seen from the top (left) and from the front (right). All measures are in [mm].*

The blue, red and green areas indicates the chamber divisions, where blue is the burning chamber, red is the gas chamber, and green is the exhaust gas. The area beneath the burning head is not included in these figures. This is not necessary as the area beneath the burning head is not included in the burning chamber.

Both the area of the water (the dark gray areas on Figure G.1 and Figure G.2) and the volume of the three chambers, and the ceramic plate can now be found. First the three water areas are found, where A_{bcw} is the area of the water which is in contact with the burning chamber. A_{gcw} is the area of the water which is in contact with the gas chamber. A_{egw} is the area of the water which is in contact with the exhaust gas.

$$A_{bcw} = 0.550 \cdot 0.340 + 2 \cdot 0.680 \cdot 0.365 = 0.683 \text{ m}^2 \quad \text{(G.1)}$$

$$A_{gcw} = 3 \cdot 0.050 \cdot 0.340 + 2 \cdot 0.850 \cdot 0.340 + 2 \cdot (0.065 \cdot 1.010 + 0.050 \cdot (0.120 + 0.040 + 0.160)) = 0.758 \text{ m}^2 \quad \text{(G.2)}$$

$$A_{egw} = (0.750 + 0.120) \cdot 0.340 + 0.850 \cdot 0.340 + 2 \cdot 0.065 \cdot 1.010 = 0.716 \text{ m}^2 \quad \text{(G.3)}$$

The volume of the ceramic plate is found in Equation (G.4).

$$\begin{aligned} V_{cp} &= \left(0.330 \cdot 0.330 + 0.035 \cdot 0.090 - 4 \cdot \left(\frac{1}{2} \cdot 0.120 \cdot 0.130\right)\right) \cdot 0.030 \\ &\quad + \left(0.330 \cdot 0.330 - 4 \cdot \left(\frac{1}{2} \cdot 0.120 \cdot 0.130\right)\right) \cdot 0.040 = 0.006 \text{ m}^3 \end{aligned} \tag{G.4}$$

The three volumes of the chambers can now be found.

$$V_{bc} = 0.340 \cdot 0.365 \cdot 0.670 - V_{cp} = 0.078 \text{ m}^3 \tag{G.5}$$

$$\begin{aligned} V_{gc} &= 0.340 \cdot (1.010 \cdot 0.065 + 0.040 \cdot 0.050 \\ &\quad + 0.120 \cdot 0.050 + 0.160 \cdot 0.050) = 0.028 \text{ m}^3 \end{aligned} \tag{G.6}$$

$$V_{eg} = 0.340 \cdot 1.010 \cdot 0.065 = 0.022 \text{ m}^3 \tag{G.7}$$

As some of the stoker measures are found from assumptions both the areas and the volumes can vary from the actual ones on the plant. This means that some of these values have to be fitted for the model to be sufficient.

Calculation of the Heat Transfer Coefficients

The heat transfer coefficients can be found from the energy balance equations for the burning chamber, the gas chamber and the exhaust gas all derived in Chapter 6. The heat transfer coefficients are isolated in these three equations and steady state values are used for inputs and state variables. As the steady state values vary depending on the solid fuel the heat transfer coefficients must be found for both wood pellets and wheat. In the equation for the burning chamber another constant is present which is the emissivity (ϵ). The emissivity is a measure of a material's ability to absorb and radiate energy. If the material is capable of absorbing all the energy it is called a black body and the emissivity for such materials is equal to one. This is however not the case in the stoker as a lot of the energy is reflected by the metal wall between the burning chamber and the water. It is therefore assumed that the emissivity lies just around 0.50, through trail-and-error ϵ_{bc} is found to 0.55 both for wood pellets and wheat. The transfer coefficient for the burning chamber can now be found from the following equation:

$$\begin{aligned} (M_{bc} \cdot c_{bc} + M_{cp} \cdot c_{cp}) \cdot \frac{\mathrm{d}T_{bc}(t)}{\mathrm{d}t} &= m_a(t) \cdot c_a \cdot T_a + m_{\mathrm{C}}(t) \cdot \left(\frac{h_{c,\mathrm{I}} + 3 \cdot h_{c,\mathrm{II}}}{4}\right) \\ &\quad + \frac{m_{\mathrm{C}}(t) \cdot n_{\mathrm{CO}} \cdot h_{c,\mathrm{V}}}{4 \cdot n_{\mathrm{C}}} + c_{\mathrm{H}} \cdot m_{sf}(t) \cdot h_{c,\mathrm{VI}} \\ &\quad - m_g(t) \cdot c_{bc} \cdot T_{bc}(t) \\ &\quad - \epsilon_{bcw} \cdot \sigma \cdot A_{bcw} \cdot (T_{bc}(t)^4 - T_w(t)^4) \\ &\quad - \alpha_{bc} \cdot A_{bcw} \cdot (T_{bc}(t) - T_w(t)) \end{aligned} \tag{G.8}$$

α_{bc} is then isolated and the time depended variables are replaced with steady state values when wood pellets are combusted.

$$\begin{aligned}
\alpha_{bc} &= \frac{1}{A_{bcw}\cdot(T_{bc}-T_w)}\cdot\left\{m_a\cdot c_a\cdot T_a + m_{\mathrm{C}}\cdot\left(\frac{h_{c,\mathrm{I}}+3\cdot h_{c,\mathrm{II}}}{4}\right)+\frac{m_{\mathrm{C}}\cdot n_{\mathrm{CO}}\cdot h_{c,\mathrm{V}}}{4\cdot n_{\mathrm{C}}}\right.\\
&\left.+c_{\mathrm{H}}\cdot m_{sf}\cdot h_{c,\mathrm{VI}} - m_g\cdot c_{bc}\cdot T_{bc} - \epsilon_{bcw}\cdot\sigma\cdot A_{bcw}\cdot({T_{bc}}^4-{T_w}^4)\right\}\Leftrightarrow\\
\alpha_{bc} &= \frac{1}{0.683\cdot(400-60)}\cdot\left\{4.531\cdot10^{-3}\cdot1005.2\cdot20+7.840\cdot10^{-3}\cdot\left(\frac{9.203\cdot10^6+3\cdot32.766\cdot10^6}{4}\right)\right.\\
&+\frac{7.840\cdot10^{-3}\cdot0.028\cdot10.103\cdot10^6}{4\cdot0.012}+0.059\cdot0.859\cdot10^{-3}\cdot141.5\cdot10^6-0.011\cdot1067.8\cdot400\\
&\left.-0.55\cdot5.67\cdot10^{-8}\cdot0.683\cdot\left(400^4-60^4\right)\right\}\Leftrightarrow\\
\alpha_{bc} &= 50.924
\end{aligned}\tag{G.9}$$

The transfer coefficient for the gas chamber can be found from the following equation:

$$\begin{aligned}
M_{gc}\cdot c_{gc}\cdot\frac{\mathrm{d}T_{gc}(t)}{\mathrm{dt}} &= m_g(t)\cdot(c_{bc}\cdot T_{bc}(t)-c_{gc}\cdot T_{gc}(t))\\
&\quad -\alpha_{gc}\cdot A_{gcw}\cdot(T_{gc}(t)-T_w(t))
\end{aligned}\tag{G.10}$$

α_{gc} is then isolated and the time depended variables are replaced with steady state values when wood pellets are combusted.

$$\begin{aligned}
\alpha_{gc} &= \frac{m_g\cdot(c_{bc}\cdot T_{bc}-c_{gc}\cdot T_{gc})}{A_{gcw}\cdot(T_{gc}-T_w)}\Leftrightarrow\\
\alpha_{gc} &= \frac{0.011\cdot(1067.8\cdot450-1034.8\cdot180)}{0.758\cdot(180-60)}\Leftrightarrow\\
\alpha_{gc} &= 35.644
\end{aligned}\tag{G.11}$$

The transfer coefficient for the exhaust gas can be found from the following equation:

$$\begin{aligned}
M_{eg}\cdot c_{eg}\cdot\frac{\mathrm{d}T_{eg}(t)}{\mathrm{dt}} &= m_g(t)\cdot(c_{gc}\cdot T_{gc}(t)-c_{eg}\cdot T_{eg}(t))\\
&\quad -\alpha_{eg}\cdot A_{egw}\cdot(T_{eg}(t)-T_w(t))
\end{aligned}\tag{G.12}$$

α_{eg} is then isolated and the time depended variables are replaced with steady state values when wood pellets are combusted.

$$\begin{aligned}
\alpha_{eg} &= \frac{m_g\cdot(c_{gc}\cdot T_{gc}-c_{eg}\cdot T_{eg})}{A_{egw}\cdot(T_{eg}-T_w)}\Leftrightarrow\\
\alpha_{eg} &= \frac{0.011\cdot(1034.8\cdot180-1017.4\cdot100)}{0.716\cdot(100-60)}\Leftrightarrow\\
\alpha_{eg} &= 32.464
\end{aligned}\tag{G.13}$$

The same procedure is used when wheat is combusted and the following three heat transfer values are found:

$$\begin{aligned}
\alpha_{bc} &= 62.095\\
\alpha_{gc} &= 24.797\\
\alpha_{eg} &= 11.560
\end{aligned}$$

As all the heat transfer coefficients are based on steady state values and assumption can it be necessary to fit the coefficients to obtain a sufficient model.

Mass of the Gas in the Chambers

The mass of the gas in the chambers are depended on the temperature and the composition of the gas where both are depended on time. As the temperature is hard to measure on-line and the composition is complex to find the mass is assumed to be constant. This is however a good assumption as both the temperature and the composition is almost constant under steady state. This means that the mass can be calculated from the volume just find in the previous section and the density of the gas. To find the density of the gas the temperature in steady state must be found and the gas composition must be known. It is assumed that the density of clean air can be used, so only the temperature must be found which is done in the following.

To find the temperature in the chambers an experiment must be conducted. As no sensors are available to measure the temperature in the burning and gas chamber, the temperature must be found otherwise. This means that the temperature only can be measured off-line which only gives an estimated value of the temperature in the two chambers. The estimated temperature can also be used in the model verification. It is however obvious that the temperature will change a lot as the exhaust gas temperature easily vary with 30°C depending on the water temperature, the reference, and the load. The temperature changes in the burning and gas chamber are even larger as these two chambers lie before where the exhaust gas temperature is measured.

The test is made by putting wolfram in the chambers. Wolfram is chosen as it has a very high melting point which makes it capable of being inside the stoker for hours without melting. The wolfram is then placed in the burning and gas chamber respectively. When the wolfram is heated up to the temperature in the respective chamber, the wolfram is taken out of the stoker and put into a water tank. The initial temperature of the water in the tank is known and the final temperature in the water is measured. From the energy given to the water, the temperature inside the chambers can be calculated. The test is performed different places in the stoker.

The result from the different test is shown in table Table G.1.

The temperature of the chambers is found from the following equation:

$$M_{\text{water}} \cdot c_{\text{water}} \cdot \Delta T_{\text{water}} = M_{\text{wolfram}} \cdot c_{\text{wolfram}} \cdot (T_{\text{wolfram initial}} - T_{\text{wolfram final}}) \tag{G.14}$$

The start temperature of the wolfram is the desired value, so the equation is rewritten to:

$$T_{\text{wolfram initial}} = \frac{M_{\text{Water}} \cdot c_{water} \cdot \Delta T_{\text{water}}}{M_{\text{wolfram}} \cdot c_{\text{wolfram}}} + T_{\text{Wolfram final}} \tag{G.15}$$

This equation is used to calculate the different temperatures inside the chambers.

In this experiment there is a lot of source of errors. These include heat lost to the surroundings, measurement uncertainties, and wrong placement of the wolfram in the chambers. Most of the source of errors will give a lower temperature than the actual one and it is therefore assumed that the calculated result is lower than the actual temperature in the chamber. The temperature tests is only made on a few different spots inside the chambers and as the burning and gas chamber are two large rooms the found temperature will only be a estimated value for the whole chamber. The temperature in the burning chamber is found to approximately 490°C. In the gas chamber is the temperature found to approximately 230°C. The results also show that there is a large temperature gab between the different tests and it is hard to decide what temperature that will be the lowest and highest possible in the different chambers. This means that this test is used to give an estimate of the temperature inside the chambers, so the mass of the gas inside the chambers and unreliable model outputs can be determined.

The density of the gas in the chambers can now be found from look-up tables and the mass of

Initial water temperature [°C]	Mass water [kg]	Final water temperature [°C]	Chamber temperature [°C]	Notes
19.7	0.741	20.1	360	On ceramic plate in the burning chamber with fan: 20 Hz and T_w: 61°C.
16.9	0.671	17.5	480	Half in fire, half on ceramic plate in the burning chamber with fan: 20 Hz and T_w: 68°C.
17.2	0.663	18	626	In the molehill with fan: 20 Hz and T_w: 65°C.
17.5	0.670	17.7	171	On the edge of the gas chamber door with fan: 20 Hz and T_w: 70°C.
17.3	0.669	17.7	286	In the middle of the gas gas chamber with fan: 40 Hz and 55° T_w: 65°C.

Table G.1: *Test results for the temperature measurements inside the burning and gas chamber.*

the gas can be calculated.

$$M_{bc} = V_{bc} \cdot \rho_{bc} = 0.078 \cdot 0.462 = 0.036 \text{ kg} \quad \text{(G.16)}$$

$$M_{gc} = V_{gc} \cdot \rho_{gc} = 0.028 \cdot 0.702 = 0.019 \text{ kg} \quad \text{(G.17)}$$

$$M_{eg} = V_{eg} \cdot \rho_{eg} = 0.022 \cdot 0.961 = 0.021 \text{ kg} \quad \text{(G.18)}$$

$$M_{\text{total}} = M_{bc} + M_{gc} + M_{eg} = 0.036 + 0.019 + 0.021 = 0.077 \text{ kg} \quad \text{(G.19)}$$

As both the volume and density is based on assumptions the mass of the gas can vary from the actual one. This means that some of these values have to be fitted for the model to be sufficient.

Appendix H

Nomenclature

This appendix present all the constants and variables used in the modelling phase. A description of the abbreviations used in the modelling phase is given along with the value and unit.

Physical Constants

This section contains all the constants used in the models. First the abbreviation of the constant is given, secondly the constant is described, and finally the value of the constant is given along with the unit of the constant.

Constant	Description	Value
A_{bcw}	Area of the burning chamber in contact with water	0.683 m^2
A_{gcw}	Area of the gas chamber in contact with water	0.758 m^2
A_{egw}	Area of the exhaust gas in contact with water	0.716 m^2
c_w	Specific heat capacity of water	4185 kJ/(kg · K)
c_{iw}	Specific heat capacity of inlet water	4181 kJ/(kg · K)
c_{bc}	Specific heat capacity of gas in burning chamber	1067.8 kJ/(kg · K)
c_{gc}	Specific heat capacity of gas in gas chamber	1034.8 kJ/(kg · K)
c_{eg}	Specific heat capacity of the exhaust gas	1017.4 kJ/(kg · K)
c_{cp}	Specific heat capacity of the ceramic plate	950 kJ/(kg · K)
$c_{a,\mathrm{O}}$	Fraction of O in supply air	0.116
c_{N}	Fraction of N in supply air	0.384
$h_{c,\mathrm{I}}$	Heat value for C reacting with O to CO	9203.2 kJ/kg
$h_{c,\mathrm{II}}$	Heat value for C reacting with O_2 to CO_2	32766 kJ/kg
$h_{c,\mathrm{V}}$	Heat value for CO reacting with O_2 to CO_2	10103 kJ/kg
$h_{c,\mathrm{VI}}$	Heat value for H_2 reacting with O_2 to H_2O	141500 kJ/kg
M_w	Mass of water	89 kg
M_{bc}	Mass of gas in burning chamber	0.036 kg
M_{gc}	Mass of gas in gas chamber	0.019 kg
M_{eg}	Mass of exhaust gas	0.021 kg
M_{cp}	Mass of ceramic plate	15.494 kg
M_{total}	Total mass of gas in the stoker system	0.077 kg

m_w	Water flow	0.35 kg/s
n_{C}	Molar mass of C atom	$12.011 \cdot 10^{-3}$ kg/mol
n_{H}	Molar mass of H atom	$1.00797 \cdot 10^{-3}$ kg/mol
n_{O}	Molar mass of O atom	$15.999 \cdot 10^{-3}$ kg/mol
n_{N}	Molar mass of N atom	$14.007 \cdot 10^{-3}$ kg/mol
n_{CO}	Molar mass of CO molecule	$28.01 \cdot 10^{-3}$ kg/mol
$n_{\mathrm{CO_2}}$	Molar mass of CO_2 molecule	$44.009 \cdot 10^{-3}$ kg/mol
$n_{\mathrm{H_2O}}$	Molar mass of H_2O molecule	$18.01494 \cdot 10^{-3}$ kg/mol
V_{bc}	Volume of burning chamber	0.078 m^3
V_{gc}	Volume of gas chamber	0.028 m^3
V_{eg}	Volume of exhaust gas	0.022 m^3
V_{cp}	Volume of ceramic plate	$5.5534 \cdot 10^{-3}$ m^3
β_{blower}	Slope rate of the relation between air flow and duty cycle	$0.267 \cdot 10^{-3}$ kg/s
ϵ_{bc}	Emissivity of metal wall between burning chamber and water	0.375
κ_{N}	Number of N atoms for each O atom in air.	3.762
ρ_{bc}	Density of gas in burning chamber	0.462 kg/m^3
ρ_{gc}	Density of gas in gas chamber	0.702 kg/m^3
ρ_{eg}	Density of exhaust gas	0.961 kg/m^3
ρ_{cp}	Density of the ceramic plate	2800 kg/m^3
σ	The Stefan-Boltzman constant	$6.57 \cdot 10^{-8}$ W/($m^2 \cdot K^4$)
υ	Transforms the O_2-level to a volume percentage value	158
χ	Fraction of primary supply air	0.8

Table H.1: *Physical constants used in the model.*

Solid Fuel Constants

In this section are all the solid fuel depended constants found. First the abbreviation of the constant is given, secondly the constant is described and finally is the value of the constant for both wood pellets and wheat given.

Parameter	Description	Value	
		Wood pellets	Wheat
c_{C}	Fraction of C in the solid fuel	0.472	0.435
c_{H}	Fraction of H in the solid fuel	0.059	0.052
$c_{sf,\mathrm{O}}$	Fraction of O in the solid fuel	0.409	0.383
β_{motor}	Slope rate of the relation between solid fuel flow and duty cycle	$95.48 \cdot 10^{-6}$ kg/s	$117.07 \cdot 10^{-6}$ kg/s
α_{bc}	Heat transfer value for the burning chamber	50.924	62.095
α_{gc}	Heat transfer value for the gas chamber	35.644	24.797
α_{eg}	Heat transfer value for the gas chamber	24.367	11.560

γ_1	Parameter depended on the solid fuel and the primary air	0.05	0.12
γ_2	Parameter depended on the solid fuel and the size of the mole hill	4	2
η_{CHO}	Fraction of C, H and O in solid fuel	0.94	0.87
$\eta_{\mathrm{H_2O}}$	Humidity of the solid fuel	0.06	0.13
κ_{H}	Number of H atoms for each C atom	1.48	1.42
κ_{O}	Number of O atoms for each C atom	0.65	0.66

Table H.2: *Solid fuel depended constants used in the model.*

Time Varying Variables

This section contains all the time varying variables used in the models. First the abbreviation of the variable is given, secondly the variable is described and finally is the unit of the variable given.

Variable	Description	Unit
$\text{duty cycle}_{\text{blower}}$	Duty cycle of the PWM signal sent to the blower	[%]
$\text{duty cycle}_{\text{motor}}$	Duty cycle of the PWM signal sent to the screw conveyor	[%]
E_{bc}	Energy in the burning chamber gas	[J]
E_{eg}	Energy in the exhaust gas	[J]
E_{gc}	Energy in the gas chamber gas	[J]
E_w	Energy in the water	[J]
h_{iw}	Specific enthalpy of the inlet water	[J/kg]
h_{ow}	Specific enthalpy of the outlet water	[J/kg]
m_a	Mass flow of supply air	[m/s]
$m_{a,\mathrm{N}}$	Mass flow of N in supply air	[m/s]
$m_{a,\mathrm{O}}$	Mass flow of O in supply air	[m/s]
$m_{a,p}$	Mass flow of primary supply air	[m/s]
$m_{bc\rightarrow gc}$	Mass flow of gas from burning chamber to gas chamber	[m/s]
m_{C}	Mass flow of C under combustion	[m/s]
$m_{\mathrm{C,char}}$	Mass flow of charcoal which is under combustion	[m/s]
m_{CO}	Mass flow of CO released under the combustion process	[m/s]
$m_{\mathrm{CO_2}}$	Mass flow of CO_2 released under the combustion process	[m/s]
$m_{\mathrm{C,gas}}$	Mass flow of C which is ignited	[m/s]
m_{eg}	Mass flow of exhaust gas	[m/s]
m_g	Mass flow of gas up through the stoker	[m/s]
$m_{gc\rightarrow eg}$	Mass flow of gas from gas chamber to exhaust gas	[m/s]

$m_{\mathrm{H_2}}$	Mass flow H_2 released under the combustion process	[m/s]
$m_{\mathrm{H_2O}}$	Mass flow H_2O	[m/s]
$m_{\mathrm{H_2O},1}$	Mass flow H_2O in solid fuel	[m/s]
$m_{\mathrm{H_2O},2}$	Mass flow H_2O released under the combustion process	[m/s]
m_{iw}	Mass flow of inlet water	[m/s]
$m_{i\mathrm{O_2}}$	Mass flow of O_2 in supply air	[m/s]
$m_{sf,\mathrm{char}}$	Mass flow of C in solid fuel which is converted to charcoal	[m/s]
m_{O}	Mass flow of O which is not used in the combustion process	[m/s]
$m_{o\mathrm{O_2}}$	Mass flow of O_2 in exhaust gas	[m/s]
m_{ow}	Mass flow of outlet water	[m/s]
$m_{\mathrm{O_2}\rightarrow g}$	Mass flow of O_2 converted to gas under the combustion process	[m/s]
$m_{\mathrm{O_2}\rightarrow\mathrm{CO_2}}$	Mass flow of O_2 converted to CO_2	[m/s]
$m_{\mathrm{O_2}\rightarrow\mathrm{H_2O}}$	Mass flow of O_2 converted to H_2O	[m/s]
m_{sf}	Mass flow of solid fuel	[m/s]
$m_{sf,\mathrm{C}}$	Mass flow of C in solid fuel	[m/s]
$m_{sf,\mathrm{H}}$	Mass flow of H in solid fuel	[m/s]
$m_{sf,\mathrm{O}}$	Mass flow of O in solid fuel	[m/s]
$m_{sf,\mathrm{O_2}}$	Mass flow of O_2 released from solid fuel under the combustion	[m/s]
$M_{\mathrm{C,char}}$	Mass of charcoal in the molehill	[kg]
$M_{\mathrm{C,gas}}$	Mass of C in the volatile gases	[kg]
q_a	Energy contained in the supply air	[W]
$q_{bc\rightarrow gc}$	Energy transferred from the gas chamber to the exhaust gas	[W]
q_{bg}	Energy from burning the gases	[W]
q_{bsf}	Energy from burning the solid fuel	[W]
q_{eg}	Energy contained in the exhaust gas	[W]
$q_{gc\rightarrow eg}$	Energy transferred from the burning chamber to the gas chamber	[W]
$q_{g\rightarrow w}$	Energy transferred from the gas to the water	[W]
$q_{g\rightarrow w,1}$	Energy transferred from the gas in the burning chamber to the water in contact with the burning chamber	[W]
$q_{g\rightarrow w,2}$	Energy transferred from the gas in the gas chamber to the water in contact with the gas chamber	[W]
$q_{g\rightarrow w,3}$	Energy transferred from the exhaust gas to the water in contact with the exhaust gas	[W]
q_{iw}	Energy contained in the inlet water	[W]
q_{ow}	Energy contained in the outlet water	[W]
T_{bc}	Burning chamber temperature	[°C]
T_{eg}	Exhaust gas temperature	[°C]
T_{gc}	Gas chamber temperature	[°C]
T_{iw}	Inlet water temperature	[°C]
T_{mh}	Molehill temperature	[°C]
T_{ow}	Outlet water temperature	[°C]
T_w	Water temperature	[°C]
τ_{gas}	Ignition time for the volatile gases	[s]
ζ_{char}	Ratio of C converted to charcoal	[·]

Table H.3: *Time depended variables used in the model.*